UNIVERSIDADE FEDERAL FLUMINENSE
INSTITUTO DE GEOCIÊNCIAS
DEPARTAMENTO DE GEOLOGIA E GEOFÍSICA
PROGRAMA DE PÓS-GRADUAÇÃO EM DINÂMICA DOS OCEANOS E DA TERRA

RODRIGO MACEDO PENNA

SEISMIC FLOW UNITS DISCRETIZATION AND PETROPHYSICAL MODELLING

NITERÓI
2022

SEISMIC FLOW UNITS DISCRETIZATION AND PETROPHYSICAL MODELLING

RODRIGO MACEDO PENNA

Thesis submitted to the Programa de Pós-Graduação em Dinâmica dos Oceanos e da Terra of Universidade Federal Fluminense in partial fulfillment of the requirements for the degree of Doctor in Science - Geology and Geophysics.

Approved by the Committee on December 08, 2022.

Committee:

_____

Ph.D. Alvaro Martini

_____

Ph.D. Emilson Ferreira Leite

_____

Ph.D. Karen Oliveira

_____

Ph.D. Leonardo Teixeira da Silva

_____

Ph.D. Sergio Oliveira

_____

Ph.D. Wagner Lupinacci – Orientador (GIECAR/GGO/UFF and INCT-GP)

Ficha catalográfica automática - SDC/BIG
Gerada com informações fornecidas pelo autor

P412s Penna, Rodrigo Macedo
SEISMIC FLOW UNITS DISCRETIZATION AND PETROPHYSICAL MODELLING / Rodrigo Macedo Penna. - 2022.
139 f.: il.

Orientador: Wagner Moreira Lupinacci.
Tese (doutorado)-Universidade Federal Fluminense, Instituto de Geociências, Niterói, 2022.

1. Geofísica. 2. Geofísica de Reservatórios. 3. Fácies de Fluxo. 4. Petrofísica. 5. Produção intelectual. I. Lupinacci, Wagner Moreira, orientador. II. Universidade Federal Fluminense. Instituto de Geociências. III. Título.

CDD - XXX

Bibliotecário responsável: Debora do Nascimento - CRB7/6368

Acknowledgements

I would like to acknowledge both Universidade Federal Fluminense and Libra JPT project for their financial support, structure and data availability. A special praise for Petrobras post-graduate program, who gave me an opportunity to continuously study and exercise science apart from my professional duties. An immense thank you to my PhD supervisor, Wagner Lupinacci, for the knowledge, support and guidance throughout the project. You've been a fantastic primary supervisor and I hope you lead many other geoscience professionals throughout your career. Thank you, also, to all the academics who helped me in any way. A special shout-out to my colleagues Leonardo Teixeira, Marcos Sebastião dos Santos, Alexandre Maul, Rodolfo Victor, André Luis Fernandes, Leonardo Rodrigues, Alvaro Martini, João Paulo Nunes, Monica Muzzette and many others for the countless technical discussions and for sharing this journey with me. The acknowledgments that I make here will be eternally insufficient considering the amount of help I received.

I am grateful to my family for the support, especially my mother and late father. You always raise me and my siblings to pursuit science above all things, and there it is: we are all post-graduates now. To my loved wife, Camilla Almeida, who support me in so many ways that I cannot write here without extrapolating this "acknowledgements section" one-page limit, unfortunately. I dedicate this thesis, above all things, to my kids Gabriela and Gustavo, whose time I had to share with this research so many times. May you two walk the path of science and may reason be always the north in your life. Long live free and accessible education for all!

Abstract

Rock typing into flow units (FU) is a well-known technique for characterizing flow heterogeneities in reservoirs and producing reliable estimations of petrophysical properties, as porosity and permeability. This thesis aims to discretize flow units in a Brazilian pre-salt reservoir through conventional core laboratory measurements and transpose this classification to the well log domain and 3D model of the reservoir, considering elastic and acoustic inverted seismic data as constraints. First, I performed core and well log data feasibility study of FU discretization, considering three different FU methods and the seismic vertical scale and resolution characteristics. This first study results provided means and grounds for the FU classification that I later chose to consider and the implications of the seismic limited vertical resolution in the classification. I noticed that porosity and permeability cumulative curves were a powerful tool for visualizing and analyzing the scale of the classification in a decametric sense, suitable for the seismic classification that the aim to achieve. The second study is a 3D FU Bayesian facies classification and petrophysical modeling considering the discretization made in the 1D domain. This is the first Brazilian pre-salt porosity and permeability 3D models constrained by both flow unit classification and elastic and acoustic inverted seismic data. The results from the second study showed that, using the FU as constraints, decametric porosity and permeability volumes are more robust in 3D approaches than considering the usual seismic lithologic classification. In the third study, I pushed the petrophysical modelling below the seismic vertical resolution, discretizing and calculating metric FU through geostatistical seismic inversion. Using the cumulative curve concept, I generated metric flow units within each decametric flow units and constrained the geostatistical inversion in this manner to generate several high-resolution porosity and permeability volumes with respect to the seismic data in the decametric scale. The results from the third generate high quality decametric and metric porosity and permeability volumes, respecting the available seismic data even below the resolution limit. Finally, I hope that the produced 3D volumes of flow units facies, permeability and porosity in decametric or metric scales can be incorporated as variables for the lateral interpolation of petrophysical reservoir parameters during the static and dynamic modelling, as well as support seismic 4D interpretations and seismic-assisted history matching.

Keywords: Flow units; seismic quantitative interpretation; presalt reservoir; 3D reservoir modelling; petrophysical modelling.

Resumo

A discretização de rochas em unidades de fluxo (FU) é uma técnica bem conhecida para caracterizar a heterogeneidade de fluxo em reservatórios e produzir estimativas confiáveis de propriedades petrofísicas, tais como porosidade e permeabilidade. Essa tese visa estabelecer uma metodologia de cálculo de unidades de fluxo em reservatórios do pré-sal da bacia de Santos por meio de medições convencionais de laboratório em testemunhos e, em seguida, transpor essa classificação para os perfis de poço e, depois, para os modelos tridimensionais do reservatório, considerando dados sísmicos elásticos e acústicos invertidos como variáveis de controle. Em um primeiro momento, realizei o estudo de viabilidade dos dados de testemunho e dos perfis de poços, considerando três métodos diferentes de discretização e as características de escala e resolução vertical da sísmica. Este primeiro estudo forneceu meios e fundamentos para a minha classificação de FU, bem como estabelecer as características e implicações da limitação da resolução vertical da sísmica na classificação. Eu notei que as curvas acumuladas de porosidade e permeabilidade são ferramentas poderosas de visualização do efeito da escala de observação na classificação, efeito este bastante adequado para uma classificação através de dados sísmicos. O segundo estudo consiste em uma classificação de fácies de fluxo Bayesiana tridimensional com modelagem petrofísica de porosidade e permeabilidade, considerando a discretização 1D feita no estudo anterior. Este é o primeiro modelo tridimensional de porosidade e permeabilidade feito no pré-sal da bacia de Santos controlado tanto pelas fácies de fluxo quanto pelos atributos elásticos e acústicos oriundos da sísmica via inversão. Os resultados do segundo estudo mostraram que, ao utilizarmos as fácies de fluxo como controle, podemos calcular porosidades e permeabilidades derivadas da sísmica com muito mais acurácia na escala decamétrica, em comparação à utilização usual de fácies litológicas. No terceiro estudo, eu promovi a classificação para além das limitações de resolução vertical da sísmica, discretizando e calculando FU na escala métrica através do uso de inversão e modelagem geoestatística. Com o conceito de curvas acumuladas da petrofísica, foram geradas fácies de fluxo métricas dentro das fácies de fluxo decamétricas, e, parametrizando a inversão geoestatística com essa hierarquia, calculei diversos modelos métricos de porosidade e permeabilidade que respeitam o dado sísmico na escala decamétrica. Os resultados do terceiro estudo mostraram que é possível gerar volumes de porosidade e permeabilidade de alta qualidade, tanto na escala métrica quanto na escala decamétrica, respeitando o dado sísmico disponível mesmo abaixo do seu limite de resolução vertical. Por fim, eu espero que os volumes

de fácies de fluxo, porosidade e permeabilidade produzidos por essa metodologia possam ser incorporados como variáveis diretas na modelagem estática e dinâmica dos reservatórios, bem como auxiliar interpretações de sísmica 4D e estudos de ajuste de histórico assistido por sísmica utilizando técnicas de filtro Kalman, por exemplo.

Palavras-chave: Unidades de fluxo; interpretação sísmica quantitativa; reservatório do présal; modelagem tridimensional de reservatório; modelagem petrofísica.

Table of Contents

List of Figures

List of Tables

Preface

In my Petrobras career, mainly as quantitative interpretation reservoir geophysicist, it always bothered me how poor was the quality of calculated porosity and permeability models through seismic data and lithologic facies as constraints. It all worked fine in the well log domain, but not so much when translating the equations and relationships for the 3D world using acoustic and elastic impedance volumes. In some cases, we had a state-of-the-art seismic, a good understanding of the local geology, a complete suite of well logs, several laboratory measurements, expensive software and algorithms, integrated workflows and, even so, the obtained results were just unsatisfactory.

The first concept of flow units I had was working together with reservoir and exploration petrophysicists along with other scientists, mainly to obtain more realistic porosities and permeabilities from magnetic resonance well logs. At the time, I tried to constrain some of the facies calculations using impedance and sonic logs, but it did not occur to me that we could later integrate the seismic data in the process and generate, maybe, some 3D flow units volumes and better petrophysical properties using these as constraints. At the time, flow units were just a 1D well log calculation translated to the 3D reservoir model using geostatistical tools in order to populate the grid.

In 2019, I joined the Universidade Federal Fluminense (UFF) as a Master's degree candidate in the *stricto sensu* post-graduation program Dinâmica dos Oceanos e da Terra, having PhD. Wagner Moreira Lupinacci as advisor. The idea, at the time, was to perform a 1D flow units feasibility study using acoustic and elastic impedance as main properties, providing means and grounds for a later study of 3D calculation. This first work (Penna and Lupinacci, 2020) was published in the SPE Reservoir and Engineering Journal.

As the Master's project continues, we realized that there was a huge potential for 3D calculation of porosity and permeability using flow units as constraints, if we could handle the vertical resolution difference of well and seismic data. We decided, then, to "upgrade" the Master's degree to a PhD. degree, extending the scope of the project to a 3D flow units calculation and petrophysical modelling in the seismic resolution (decametric) and, also, below the seismic resolution (metric). This work progression, in both decametric and metric scales, led other two publications: Penna and Lupinacci (2021) published in the Marine and Petroleum Geology Journal and Penna and Lupinacci (2022), published in XXXX.

All of the work presented henceforth was conducted along with the GIECAR group, in the Universidade Federal Fluminense. The project is sponsored by Petrobras and Libra JPT group, who provided data access for the project. I hope that the academic contributions that we achieve can add a little more insight to the reservoir quantitative seismic interpretation subject, especially considering the challenges of using seismic data in Brazilian pre-salt reservoirs.

1. Introduction

In geology and reservoir characterization, the subject “reservoir modelling” is often refereed as the practice of representing the subsurface complexity through porosity and permeability parameters, aiming to produce realistic dynamic and static models for oil production (Doyen, 2007). This process become especially harder when the reservoir being modelled comprises a series of heterogeneous rocks with several diagenetic phases, complex structural framework and, for the most cases, hard-to-acquire data for uncertainties minimization, such as the Brazilian pre-salt carbonate.

In a 1976 publication the statistician George Box said the well-known phrase “all models are wrong”, that later he corrected for “all models are wrong, but some are useful” (Box, 1976). This sentence is more and more the reality for any geoscientist working with limited resources and high uncertainties in complex environments. We are all aware of our models limitations, but we try the best to represent the local geology heterogeneity with just a few useful parameters. Surprisingly, at the end, models sometimes can indeed represent, with a satisfactory level of accuracy, the subsurface geology and fluid flow, supporting the decision-making process of the reservoir characterization process.

In that sense, pursuing methods and workflows that can calculate better inputs and parameters for the model building workflow is the daily goal for any geoscientists working inside a reservoir asset team. Several publications show that, in the presence of complex geological settings with differential diagenesis, the estimation of porosity (ϕ) and permeability (k) performed on a flow unit (FU) basis should be more accurate than the estimation made on lithological or sedimentary facies, as discussed by Aggoun et al. (2006), Daraei et al. (2017), Hatampour et al. (2018) and Ghanbarian et al. (2019).

Flow units classification is a well-known technique for petrophysicists since the 1980 decade, but the available bibliography is very limited to core and well-log data, like Amaefule and Altunbay (1993); Altunbay et al. (1994); Abbaszadeh et al., (1996); Chen et al., (2017); Gunter et al. (1997); Kolodzie (1980) and Oliveira et al. (2016). It is very uncommon to see publications that effectively extrapolate flow units and its porosity and permeability estimations away from the well location, generating tridimensional models for reservoir classification. Even latest methods, like the mercury injection based Winland R35 (Pittman, 1992), FZI-star

(Mirzaei-Paiaman et al., 2018) and electrical formation factor (Ghanbarian et al., 2019) are very restrict to well core data and control (Rebelo et al., 2022).

There are, in fact, a few available publications who aims toward a tridimensional flow units modelling, producing discrete FU facies volumes and petrophysical parameters derived from them (Martin et al., 1997; Udegbunam and Amaefule, 1998; Porras and Campos, 2001; Svrsky et al., 2004; Aggoun et al., 2006; Li et al., 2018 and Zhang et al., 2018). However, most of these works consider the lateral extrapolation of flow units, porosity and permeability away from the well domain merely a geostatistical matter, there is, a kriging extrapolation (or any other extrapolation technique) without the constraint from a spatially acquired data, which, in our case, is seismic data. Although this is a rather commonly used technique in the industry, it can result unrealistic static and dynamic models, especially in complex geological settings where porosity and permeability can change rapidly due to diagenetic and sedimentary factors.

For quantitative interpretation geophysics working with flow units to generate porosity and permeability estimations there is a limited number of publications available in the literature addressing this matter. Reference books like Avseth et al. (2005), Simm and Bacon (2014), Dvorkin et al. (2016) and Vernik (2016) do not comment about this method or mention any procedures or technique to incorporate flow units into the usual quantitative interpretation workflow through acoustic and elastic parameters. In fact, in literature, flow units methods are restricted to classical petrophysics works, especially core-related data and analysis in a variety of geological settings and samples.

One of the first publications correlating flow units and geophysics (more specifically P-wave velocity) is, perhaps, Prasad (2003). Although in this work the author's objective was not to obtain better reservoir properties but to study P-wave attenuation through Biot theory using flow units as a template; the study shown that a positive correlation between velocity and permeability can be established using grouped flow units as constraints. Using FZI values for pore space properties the modeled data agrees well with measure data, there is, flow properties can be predicted. This intrinsic FZI characteristic representing pore space properties (more specifically pore throat space) is also mentioned by Hasan and Hossain (2011).

Recently, a limited number of works aiming to characterize better reservoir properties through flow units were published, such as Rastergania and Kadkhodaie (2013), Emami-Niri and Lumley (2014), Rastergania et al. (2016), Iravani et al. (2018) and Xin et al. (2022). However, most of these publications consider a small amount of flow units (two, for most cases)

in a rather simple geological setting, like sand and shale horizontal layering. Concerns like the total number and the upscaling of FU, seismic vertical resolution limitation, uncertainties in seismic facies classification and other intrinsic quantitative seismic interpretation problems are not needed in these cases. For our purpose, in a more complex geological environment, we must take all these details under account to estimate adequate porosity and permeability according to seismic characteristics.

It is important to mention that Santos Basin pre-salt carbonates are, to date, the most prolific hydrocarbon producer in Brazil, with great sediment column thickness and wide lateral extension. Specifically, Mero reservoir, the studied area in this thesis, accounts for more than 10,000 million of bbl. in place, the third largest reservoir in Petrobras (ANP, 2021). Its complexity in term of sedimentation process, igneous rock presence, structural framework, diagenesis, operational challenges and production costs, however, implies the need of a risk mitigation from geologists, engineers and geophysics working in the project. Due to the reservoir scale, a small error in the porosity or permeability estimation can lead to large miscalculations in the end of the process, there is, production and injection frameworks, production platform scaling, well drilling estimation costs and reservoir management. Given that, the motivation of this thesis is to provide means and workflows to produce better petrophysical properties of the reservoir according to the local geology characteristics and the available seismic data. First, using core data, I performed a flow unit classification that later was translated to the well log and later to the 3D seismic using a sequence stratigraphy reasoning for upscaling. I classified decametric flow units facies using the p-impedance and s-impedance attributes through a Bayesian inference, calculating porosity and permeability volumes. Then, I pushed the classification below the seismic resolution limit, using a Bayesian geostatistical seismic inversion producing a larger number of metric FU.

To achieve these objectives, I subdivided the thesis into three main steps: (1) a core data feasibility study; (2) 3D classification of four decametric flow units facies through Bayesian inference and (3) 3D classification of eight metric flow units through geostatistic inversion. All of these steps correspond to specific publications in scientific journals.

The first stage, a feasibility study of several flow units classification methods adequate to the data available, was published in SPE Reservoir Evaluation and Engineering journal (Penna and Lupinacci, 2020). Using core data from both Barra Velha and Itapema formations, we considered Lorenz plots (Gunter et al., 1997); FZI classification (Amaefule and Altunbay,

1993), which we decided to use further, and electrical quality index method (Soleymanzadeh et al., 2018). In this publication, we noticed how cumulative porosity and permeability curves can be a powerful graphical tool for upscaling flow units into the seismic vertical resolution (decametric). Then, we defined the FZI classification template and studied the discretization of FU using filtered well log data, simulating how accurate was the estimated porosity and permeability and how them would behave when applied to real seismic data.

The outputs from this work were the FZI template chosen for decametric flow units discretization and the upscaling method using a sequence stratigraphy reasoning through cumulative porosity and permeability curves. We later used all the classification stablished in this 1D study for the Bayesian 3D facies classification and geostatistical inversion.

The second study and article from this thesis was published at the Marine and Petroleum Geology journal and comprises the application of the FZI template stablished in the 1D feasibility study through a FU facies Bayesian 3D volumetric classification (Penna and Lupinacci, 2021). Using p- and s-impedance volumes, as well as k-ø relationship per FU facies, we calculated posterior occurrence probability volumes that we later used as constraints for the estimated porosity and permeability. We compared the FU petrophysical attributes with lithologic facies petrophysical attributes and noticed that we had much better accuracy when we considered flow units as template for the calculation.

From this work, we proved that, with an adequate upscaling of FU according to the seismic vertical resolution characteristics, we can calculate facies, porosity and permeability volumes from p- and s-impedance data that are much more accurate than using conventional lithologic facies. We expect that these output volumes can be instantaneously incorporated into 4D seismic interpretation studies workflows, as well as seismic assisted history matching and production/injection framework optimization.

In the third study, we pushed the classification below the seismic resolution limits, calculating eight metric flow units (MFU) within each of the four decametric flow units (DFU) used in the second study. First, we stablished the relationship in core data, and later in well log data. Then, using geostatistical inversion for p- and s-impedance attributes, we simulated metric flow units constrained by the seismic data in the decametric scale. Given each of the eight metric flow units and its petrophysical distribution as pdfs (probability density functions), we co-simulated porosity and permeability generating a significant number of feasible models for Mero reservoir (Penna and Lupinacci, in preparation).

The last study results showed that it is possible to simulate flow units below the seismic resolution limit, but also respecting the seismic data in the decametric scale. This is equivalent to say that if we convolve a specific wavelet with any of the simulated impedance or porosity models (given a rock physics model) in the metric scale, the resultant synthetical seismic would be almost identical to the real seismic in the decametric scale. From these results we can estimate pessimistic, optimistic or base case scenario for the porosity in the reservoir, as well as any other probabilistic analysis in the results.

It is important to mention that this is the first attempt to incorporate pre salt flow units into the seismic quantitative interpretation workflow, producing more accurate porosity and permeability volumes constrained by this FU classification. In this subject, we consider the scale recognition of the FU characteristics an important matter, and we acknowledge the upscaling based on a sequence stratigraphy reasoning as a crucial step. Finally, this thesis is structured in the presentation of each of the published papers previously mentioned. At the end I wrote final considerations for all the studies and future expectations in flow units topic.

2. Decameter-Scale Flow-Unit Classification in Brazilian Presalt Carbonates

Article published in

SPE Reservoir Evaluation & Engineering, Vol. 23, 2020.

Impact Factor: 2.67

Authors: Rodrigo Penna and Wagner Moreira Lupinacci

2.1 Abstract

Rock typing into flow units (FUs) plays a pivotal role in constructing static and dynamic models of petroleum reservoirs. Decisions made by asset teams mostly depend on predictions of how fluids will percolate through the subsurface during the reservoir life cycle. In carbonate settings, dealing with rock typing is complex and can generates a large quantity of units, due to diagenetic processes like dissolution, cementation and silicification. Most rock typing methods in carbonates successfully classify small-scale flow heterogeneity in well resolution but fails when interpolating those facies further away from the 1D domain, because of the lack of correlation between flow units and spatial data. Seismic data can be used to detect large-scale FUs and assist the interpolation of small-scale FUs in 3D reservoir volume, thus producing more realistic static and dynamic models.

We propose a modification of the classical rock typing methods based upon permeability (k) versus porosity ($\emptyset$) plots and electrical properties, using a dataset from the Mero Field, part of the Libra giant field of pre-salt carbonate reservoirs in offshore Brazil. From the permeability cumulative S-curve analysis, we established major large-scale flow units that maintain part of the carbonate flow heterogeneity and correlate them with the elastic attributes: p-impedance (PI) and s-impedance (SI). In addition, we established a priori PI and SI correlations with the formation factor (F) parameter to categorize large-scale flow units using the F versus k methodology.

With the large-scale FUs mapped in seismic datasets, core plug-scale FUs can be populated into the 3D static and dynamic models using geostatistics tools, thus creating more realistic reservoir models and assisting asset teams in the decision-making process.

2.2 Introduction

Hydrocarbon reservoirs are heterogeneous and not uniform, which can be divided into multiple homogeneous groups, called Flow Units (FUs). Each unit presents similarities in terms of grain size, texture, cementation, pore distribution, porosity and other physical characteristics controlled by the sediment depositional environment and diagenesis (Altunbay et al., 1994). FUs for reservoir characterization are an effective way to simulate fluid movement and oil production behavior. According to Ebanks (1987), "a flow unit (FU) is a representative elementary volume of the total reservoir rock, within which geological and petrophysical properties that affect fluid flow rate are internally consistent and predictably different from properties of other rock volumes."

Rock typing for FU in reservoirs has been a source of debate for geoscientists. Rebelle and Lalanne (2014), for instance, point out issues of rock typing driving techniques (geological, petrophysical and production driving), especially when considering data with different scales available in a reservoir. Considering rock typing essentially a petrophysical attributes clustering technique, finding correlations between this type of classification, with sedimentary-driven geological models at different scales, is always challenging.

All rock typing methods available have advantages and limitations, especially considering the complexity degree of the geological setting and the quantity of data available. However, all share the same limitation: the lack of integration with different resolutions and data scales. In many examples, rock typing is able to quantify core plug-scale flow characteristics in the core domain but fails when upscaling these properties to well logs, not to mention for the entire field.

Considering that rock typing into flow units is purely a petrophysical matter, as pointed by several authors, geological parameters (i.e. depositional environments, sedimentological texture and diagenesis), in any scale of observation, are not considered during the process. Because of the data absence in early stages of reservoir development and high geological heterogeneities, propagation of petrophysical properties, like flow units, away from the wells and into the 3D geological model, can be very problematic and sometimes results in non-realistic flow models. Due to the lack of correlation of spatial acquired data (e.g. seismic) and the petrophysical properties, spatial geostatistics and stochastic models without constraints are often used in the pre-salt carbonate geological model construction. In other geological context,

authors have proposed multidisciplinary methodologies for adding geological significance into the rock typing workflow, as described in Rebelle and Lalanne (2014), Daraei et al. (2017) and Riazi (2018). However, in complex geological settings where a large number of flow units are present, the interpolation largely depends on statistical parametrization, as large-scale flow units are not mapped and acquired spatial data, like 3D seismic volumes, is not considered in the process.

Recent works attempts to correlate petrophysical flow units with multiple seismic attributes. Iravani et al. (2018) used a single FU regression from well-log data and then applied to the whole reservoir, having an acoustic impedance seismic volume as constraints. Rastergania et al. (2016) and Hatampour et al. (2018) used intelligent systems, like probabilistic neural networks and radial basis function networks, to obtain linear relationships between the discrete FU and seismic attributes. However, those methods are an extrapolation of the well FU classification in the seismic, regardless of the scale difference between data types. In complex geology settings, where a great number of FU are calculated, the lack of seismic vertical resolution is a problem to address.

The present study is an approach to characterize large-scale reservoir flow units that can correlate with seismic attributes, like p-impedance (PI) and s-impedance (SI). To achieve this goal, we propose a modification of the classical flow zone indication (FZI) permeability versus porosity rock typing, analyzing a cumulative S-curve like the Lorenz method. In addition, using the electrical formation factor method, we calculated flow units (FU) based on well logs of PI and SI using the formation factor to discretize the rock typing into FU. Using data from the Mero Field, we calculate four major flow units that respond to large-scale flow characteristics in the reservoir and are still able to measure some level of flow complexity and correlate with elastic attributes. Once those FU are detectable in seismic volumes, we expect to achieve lateral predictability, thus providing conditions for the interpolation of core plug-scale FU into 3D static and dynamic models.

2.3 Rock Typing Methods

Rock typing methods for flow units are available in literature, being widely used in reservoir characterization in many reservoir settings. For our purpose, we grouped the most common FU rock typing methods into two different categories, named as Porosity-Permeability Method, and Electrical Method.

2.3.1 Porosity Permeability Methods

Flow Zone Indication

Since Amaefule and Altunbay (1993) introduced the flow zone indication (FZI) concept based on the Carman-Kozeny model, FZI is widely used to classify rocks with similar flow behavior. Studies have shown that the FZI classification correlates with many petrophysical properties, such as surface area, pore size distribution, mean pore throat size and nuclear magnetic resonance (NMR) relaxation data (Ohen and Ajufo 1995; Basbug and Karpyn 2007; D'Windt et al. 2018). FZI is considered a robust method of permeability estimation and reservoir prediction in terms of flow heterogeneities, due to petrophysical correlations between permeability and flow units (see e.g.: Again et al. 2006; Pritchard et al. 2010; Emami Niri and Lumley 2016 and Iravani et al. 2018).

In the FZI analysis, the first step is to calculate the reservoir quality index (RQI) defined as:

$$\mathrm{RQI} = 0.0314 \,.\, \sqrt{\frac{\mathrm{k}}{\phi_{\mathrm{E}}}}, \tag{1}$$

where ϕ_{E} is the effective porosity and k is the permeability. Then, the FZI is calculated as:

$$\mathrm{FZI} = \frac{\mathrm{RQI}}{\phi_{\mathrm{Z}}}, \tag{2}$$

with ϕ_{Z} defined as:

$$\phi_{\mathrm{Z}} = \frac{\phi_{\mathrm{E}}}{1 - \phi_{\mathrm{E}}}. \tag{3}$$

Considering a constant value of FZI, a log-log plot of RQI versus ϕ_{Z} produce a straight line. Samples with similar flow characteristics and FZI values cluster around a corresponding unit-slope, determining a flow unit. Samples with different FZI values are plotted on different parallel lines. A graph analysis discretizes the sample space into n flow units, but works like introduced a way to automate and minimize display errors from a variable named as Hydraulic Units (HU):

$$\mathrm{HU} = \mathrm{Round}\,[\,2\,.\ln(\mathrm{FZI}) + 10.6]. \quad (4)$$

Some authors use RQI to cluster similar flow units applying log to both sides of Eq. 1 (Xu and Torres-Verdín, 2012). However, Nabawy and Al-Azazi (2015) stated that simultaneous usage for both RQI and FZI for reservoir rock typing is not recommended, due to some differences in the ranks raised during processing. Instead, they recommend applying the reservoir potential index (RPI), which is an average of reservoir quality obtained from both parameters.

Lorenz Plots

Gunter et al. (1997) applied the so-called stratigraphic modified Lorenz plot (SMLP) to evaluate the number of flow units based on a cumulative storage capacity versus cumulative flow capacity S-curve, ordered in the stratigraphic sequence. The equation to calculate a single value of cumulative flow capacity (k_H) is:

$$\mathrm{k_H} = \mathrm{k_1(H_1 - H_2) + k_2(H_2 - H_3) + \cdots k_i(H_i - H_{i+1})}, \quad (5)$$

where the term $\mathrm{H_i - H_{i+1}}$ is the depth difference between subsequent samples i and $\mathrm{i + 1}$. A similar equation calculates the cumulative storage ($\emptyset_{\mathrm{H}}$) capacity:

$$\emptyset_{\mathrm{H}} = \emptyset_1(\mathrm{H_1 - H_2}) + \emptyset_2(\mathrm{H_2 - H_3}) + \cdots \emptyset_{\mathrm{i}}(\mathrm{H_i - H_{i+1}}). \quad (6)$$

The slope variation analysis in the segments of the k_H versus $\emptyset_H$ plot is interpreted as the main flow units in the dataset. Steeper parts of the curve are called “speed zones” and relates with better quality facies in terms of flow capacity. On the other hand, flat segments are interpreted as seals or baffle zones. Some authors have used an integrated approach with other methods, like FZI and mercury injections to determine the minimum amount of flow units, as shown in Alhashmi (2016), Daraei et al. (2017) and Riazi (2018).

2.3.2 Electrical Methods

Electrical Quality Index

Electrical properties of reservoir rocks are important for calculating water saturation. In laboratory, these properties are determined by testing rock samples under simulated temperature and overburden pressure conditions.

An analogy between hydraulical and electrical rock properties can be made based on the concept of transmissibility. Permeability or hydraulic conductivity is the ability of a porous medium to conduct a fluid. Permeability can be determined from Darcy's equation. Electrical conductivity of a saturated sample is the capacity of this rock to allow electrical transmission through its pore structure. Ohm's law calculates rock electrical conductivity. Both Darcy and Ohm equations are transport equations whose general form is:

$$Q = \text{Transport property of the medium x A x } \frac{d\emptyset}{dl}, \tag{7}$$

where Q is the transfer rate, A is the cross-sectional area and $\frac{d\emptyset}{dl}$ is the potential gradient that is the driving force. If the transport property in Eq. 7 is considered as permeability and electrical conductivity, $\frac{d\emptyset}{dl}$ is assumed as pressure gradient (in Darcy's law) or voltage drop (in Ohm's law); then Darcy's and Ohm's equations are obtained respectively. Therefore, it is evident that there is an analogy between permeability and electrical conductivity of a rock sample.

The resistivity of a rock is mainly function of matrix porosity, pore geometry and resistivity of the fluid filling the porous space. For a fully water saturated rock, Archie (1942) defined the following relationship:

$$R_0 = F \,.\, R_w, \tag{8}$$

where R_0 is the formation resistivity at 100% brine saturation, R_w is the brine resistivity and F is the formation resistivity factor (or formation factor). Then, the formation resistivity versus porosity in a log-log graph can display the following linear trend:

$$F = \frac{\alpha}{\emptyset^m}, \tag{9}$$

where α is defined as a tortuosity factor (considered as equal to 1 in this work) and m is called cementation factor, also porosity exponent.

The resistivity of a clean rock (R_t) is a function of water saturation (S_w), formation water resistivity (R_w) and rock structure, which is represented by the formation factor F:

$$R_t = F \,.\, R_w / S_w^n, \tag{10}$$

where n is the saturation exponent. The cementation factor, saturation exponent and tortuosity factor are electrical parameters and are used in the Archie equation for calculating water saturation from resistivity logs. The cementation factor and tortuosity factor are dependent on pore geometry, which it is controlled by various textural rock properties. Authors like Hassani-Giv and Rahimi (2008) and Ghanbarian et al. (2019) provide considerations about the influence of these parameters in reservoirs. In fact, some researchers show that the cementation factor and tortuosity are interdependent, that is, a rock sample with higher tortuosity generates a longer path for electric flow, which implies higher values of m (Rezaee et al. 2007).

Based on an analogy of the RQI defined in Eq. 1, Soleymanzadeh et al. (2018) defined the parameter EQI (electrical quality index) as:

$$\mathrm{EQI} = \sqrt{\frac{\sigma_0}{\emptyset}\frac{1}{\sigma_w}} = \sqrt{\frac{1}{F\,\emptyset}}, \tag{11}$$

where σ_0 is the electrical conductivity of water-saturated rock, σ_w is the electrical conductivity of saturant water, F is the formation factor and $\emptyset$ is the porosity. Soleymanzadeh et al. (2018) state that permeability and electrical conductivity are two equivalent transport properties. Therefore, clustering rock samples with similar EQI plays the same role as grouping similar RQI rocks in terms of fluid flow properties. In other words, rock samples with similar values of EQI are expected to have similar electrical behavior and the EQI value can be used to categorize F data into distinct groups. Each of these groups represent a linear trend on a log-log plot of F versus $\emptyset$.

Formation Factor Mehod

Ghanbarian et al. (2019) proposed a method for clustering flow units based on the permeability and the formation factor. They state that most rock typing methods calculated through permeability (k) versus porosity ($\emptyset$) templates ignore the effect of the formation factor. In the Archie method, for instance, the cementation exponent in Eq. 9 represents this effect indirectly. This is because both k and F are complex functions of the porosity, while the porosity is only a measure of the pore volume and does not provide information on the dynamically connected pores.

Instead of using the k versus $\emptyset$ template, Ghanbarian et al. (2019) used a rock typing classification based on k versus $-1/F$ plot, grouping samples with similar connected pores.

According to the authors, this would avoid non-connected pores induced errors into the classical permeability versus porosity templates.

2.4 Considerations about Seismic Scale, Sequence Stratigraphy and Flow Units

Geological stratigraphic cyclicity can be observed at different scales, as discussed by Strasser et al. (2007) and Catuneanu (2019). At each scale of observation (i.e., core and plug data, well log, and seismic data), the construction of stratigraphic framework for a reservoir is represented by sequences, and their component systems tracts and depositional systems.

Catuneanu (2019) defines that at core plug-scales, system tracts and component depositional systems consist of sedimentological cycles (for example, beds and bedsets), commonly observed at scales of 1 to 10 meters. At larges scales, systems tracts and depositional systems consist of lower rank stratigraphic cycles, which are called sequences (hundreds of meters thick). For instance, on shorter timescales, stratigraphic cyclicity is controlled by tidal cycles, storm-fairweather cycles, and seasonal changes. Tectonic events, compaction and long glacial cycles define long-term changes, which define the sequences.

This cyclicity reasoning also applies to FU definition, as one of the major factors controlling porosity obliteration and dissolution are related to stratigraphic events, in shorter or longer time scales of observations. Rock typing for flow units in centimetric data (like well logs) and metric data (like seismic) produces different results, although all represent the same geological construction process. Core plug-scale flow unit definition has great relevance in dissolution and dolomitization numerical studies. Therefore, large-scale flow unit correlate directly with flow simulators and 4D seismic studies, as oil, water and gas fronts will be detected according to seismic vertical resolution and the cell dimension of the flow simulator, usually dozen of meters.

Determining the core plug-scale flow performance, as well as large-scale, are equally important, and comprises different stages of the geological building process from a reservoir.

2.5 Study Area and Data Available

The Mero Field is a part of the giant Libra discovery, located in the northeastern portion of the Santos Basin, in the ultra-deep water of the Atlantic Ocean (Fig. 1). In 2013, the first bidding round executed by the Brazilian government under the new production-sharing contract

for pre-salt areas offered the Libra area. The winning consortium is comprised of Petrobras (operator), Shell, Total, CNOOC and CNPC, overseen by PPSA (Pré-Sal Petróleo SA).

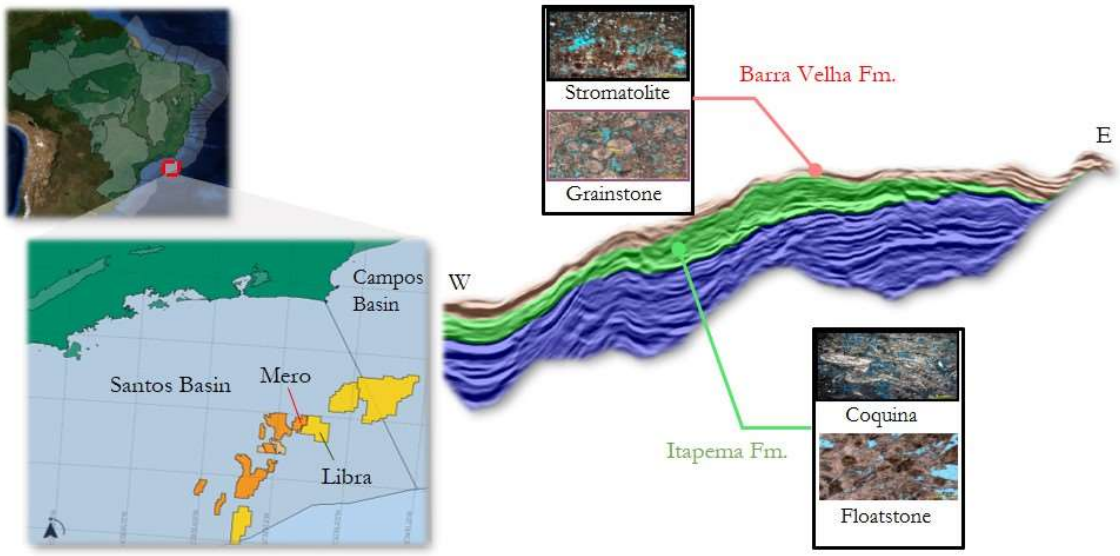

Fig. 1 — (left) Mero Field and Libra location in Santos Basin, southeast Brazil. (right) Typical W-E seismic section in Mero Field. The main plays, displayed as thin sections, are stromatolites from Barra Velha Formation and coquines from Itapema Formation.

Libra initial estimates indicate an oil in place volume of between 8 and 12 billion BOE in carbonate reservoirs (Carlotto et al. 2017), with high geological complexity in terms of stratigraphic facies (Penna et al. 2019). The discovery well found reservoirs with high porosity and permeability in the Itapema and Barra Velha formations (Barremian and Aptian ages, respectively), with about 600m net-pay column. Since then, 17 wells were drilled in the area. The main plays are coquinas from the Itapema Formation and stromatolites from the Barra Velha Formation, although high porosity is also found in grainstones, floatstones and others carbonate facies (Jesus et al. 2019). Fig. 2 shows the structural map of the salt base and the main pre-salt lithologies drilled in the area. Low porosity fine-grained carbonates, such as mudstone (classified, for simplification, as microporous sediments) are distinguishable, as well as extrusive and intrusive igneous rocks.

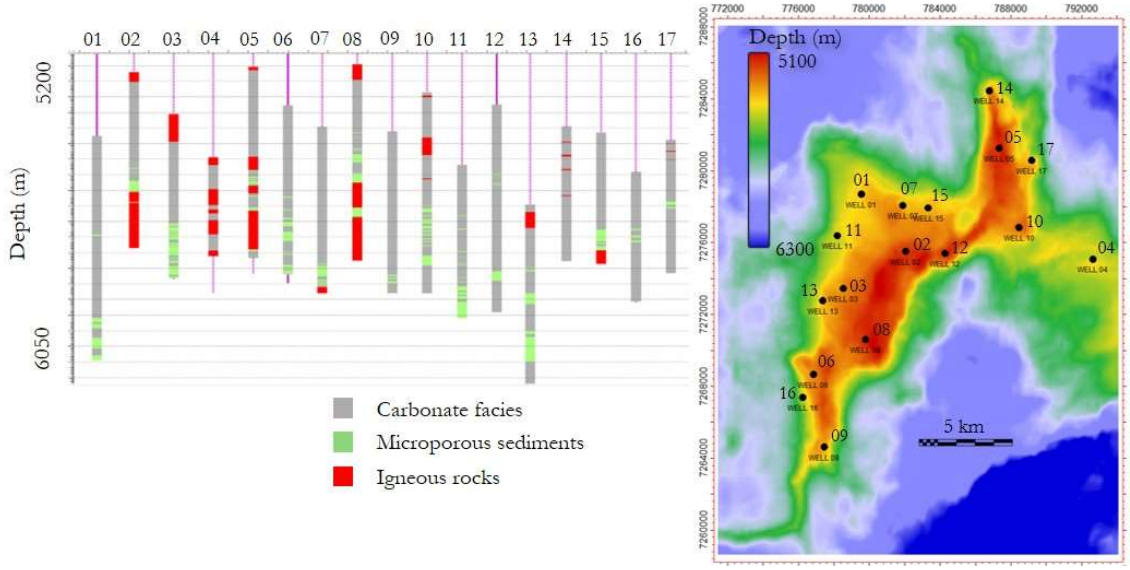

Fig. 2 —(left) Main subsalt facies in the Mero Field. (right) Structural map of the salt base and well positions.

One of the characteristics of fluid produced in the Mero Field is the high content of CO2 (44% in the gas phase). So, performing a conventional extended well test (EWT) would lead to a very limited oil rate, due to the gas-flaring limit imposed by the environmental agency. For this reason, Petrobras proposed to contract a Floating Production Storage and Offloading (FPSO) designed to reinject all gas produced during the EWT, which started in the end of 2016 and became the first offshore well test with gas reinjection in the world (Moczydlower et al. 2019). This FPSO is used in wells of the field performing EWT in different production-injection pairs. In order to accelerate production, the wells drilled by the consortium are keepers, and will be used as producers or WAG (water alternating gas injectors). A total of 11 drill stem tests (DSTs) have been performed in 8 wells and 9 production logging tests (PLTs) was realized in this field.

Almost 500m of cores were taken in different stratigraphic intervals. The dataset comprises about 1700 core and plug porosity measurements and horizontal permeability measurements from the 17 wells in the field, containing both the Barra Velha and Itapema formations. 15 electrical petrophysical analysis from one well are also available, mostly in grainstones and rudstones facies from both geological formations.

We used the Dykstra-Parsons coefficient (V_{dp}) to quantify the level of heterogeneity in the Barra Velha and Itapema reservoirs, which is defined as:

$$V_{dp} = \frac{(k_{50} - k_{84.1})}{k_{50}}, \tag{12}$$

where k_{50} and $k_{84.1}$ are, respectively, the permeability value at the 50th percentile (median) and 84.1 percentile in decreasing permeability ordered data (Fig. 3). The heterogeneity value of k, considering all the samples from the conventional core analysis, is 0.99. Typical k values ranges go from zero (homogeneous) to 1 (highly heterogeneous).

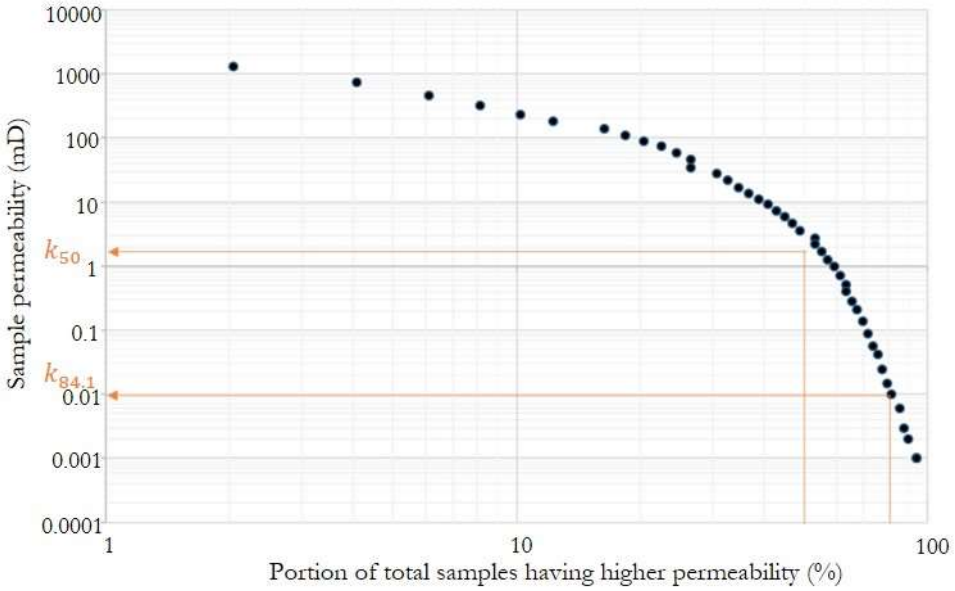

Fig. 3 — Dykstra-Parsons coefficient plot. The level of heterogeneity calculated is about 0.99. Typical ranges go from 0 (homogeneous) to 1 (highly heterogeneous).

2.6 Flow Units Classification

We used three methodologies for the flow unit classification. First, we analyzed the stratigraphic modified Lorenz plots using core permeability and porosity values to determine the minimum number of FUs. Then, considering speed zones as steep curves segments and seals/baffle zones as flat segments, we suggest a modification of the classical FZI method, analyzing the derivatives of cumulated percentiles of the permeability versus log(FZI) S-curve to discretize flow units.

Based on the results of the core electrical property analysis, we calculated logs of electrical formation factor (F) and cementation factor (m) using the well log data. Then, we discretize in flow units applying threshold values in the histogram of the formation factor results on a p-impedance versus s-impedance crossplot.

Fig. 4 summarizes the workflows for the three methods proposed in this work, considering that "core domain" is related to data analysis and interpretations made in the Mero Field core and plug dataset; "well domain" are the calculations using well-log data and "seismic frequency domain" are the analysis made with filtered versions of well-logs.

2.6.1 Stratigraphic Modified Lorenz Plots (SMLP)

We calculated the storage capacity and flow capacity for the Barra Velha and Itapema formations using the Eqs. 5 and 6 and re-ordering the data in crescent depth values. The SMLP is constructed plotting the normalized values of both variables, as shown in Fig. 5. Analyzing the slope variation of the curve, we can deduce a minimum number of four main flow units for the reservoir of the Mero Field, although it is possible to observe more FUs as a higher frequency variation. We are considering four flow units as a minimum amount of units to guarantee a correlation with the spatial data available – seismic data, which has lower vertical resolution. Considering the level of flow heterogeneity present, this will result in some calculation errors. However, we expect to obtain lateral predictability with flow units that can correlate vertically and spatially with seismic volumes.

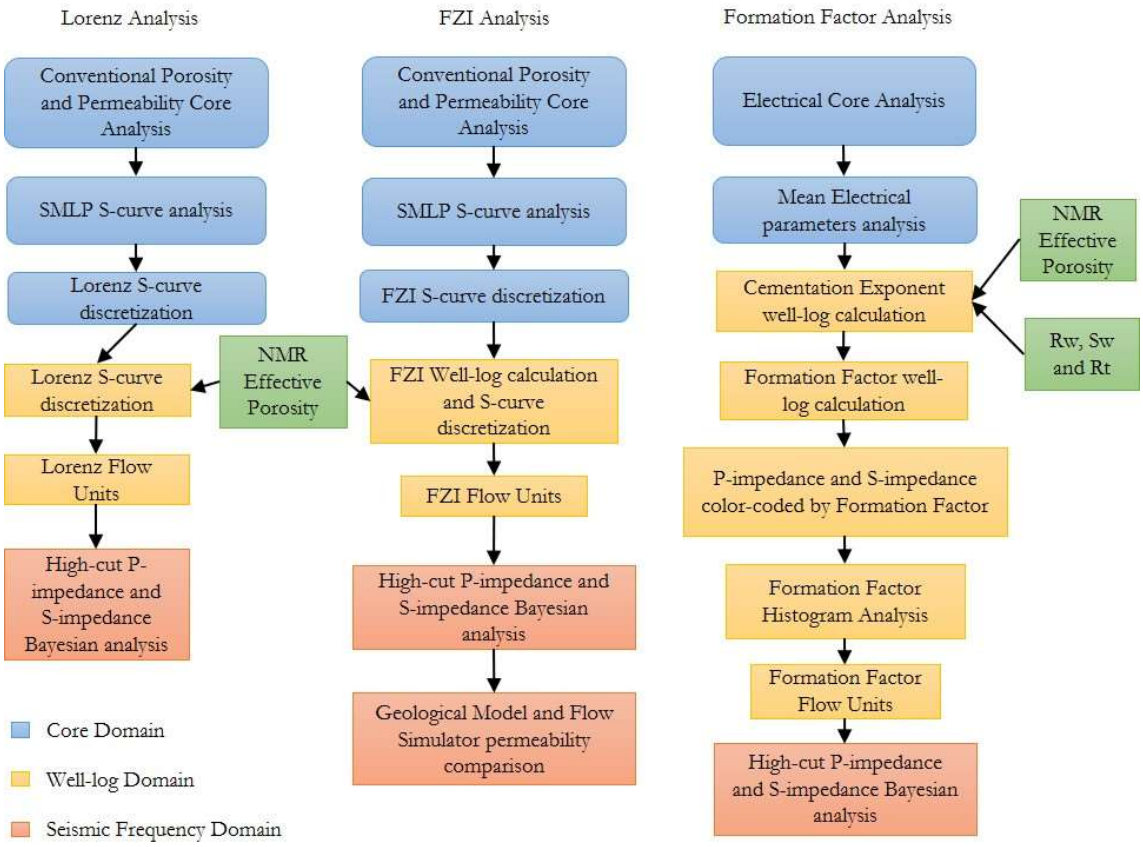

Fig. 4 — Workflow summarizing the methodologies proposed in this work.

An approach from the Lorenz method proposed in this study is to analyze a cumulative S-curve of permeability versus porosity, which removes vertical core and plug sampling bias present in Eqs. 5 and 6. Porosity values were sorted in increasing order and with the accumulated sum of the corresponding permeability was constructed the graph shown in Fig. 6. Then, we determined porosity cut-offs values to discretize the LPFU (Lorenz Plot flow units) analyzing the changes of the S-curve slope. This was also described in Lalanne and Massonnat's (2004), as they noticed that applying cut-offs to cumulated curves of net volumes generate discrete facies data, which produce less previsibility errors in the final reservoir model and reduced upscale bias. In summary, the following steps are used to construct the Lorenz's S-Curve:

1. Calculate percentiles of porosity and permeability core and plug dataset;
2. Porosity values are sorted in increasing order;
3. Accumulate and normalize the percentiles of permeability values;
4. Calculate the slope of the curve for each sample.

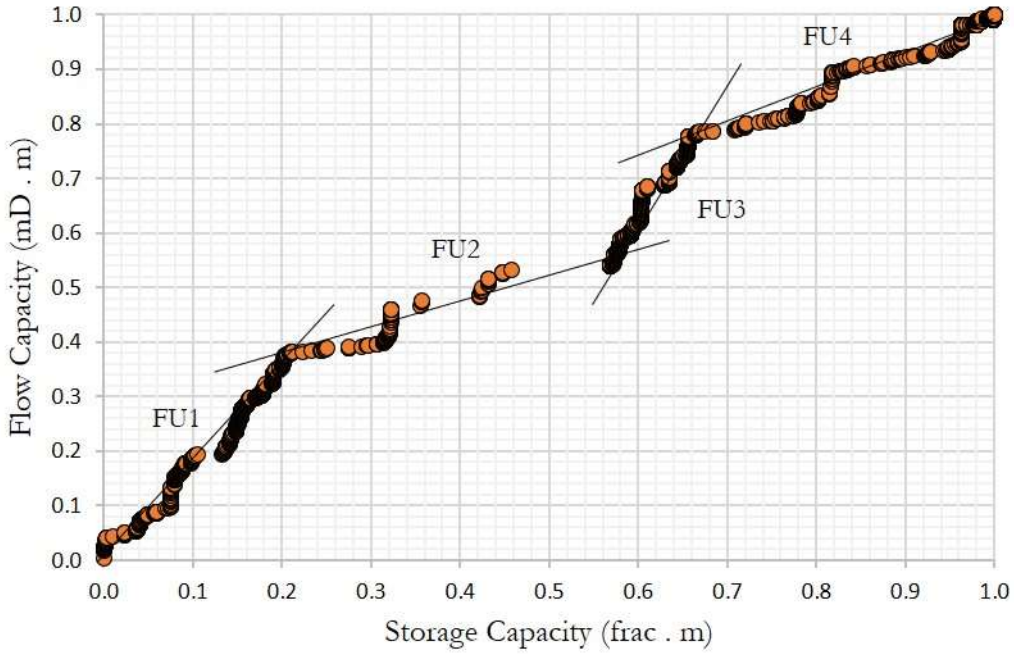

Fig. 5 — Stratigraphic Modified Lorenz plot discretizing a minimal of four large-scale flow units (FU) in the Barra Velha and Itapema formations. Steeper segments correspond to better zones in terms of flow capacity, while flat segments are related to barriers and baffle zones. Core plug-scale flow can be identified analyzing each steep/flat segment of the curve.

The interpretation of each LPFU is similar as described by Gunter et al. (1997). Flat segments can have storage capacity, depending on the porosity value, but little or no flow capacity. Steep segments are speed zones and add great value for the reservoir flow. LPFU1, where the curve does not show any detachment from the horizontal axis and none or little cumulative permeability, can be considered a flow barriers or no-flow zones in reservoir dynamic modelling, if laterally extensive.

LPFU2 is interpreted as the beginning of the curve detachment from the X-axis until the first ramp up of the line. This unit also has little storage capacity but shows a better flow capacity than the first. In aquifers, for instance, mapping LPFU2 can be crucial for understanding pressure maintenance in reservoir and the underlying aquifer studies.

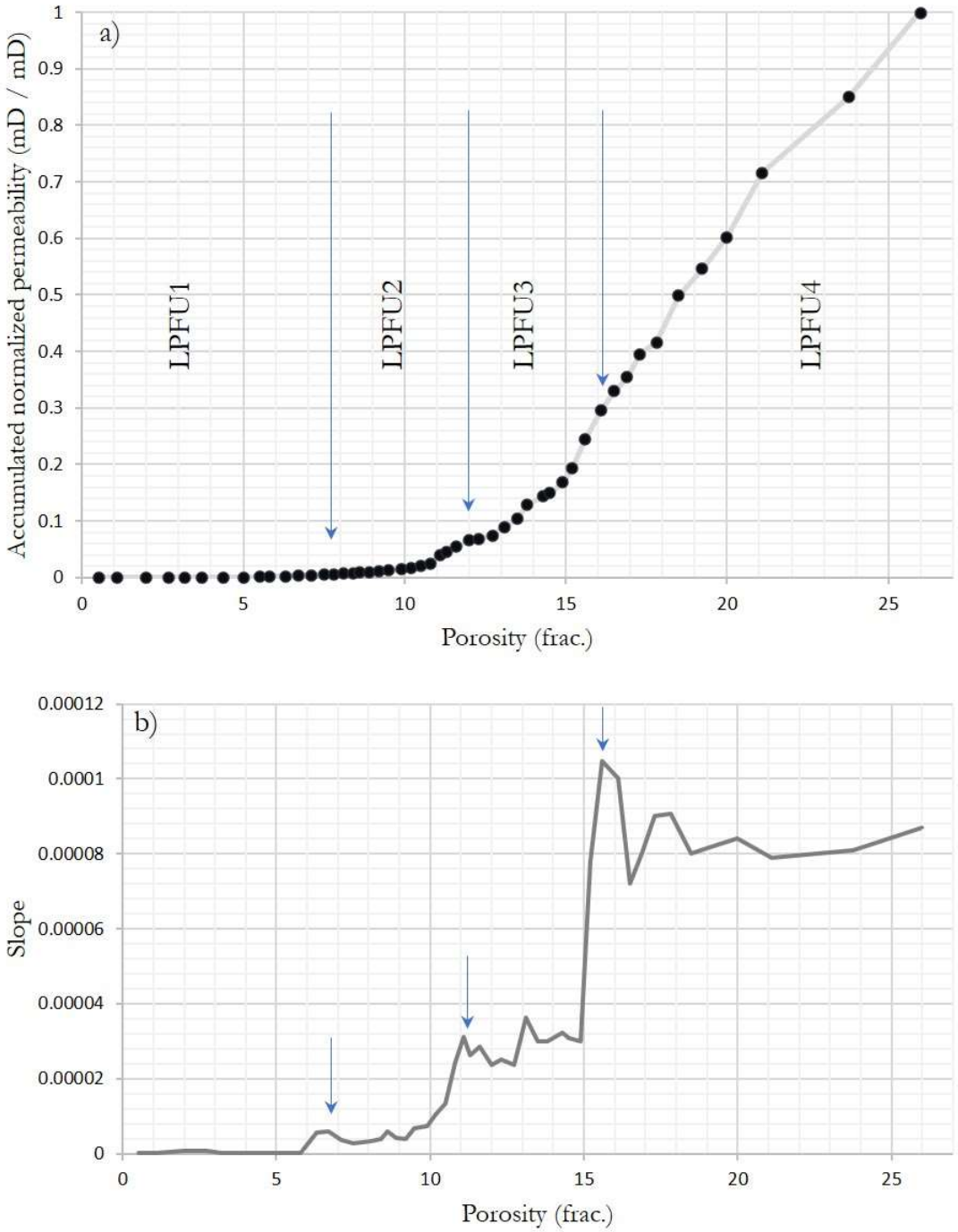

Fig. 6 — Cumulative permeability S-Curve plot for the Modifed Lorenz Plot flow units classification (LPFU). The porosity cut-offs to discretize the LPFUs were interpreted as the major changes in the slope.

LPFU3 and LPFU4 are interpreted as the subsequent major changes in the slope, having better porosity and permeability properties. LPFU3 denotes medium to good reservoir facies in terms of fluid performance, with porosities varying from 11 to 15% and decent flow capacity. LPFU4, presenting a steeper ramp (speed zone), is the best flow unit, and significantly contributes to the reservoir flow performance. Table 1 describes the cut-off ranges used considering the classification in both the Barra Velha and Itapema formations.

As seen in the SMLP (Fig. 5), the cumulative S-curve (Fig. 6) also suggests a larger number of flow units to the reservoir. However, we chose to interpret only major changes in flow performance, i.e., greatest slope variations in the Lorenz plots. This is similar in higher frequency sequence stratigraphic interpretations, when geologists separate between higher order (low frequency) changes in the base level caused by regional subsidence/upwelling and low order (high frequency) changes in the base level due to seasonal and diurnal variations. As seismic data lacks vertical resolution, higher order variations are detected in p-impedance and s-impedance volumes.

Fig. 7 shows the core and plug S-curve hydraulical unit discretization applied to two wells in the Mero Field using the well logs. As expected, areas with low porosity/permeability values are concentrated within LPFU1 and LPFU2 facies, while areas with better flow performance relate to LPFU3 and LPFU4.

Table 1 — FU and porosities cut-offs used in the S-curve of Fig. 6.

	Porosity cut-offs
LPFU1	below 6 %
LPFU2	6 to 11 %
LPFU3	11 to 15 %
LPFU4	above 15 %

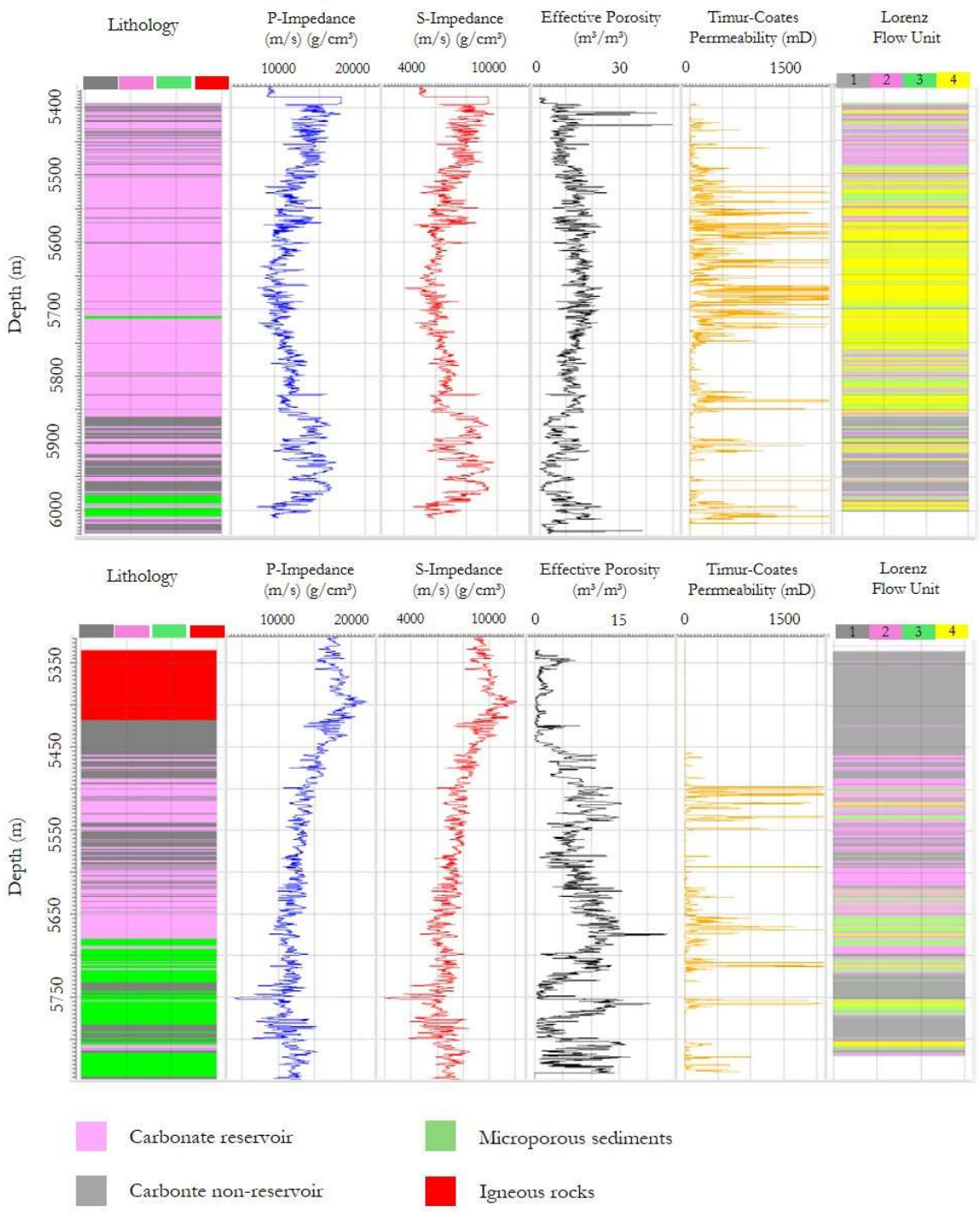

Fig. 7 — Lorenz S-curve classification of LPFU applied to wells 01 and 03.

2.6.2 FZI Classification

As detailed in section 2.3.1, FZI classification is a very popular method of reservoir rock typing for flow units. The reservoir quality index (RQI) defined in Eq. 1 is the net result of the porosity contribution to the permeability, which, in turn, are ruled by the pore size, shape and distribution. RQI and FZI are the key parameters for measuring the potential of petrophysical properties of a rock sequence, assessing the ability of the reservoir for storing and accumulating hydrocarbons (Li et al. 2017). However, diagenetic factors can obliterate the primary porosity or generate connected or isolated karsts and vugular structures. Herlinger et al.'s (2017) pre-salt studies, located in the Campos Basin, shows how the balance between dissolution and neomorphism, redeposition of sediments into deep lacustrine settings, replacement of minerals and dolomitization affect many levels of porosity in Brazilian carbonate rocks.

Considering the presence of such level of heterogeneity, the usual workflow of FZI/RQI rock typing (Eqs. 1 to 4) produces a large number of flow units, as shown in Fig. 8. Workflows based on neural networks (Dezfoolian, 2013 and Hatampour et al. 2014) also reproduce the heterogeneity and create many units. Dealing with this amount of FUs during the construction of the geologic and dynamic modelling is quite problematic, as FUs often have no correlation with the stratigraphic depositional facies 3D modelling trends usually made in most reservoir characterizations. In that sense, we prefer to discretize FZI rock typing in permeability cumulative S-curve, using percentiles of the k and ∅ dataset and analyzing the slope variation, like the workflow described in 2.6.1 section. This is like the Lorenz method, considering that the FZI value itself is an estimation of pore throat size.

Steps to construct the FZI S-curve:

1. Calculate porosity and permeability percentiles of the core and plug dataset;
2. Calculate RQI and FZI using Eqs. 1 to 3 and the percentiles values;
3. Order the data with increasing values of $log(FZI)$;
4. Accumulate and normalize the percentiles of permeability values;
5. Calculate the slope of the curve for each sample.

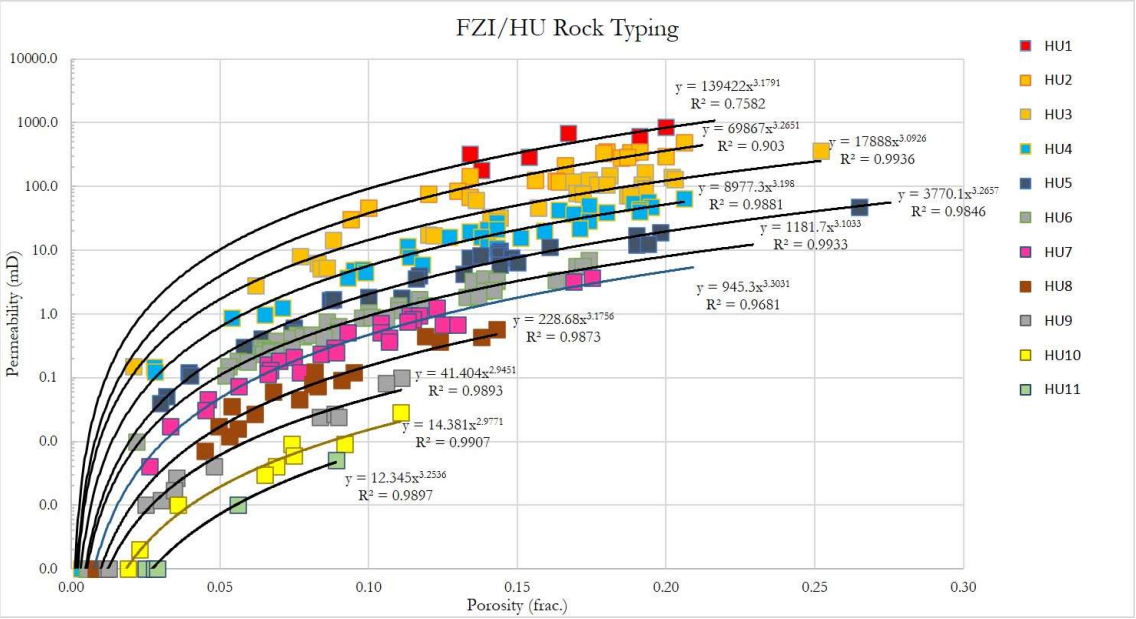

Fig. 8 — Usual FZI/HU workflow applied to Mero Field reservoirs, calculating 11 hydraulic units in the Barra Velha and Itapema formations.

Fig. 9 shows the S-curve percentiles plot of permeability versus $log(FZI)$. We discretize the FU analyzing the values of $log(FZI)$ corresponding to major changes in the slope, like the Lorenz plots described before. We identified four major flow units and named them as FZI1, FZI2, FZI3 and FZI4.

FZI1 corresponds to the initial flat segment of the curve, with poor flow performance and probably a barrier or baffle zone. FZI2 relates to the initial detachment of the curve, with reduced but considerable flow capacity in the seismic scale. FZI3 relates to the first ramp up after the FZI2 cut-off value and an increasing steep curve. This is a higher permeability reservoir rock. Finally, FZI4 corresponds to the better flow characteristics and relates to the final step of the S-curve.

Table 2 summarizes the $log(FZI)$ rock typing using the FZI method.

Table 2 — FU and log(FZI) cut-offs used in the S-curve of Fig. 9.

	Log(FZI) values
FZI1	below -0.5
FZI2	-0.5 to 0.67
FZI3	0.67 to 1.49
FZI4	above 1.49

Fig. 10 shows the cut-off application and FU classification in two well logs in the Mero Field. Note that igneous rocks and carbonates with recrystallized silica are classified as FZI1, with low porosity-permeability values. This is shown in the top of the Well 03 (where a massive intrusive igneous rock is present in the salt / carbonate interface) and in the middle of the well 03 and end of well 01, where primary porosity is obliterated by secondary processes. Low-energy carbonates with fine sediments, as laminite and siltites, are classified as FZI2, as seen in the final part of the well 03. Better porosity carbonates are divided between FZI3 and FZI4, depending on the porosity/permeability conditions.

Fig. 11 exemplifies how the classification segments the data in the semilog plot of permeability versus porosity. It is quite evident that there is a scatter around each FU, suggesting that a high frequency order of classification is possible. Analyzing each variation of the slope in Fig. 9 would probably lead us to the 11 FUs mentioned before. However, interpreting only major changes in the percentiles of the cumulative S-curve allow us to obtain the main flow zones in the reservoir at a larger scale, which are more likely to be detected in seismic volumes. Pursuing the seismic data constraint, we will gain lateral detection of the FUs, but lose vertical resolution. This is a trade-off that we need to manage for data integration with different resolutions.

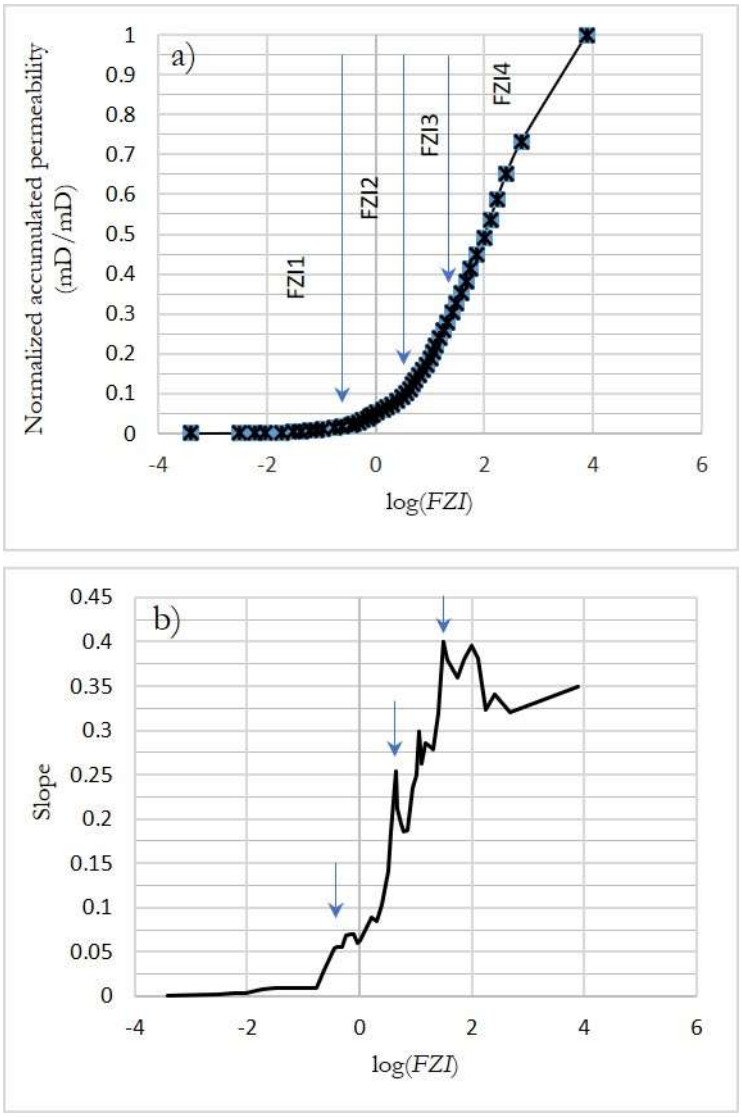

Fig. 9 — (a) Cumulative permeability S-Curve plot; (b) The log(FZI) cut-offs to discretize the FUs were interpreted as the major changes in the slope.

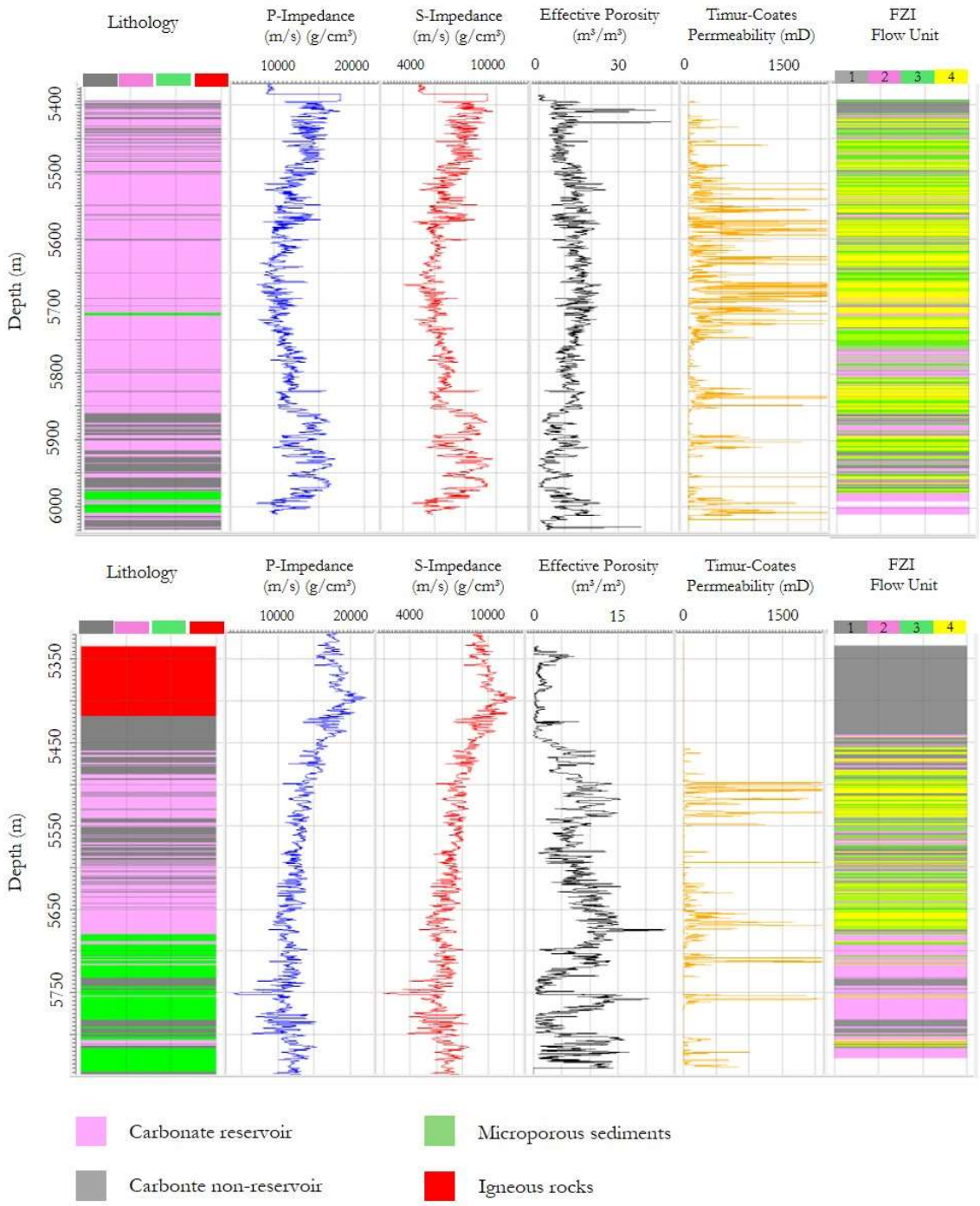

Fig. 10 — FZI cumulative S-curve classification of flow units applied to wells 01 and 03.

We compared the calculated permeability (using the equations per facies shown in Fig. 11) versus the measurement permeability in conventional core analysis (Fig. 12) to evaluate the proposed classification. It is observed that the majority of scattering occurs at the lowest permeability values, while for higher values above 1 mD the relative error is about 5%.

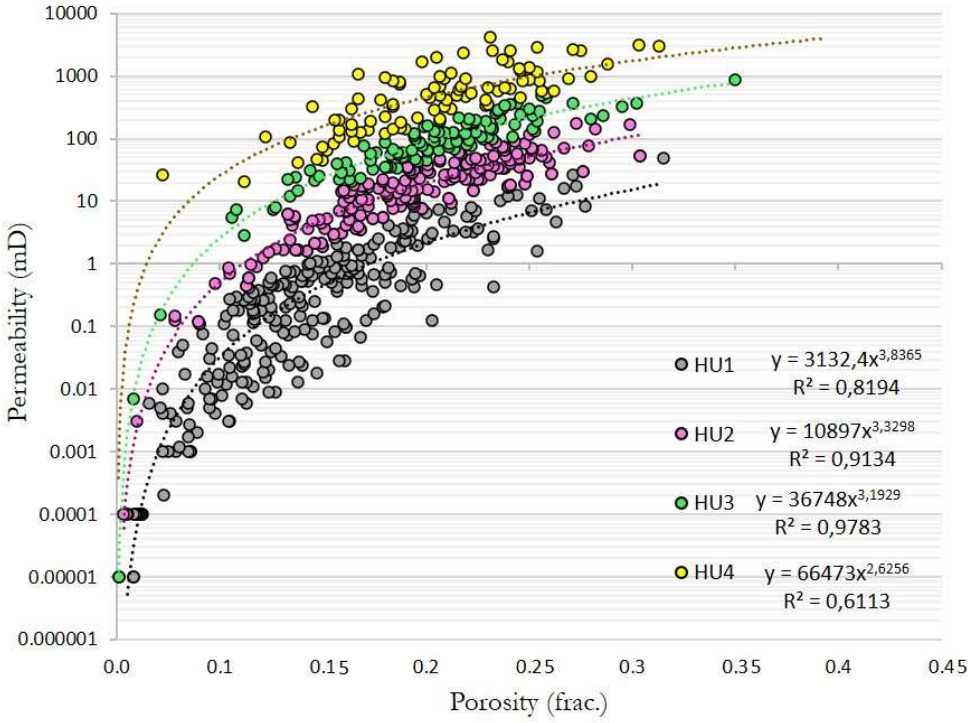

Fig. 11 — FZI flow units calculated from the S-curve segmentation in Fig. 8. Each of the four HU correspond to a permeability versus porosity fit in the semilog plot.

An example of how difficult it is to incorporate FZI flow units into geological models is exemplified in Fig. 13. Each FU shows a wide variety of sedimentary facies, with no relationship between FU facies and carbonate facies. For example, FZI3 and FZI4, which corresponds to the better flow performance in the reservoir, are not directly related to stromatolites (boundstone) and coquinas, the main facies in the Mero Field. Importantly, most static models are based upon modern analogs, geological setting premises and sedimentary facies distribution.

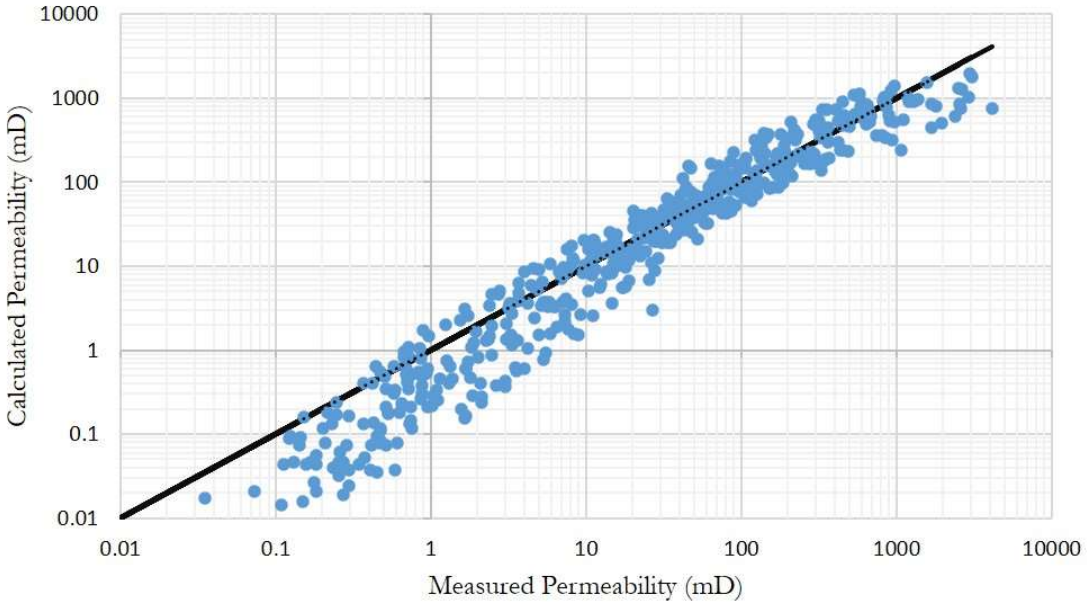

Fig. 12 — Measured versus calculated permeability through the S-curve analysis using the log(FZI) values. Note how most of the dispersion occur at low values of permeability.

2.6.3 Formation Factor

The formation factor, F, can be used to classify and cluster FU in a k versus -$1/F$ plot, as proposed by Ghanbarian et al. (2019). They argue that methods based on k versus $\emptyset$ plots ignore the effect of dynamically connected pores. In the formation factor (FF) and electrical methods, this connectivity effect is represented indirectly by the cementation exponent m, providing a better porosity estimation than usual methods based only in permeability and porosity ratios.

Adapting ideas of Ghanbarian et al. (2019) and considering our objective of obtaining a rock typing suitable to seismic resolution, we propose a classification of flow units by analyzing the formation factor distribution on the p-impedance versus s-impedance crossplot filtered for seismic data sampling rate (4ms). It is important to mention that the Mero Field has only 12 raw electrical measures in core and plug samples (4 and 8 samples in the Barra Velha and Itapema formations, respectively). Therefore, it was necessary to supplement the classification using well log information.

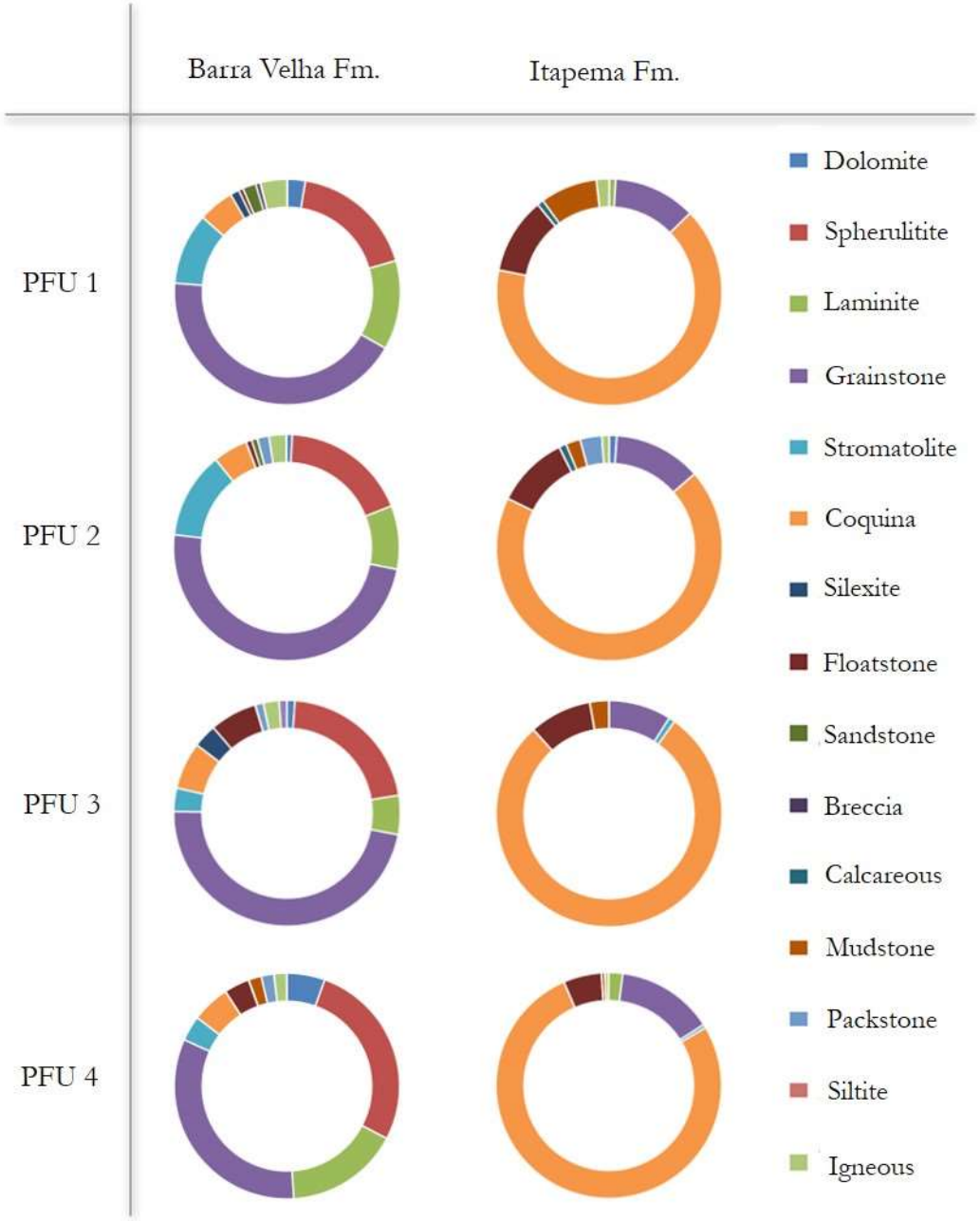

Fig. 13 —Sedimentary facies descriptions and distribution in each of the flow units calculated in the core samples of the Mero Field.

We analyzed the porosity versus formation factor to verify its linearity and whether, accordingly, Archie's law applies to our dataset. In Fig. 14, the gradient of the line is the cementation factor, m, and the intercept is the tortuosity factor. Table 3 summarizes the mean values of the electrical measurements in the Mero Field samples from Barra Vela and Itapema formations.

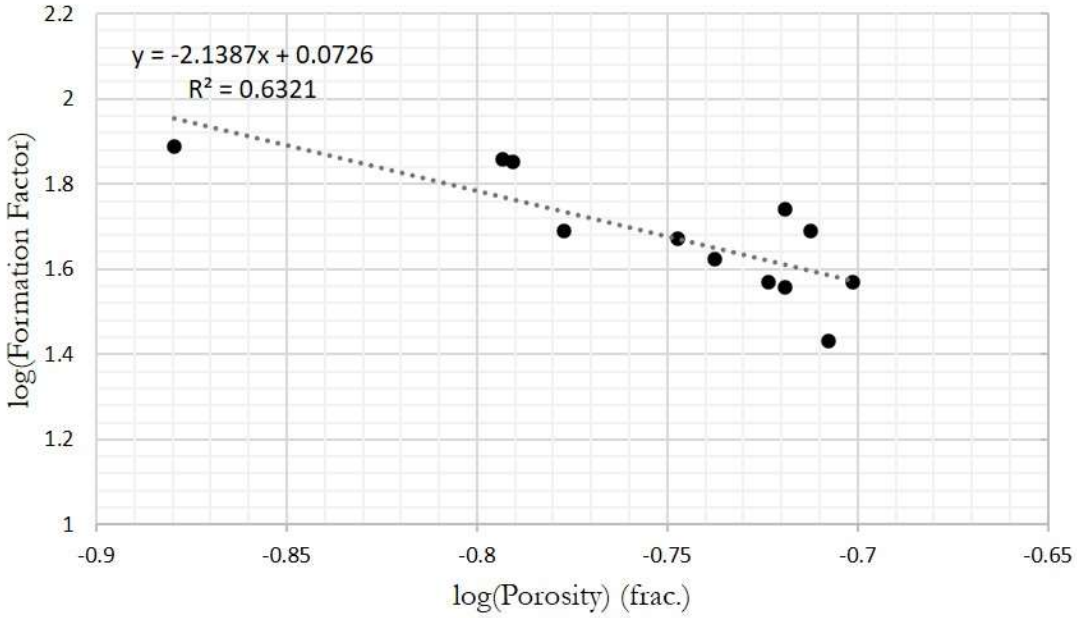

Fig. 14 — Porosity versus formation factor crossplot from core and plug electrical measurements of the Mero Field.

Table 3 — Mean and standard deviation (STD) from electrical measurements in core and plug samples.

Barra Velha Formation	Mean	STD
Permeability (k, mD)	63.64	44.66
Porosity (ϕ, frac.)	18.48	1.17
Water Saturation (Sw)	20.96	2.76
Formation Factor (F)	40.4	7.89
Cementation Exponent (m)	2.17	0.08
Saturation Exponent (n)	4.5	1.16

Itapema Formation	Mean	STD
Permeability (k)	237.72	291.22
Porosity (ϕ)	17.94	2.62
Water Saturation (Sw)	19.15	5.47
Formation Factor (F)	73.6	30.06
Cementation Exponent (m)	2.45	0.3
Saturation Exponent (N)	4.27	1.08

Formation factor logs can be calculated using Eq. 9, the effective porosity from NMR log and the mean values for m and α. However, this can lead to error in rock typing classification, because the use of a value for the cementation and the tortuosity factor neglect the importance of those elements. As described in El Sharawy and Nabawy (2018) and Soleymanzadeh et al. (2018), m depends greatly on diagenetic processes.

The cementation factor log can be calculated from Archie's empirical relationship:

$$\mathrm{RI} = \frac{\mathrm{R_T}}{\mathrm{R_0}} = \frac{1}{\mathrm{S_w^n}}, \tag{13}$$

where RI is the resistivity index (in Ω.m), $\mathrm{R_T}$ is the formation resistivity (in Ω.m) and $\mathrm{R_0}$ is the water saturated rock resistivity (in Ω.m). Replacing $\mathrm{R_0}$ from Eq. 8 in Eq. 13 obtain:

$$\mathrm{F.R_w} = \mathrm{R_T}\,.\,\mathrm{S_w^n}, \tag{14}$$

$$\frac{1}{\emptyset^{\mathrm{m}}} = \frac{\mathrm{R_T}.\ \mathrm{S_w^n}}{\mathrm{R_w}}, \tag{15}$$

Applying log to both side of equations and isolating the cementation exponent:

$$m = \frac{log(R_w) - n\,log(S_w) - log\ (R_T)}{log\ (\emptyset)}, \tag{16}$$

where R_T is the formation resistivity (or the deepest resistivity log, in Ω.m), S_w is the matrix water saturation log, R_w is the formation water resistivity (0.016 Ω.m in the reservoirs) and n is the saturation exponent (it was used the mean value obtained from core and plug data).

Fig. 15 shows the formation factor log estimated in well 12. It can be observed that F correlates directly with the p-impedance and s-impedance logs and inversely with the porosity and permeability logs. Areas with low porosity, igneous and cemented carbonate rocks, show high values of impedances and F. As expected, reservoir rocks with good permo-porous conditions show low values of impedances and F.

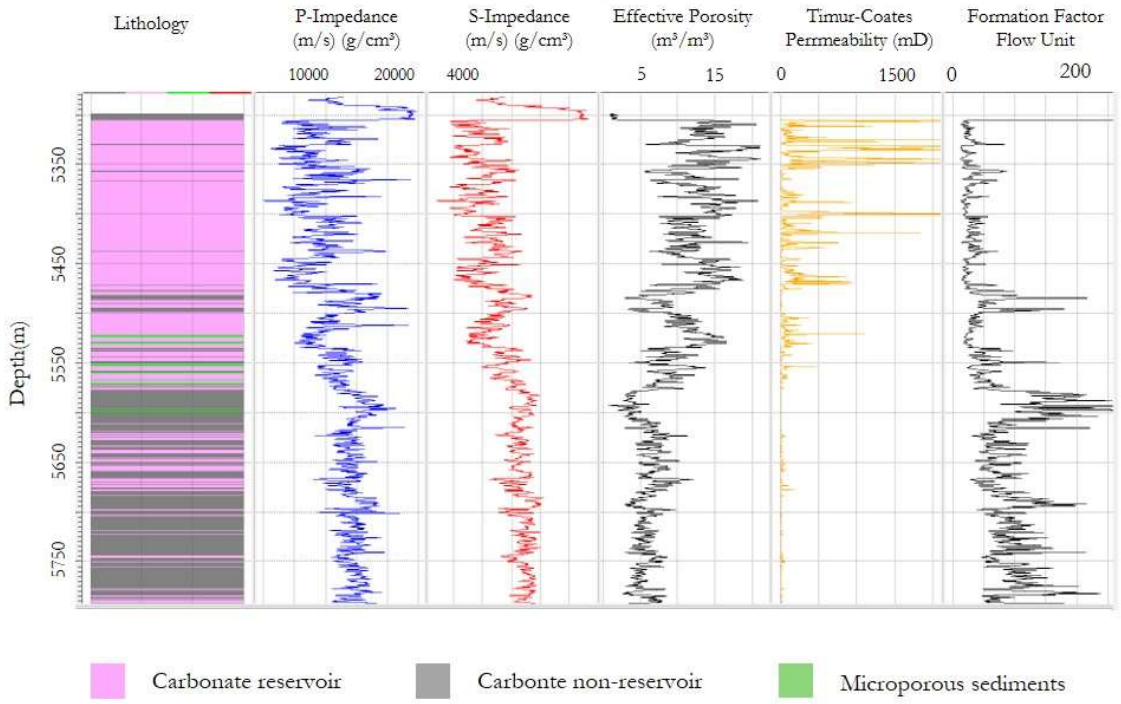

Fig. 15 — Formation factor log calculation using variable values of cementation factor m. Note how the F correlates with both p-impedance and s-impedance logs.

The impedance-p (PI), impedance-s (SI) and formation factor logs of Fig. 15 were filtered for seismic resolution to analyze their correlations. Fig. 16 shows the crossplot of the PI versus SI color coded by F values. It is possible to distinguish the trend of PI versus SI and F, with better quality reservoir rocks in the bottom left of the plot and igneous and cemented carbonates concentrated in the upper right. This trend was also observed considering lithology related seismic facies (Penna et al., 2019).

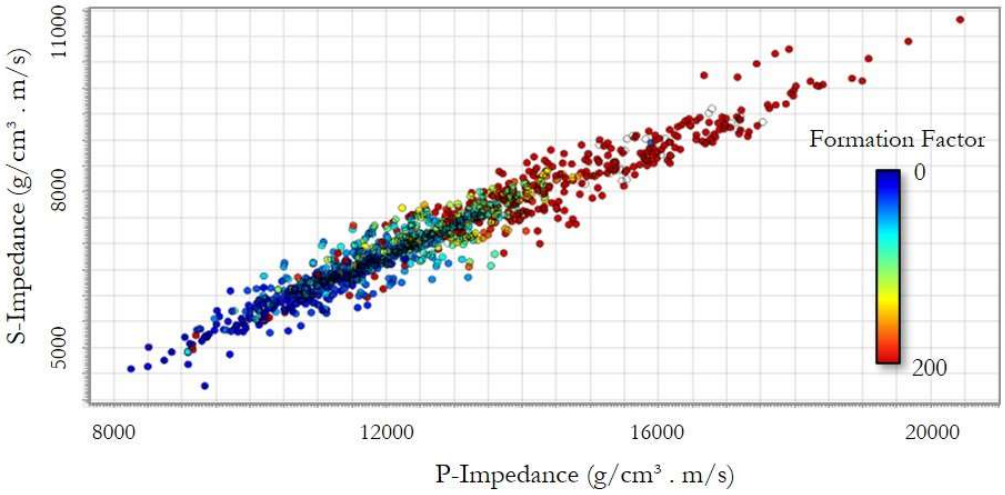

Fig. 16 —P-impedance versus s-impedance crossplot color-coded by the formation factor. Good quality reservoir rocks occur mostly on the bottom-left side, while cemented carbonate and igneous rocks cluster in the upper-right.

Cumulative S-curves of F versus k core measurements can be analyzed in terms of steep and flat segments (Fig. 17), like that shown in the SMLP and FZI methods (Fig. 6 and Fig. 9). Due to the lack of numerous electrical experimental measurements (only 12 samples), we only see a small portion of the real S-curve, missing where occurs the major changes in the flow performance.

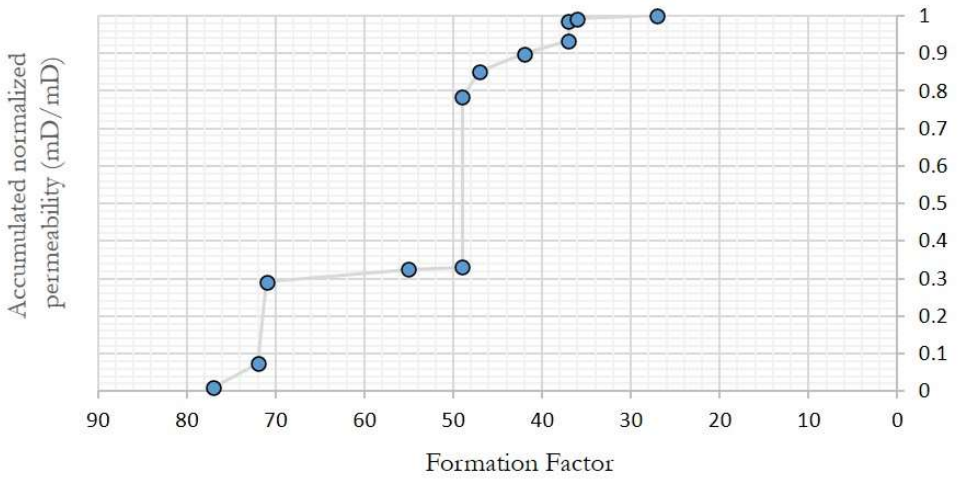

Fig. 17 —Formation factor versus cumulative normalized permeability from the core and plug electrical analysis. We choose not to use the S-curve segmentation to produce the F rock typing due to the limited number of samples.

The proposed approach to detect the major changes in F values is to analyze the histogram of F values from the well log data. As shown in Fig. 18, major changes in the F distribution can be interpreted as considerable jumps in the histogram. To maintain the same meaning of FUs used in the Lorenz and FZI methods, we classified FF1 as the flat final part of the histogram with higher values of F (hence, low quality rocks in permo-porous terms), while FF4 is the initial segment of the histogram with lower F values and a constant rate of variation. FF3 is interpreted as the first major change in the histogram, while FF2 is defined between the beginning of the ramp down until the flat final part that characterizes FU1. Table 4 summarizes the cut-offs defined in the histogram in Fig. 18.

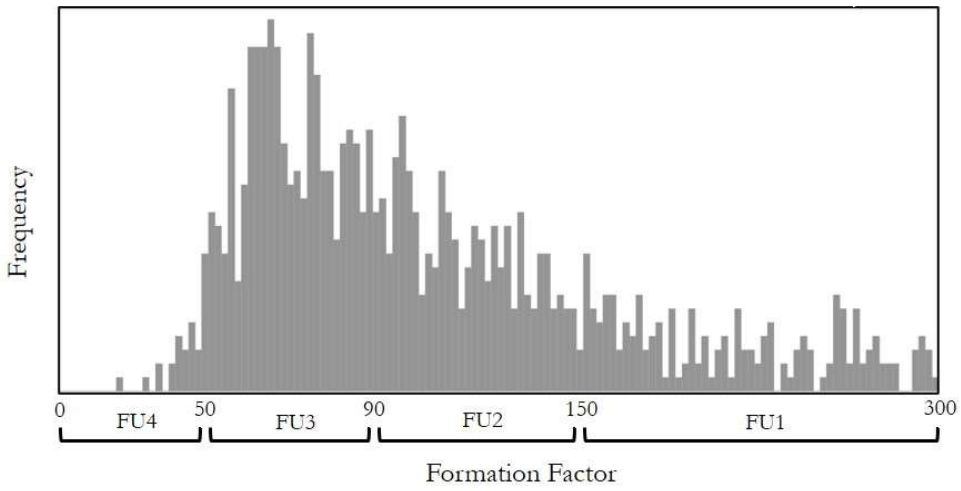

Fig. 18 —Histogram of formation factor well log and discretization based on the major changes of F values.

Fig. 19 exemplifies the segmentation proposed in Fig. 18 applied to wells 01 and 03. Both FZI and F classifications have aspects in common, although some differences occur. The cut-off range choices in the S-curve analysis and in the histogram have influence on the classifications, once it is a qualitative segmentation. We believe that the rock connectivity of the porous structure plays an important role in the formation factor analysis. The FZI method neglect this effect, because it approximates only the pore throat radius, as discussed by Ghanbarian et al. (2019). Fig. 20 shows the comparison of the FZI and FF rock typing classifications in a section of the Itapema Formation with high degree of carbonate dissolution, identified in the acoustic image log, in a cemented matrix interval. Because of the vugular porosity, this segment present great storage capacity, but reduced flow capacity, due to low connectivity of the pores. Note that the FZI method classifies this interval as FZI3, with good

permo-porous characteristics, while the FF method identified as FF1. According to Ghanbarian et al. (2019), this is the expected effect when using the formation factor instead of the porosity.

Table 4 — FU and Formation Factor cut-offs values used in the histogram of Fig. 18.

	F values
FF1	above 150
FF2	90 to 150
FF3	50 to 90
FF4	below 50

2.7 Flow Units and Elastic Parameters Correlations

Large-scale flow units can be correlated with seismic attributes to assure their spatial detections in acquired 3D data. Therefore, the resulting rock typing must separate a FU from another in the elastic space. To check how much the seismic dataset available can detect the major flow units in the elastic domain, we perform a 1D feasibility study considering p-impedance and s-impedance crossplots color coded by rock typing discretization methods. We analyze the flow units correlation with the elastic parameters at both the well and seismic scales, using high-cut frequency filtered version of the logs in order to represent the seismic vertical sampling of the area (to generate high-cut well logs, we considered a peak frequency of 20Hz with maximum 40Hz, compatible to the frequency characteristics of the seismic dataset).

Fig. 21 shows the Lorenz S-curve rock typing using the cut-offs defined in Table 1. LPFU, FZI and FF flow units 1 to 4 are better defined in the elastic domain for both well log and seismic scales. Each flow units can adjust a probability density function (pdf) and classify flow facies through probabilistic methods, using p-impedance and s-impedance volumes.

The same analysis of flow units and elastic parameters, in both well log and seismic scales, was performed using the rock typing provided by the FZI S-curve and formation factor (FF) approaches. (Fig. 22 and Fig. 23, respectively). It is observed that the LPFU classification is slightly better defined in the elastic domain, compared to the other two approaches. This is an expected result, considering the classical impedance – porosity relationship that forms the basis for most petrophysical studies using compressional and shear velocities.

A quantitative analysis was performed to verify whether rock typing can be distinguishable using elastic parameters in seismic scale. We used high-cut filtered versions of the p-impedance and s-impedance logs in a Bayesian facies classification workflow to analyze the FZI S-curve classification according to the seismic resolution.

Bayesian's theorem describes the posterior probability $p(m \mid z)$ of the parameters model m given the observed data z from:

$$p(m \mid z) = \frac{p(m)\,.\;p(z \mid m)}{p(z)}, \tag{17}$$

where $p(m)$ and $p(z)$ are the probabilities of observing m and z independently, respectively, and $p(z \mid m)$ is the conditional probability the z given m.

Considering our purpose to classify FU from the PI and SI, Eq. 17 can be written as:

$$p(FU \mid PI, SI) = \frac{p(FU)\,.\;p(PI,\ SI \mid FU)}{p(PI,\ SI)}. \tag{18}$$

For seismic facies classification, $p(FU)$ corresponds to a priori estimation of the probability of each facies at well scale. The term $p(PI,\ SI \mid HU)$ is the probability density function adjusted for each FU in the p-impedance versus s-impedance crossplot and $p(PI,\ SI)$ is a normalization factor (joint probability of PI and SI). Fig. 24 shows the FU classification and the posteriori probabilities of the FUs from the Bayesian classification, considering high-cut filtered versions of the PI and SI logs as inputs mimicking the seismic vertical sampling condition. Analyzing Fig. 24 is reasonable to mention that the lack of seismic vertical resolution acts as a smoothing factor of the rock typing. This effect is a trade-off that the method we are proposing must deal with, considering the loss of vertical discretization capacity.

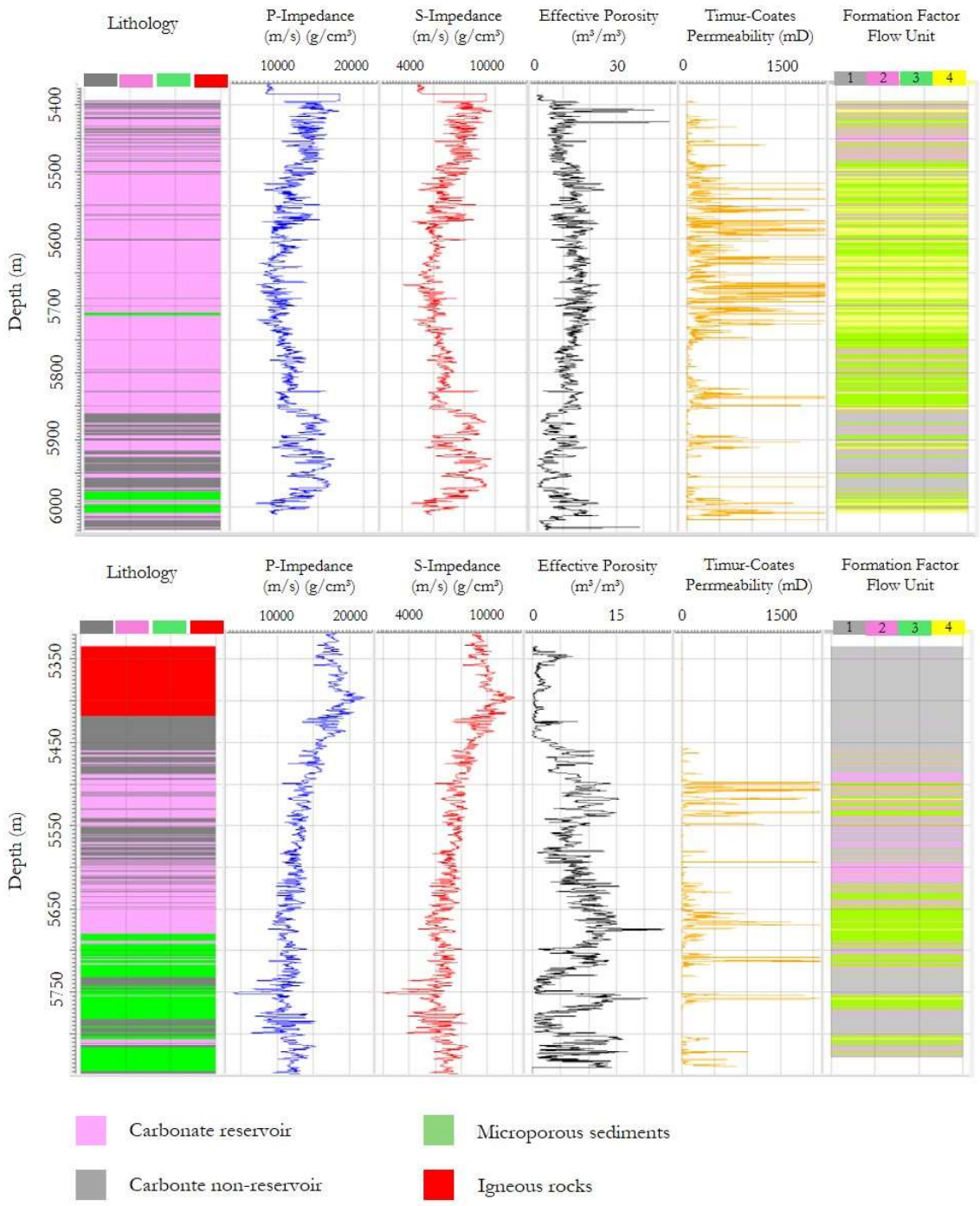

Fig. 19 —Classification of flow units from the formation factor histogram classification applied to wells 01 and 03.

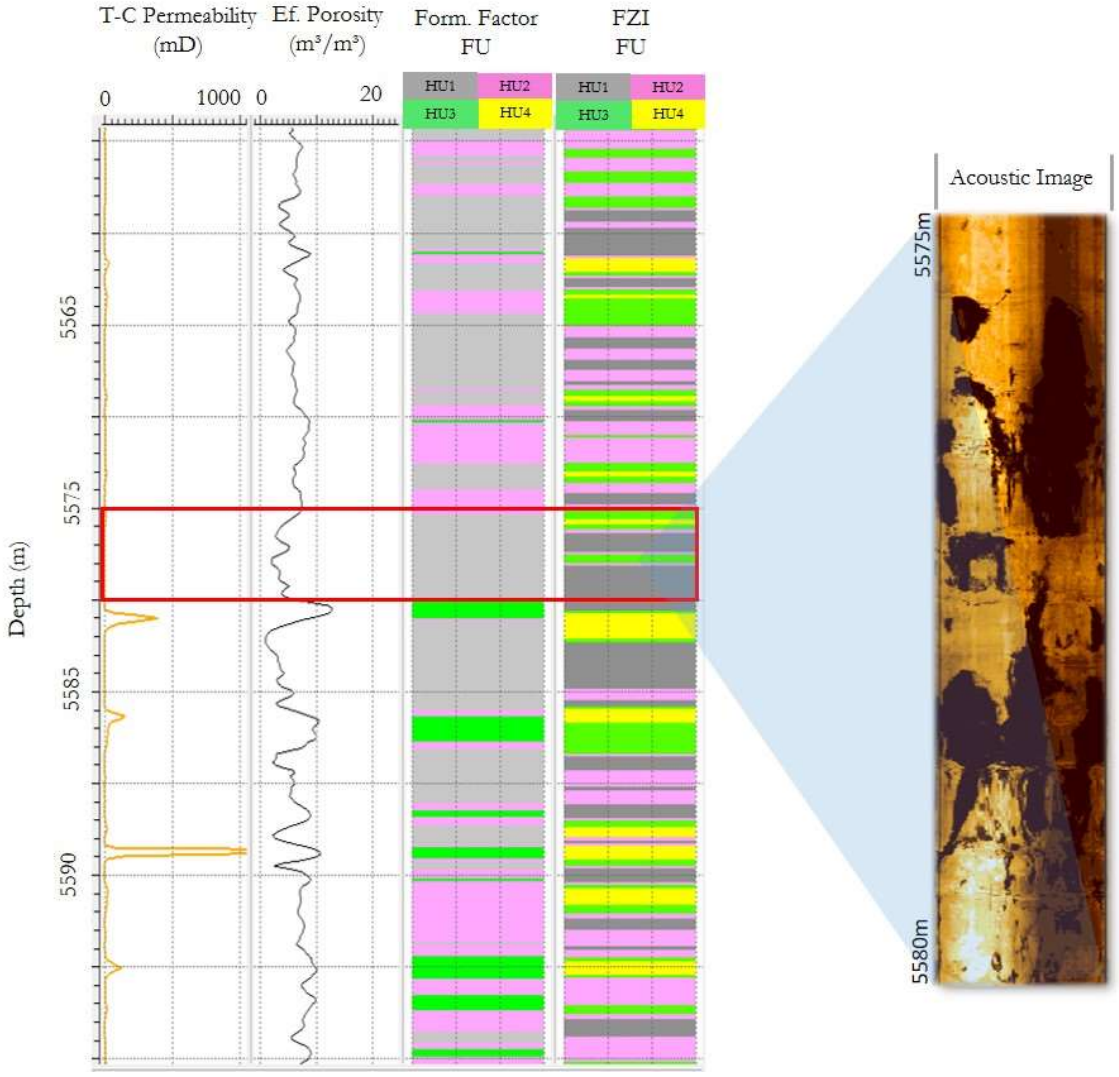

Fig. 20 —Classifications from the FZI S-curve and formation factor histogram analysis. The region with non-connected vugular porosity is classified as FZI3 by the FZI rock typing and as FF1 in the *F* rock typing.

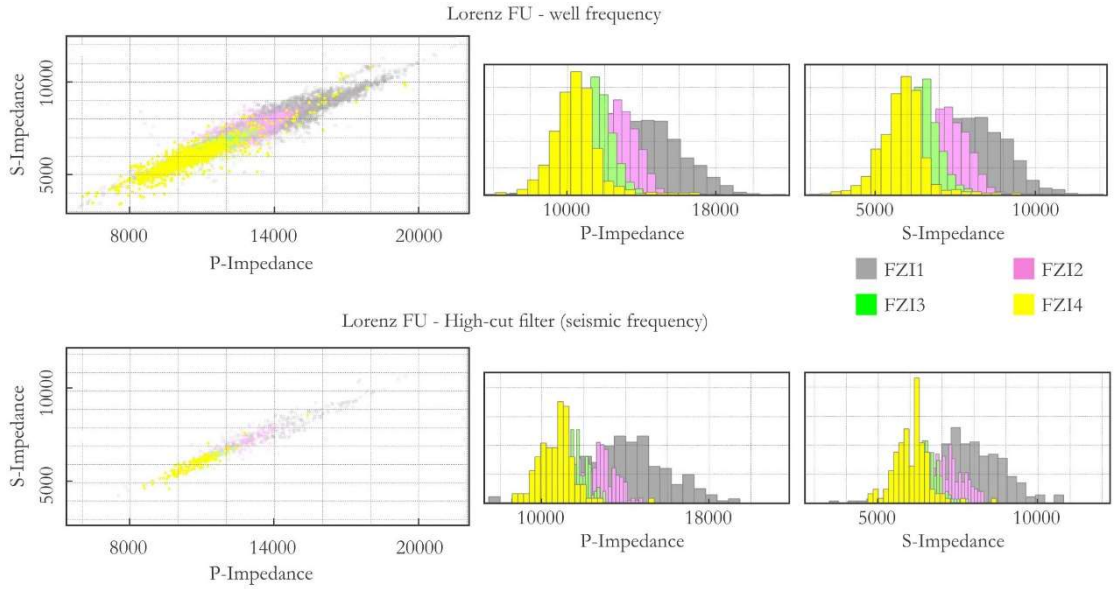

Fig. 21 —PI and SI coded by the Lorenz rock typing classification in the well log sampling (above) and in the seismic sampling (below). Flow units 1 to 4 are well defined in the elastic domain, even considering the low vertical resolution of the Mero seismic dataset. P-Impedance and S-Impedance in units of (m/s) (g/cm3).

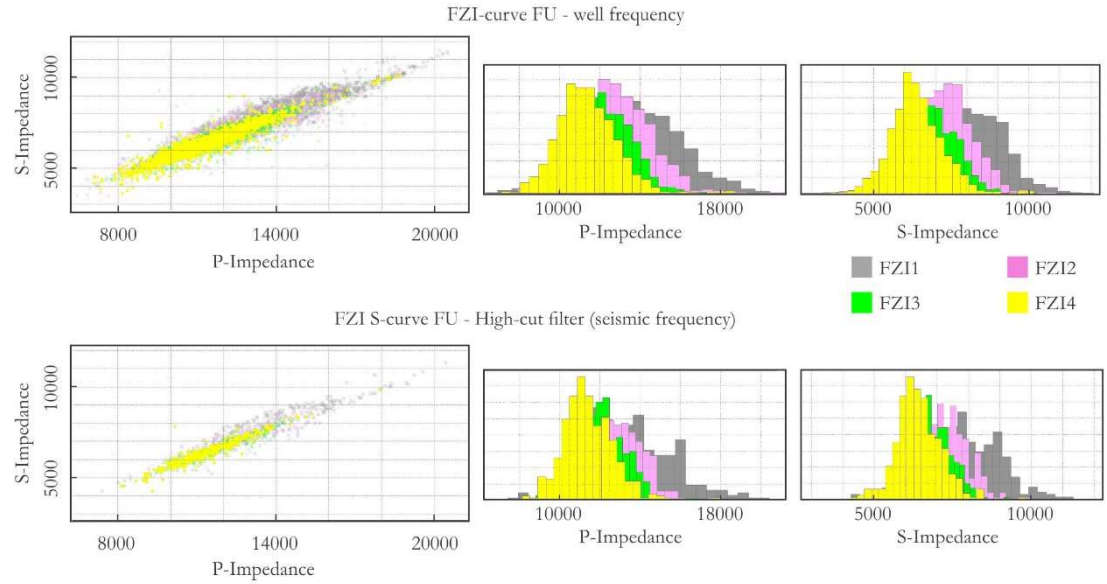

Fig. 22 —PI and SI coded by the FZI S-curve rock typing classification in the well log sampling (above) and in the seismic sampling (below). Flow units 1 to 4 are well defined in the elastic domain, even considering the low vertical resolution of the Mero seismic dataset. P-Impedance and S-Impedance in units of (m/s) (g/cm3).

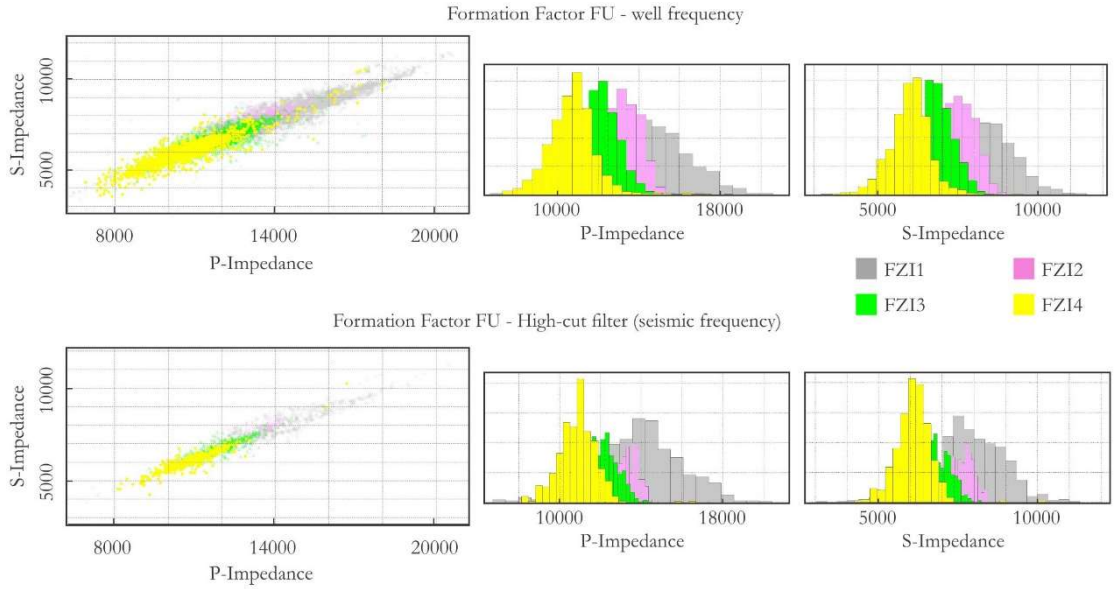

Fig. 23 —PI and SI coded by the formation factor rock typing classification in the well log sampling (above) and in the seismic sampling (below). Flow units 1 to 4 are well defined in the elastic domain, even considering the low vertical resolution of the Mero Field seismic dataset. P-Impedance and S-Impedance in units of (m/s) (g/cm3).

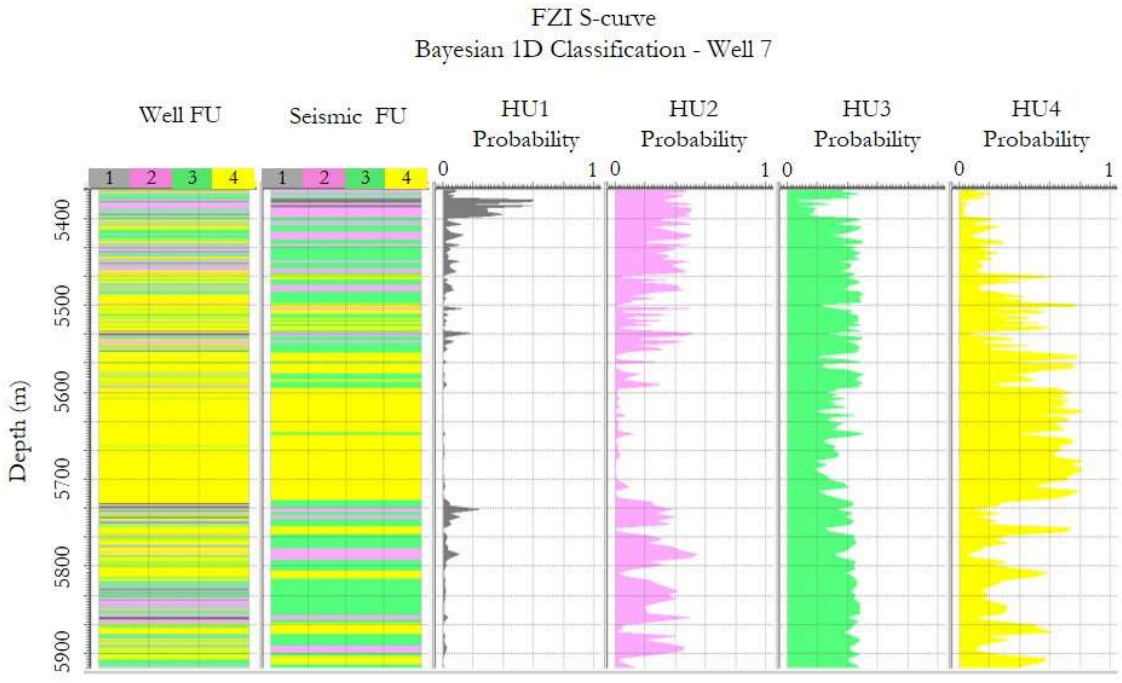

Fig. 24 —Bayesian 1D classification of the FZI S-curve FU in seismic scale from the PI and SI logs. Note that the seismic resolution acts as a smoothing factor of the rock typing.

As an example, for assessing the reliability of seismic resolution results, we compared the absolute permeabilities obtained from the large-scale FZI, the geological model and the extended well-test (EWT) adjusted in flow simulator (Fig. 25). The large-scale FZI absolute permeability was calculated per flow unit using the equations shown in Fig. 11, while the absolute permeability from the geological static model consists of a complex sedimentological facies-based 3D modelling populated with geostatistics constraints and conceptual model inferences built by the Mero Field asset team. Some details about the general methodology of the 3D depositional building can be found in Faria et al. (2017). Absolute permeability and porosity values where populated in a fine-grid with stochastic simulation considering each depositional facies and the corresponding conventional core analysis results. The geological fine-grid were upscaled to the flow simulator using a tensor technique. After the extended well-test performed in the reservoir, the flow simulator has been updated considering the observed dynamic results. Some high-permeability corridors where manually constructed and given zones penalized or increased in terms of absolute permeability and porosity values, resulting in an adjusted absolute permeability. As seen in Fig. 25, in several well segments, the large-scale FZI provides a closer result than the geological static model, considering the EWT adjusted permeability as a benchmark. This result suggests that the incorporation of large-scale flow units as constraints during the conceptual geological model building would provide results that are more accurate to the dynamic data of the reservoir.

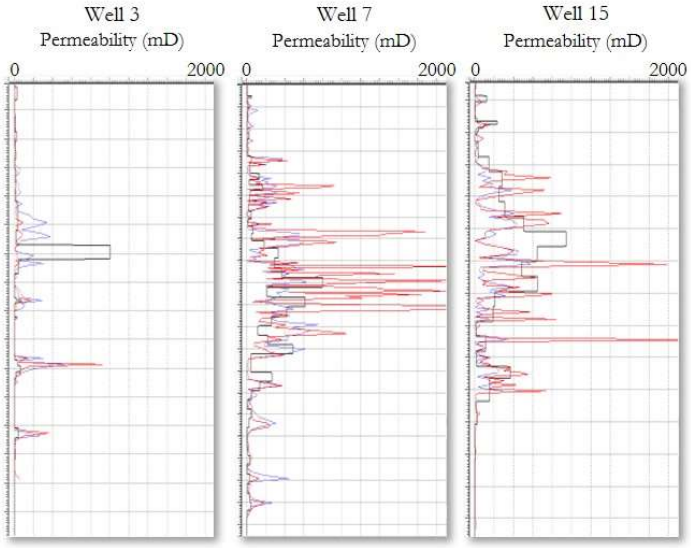

Fig. 25 —Comparison of the permeabilities obtained from the large-scale FZI (blue line), the geological static model (red line) and the adjusted EWT flow simulation model (black line). The large-scale FZI permeability is closer to the EWT adjusted data in several sections.

2.8 Conclusions

Conventional rock typing workflows in well log resolution are accurate describing flow behavior in the pore and core domain. However, interpolating flow units to the whole reservoir are typically difficult due to the lack of correlation with sedimentary facies and data integration at different scales. In most situations, upscaling and downscaling only dilute this problem, and the interpolation are greatly dependent of geostatistical constraints. We argue that large-scale flow units calculated through a cumulative S-curve are those that respond for major fluid movements in the reservoir and must be considered for flow simulation, especially when incorporating time-lapse seismic interpretations and seismic assisted history matching. We argue that maps and spatial data based on these flow units like maps and volumes will provide valuable insights into any flow simulation workflow.

As seen in the 1D feasibility study, large-scale flow units can be successfully identified in seismic through elastic inversion volumes, providing lateral predictability and supporting the geological and the flow simulator 3D building, with results more appropriate to the dynamic data of the reservoir. When comparing the permeability derived from the conceptual geological model with the permeability obtained by the FZI S-curve analysis, we noticed that the large-scale flow units provide a better estimation of the absolute permeability, considering the flow simulator adjusted permeability with the extended well-test results as a benchmark.

At the well scale, we noticed that rock typing for formation factor presents an advantage over the FZI method, as it considers the connected pore structure present in the rock sample. Cemented carbonates with vugular porosity zones where better classified in the formation factor rock typing method in terms of flow capacity.

3. 3D Modelling of Flow Units and Petrophysical Properties in Brazilian Presalt Carbonate

Article published in

Marine and Petroleum Geology, Vol. 124, 2021.

Impact Factor: 5.361

Authors: Rodrigo Penna and Wagner Moreira Lupinacci

3.1 Abstract

Rock typing into flow units (FU) is a well-known technique for characterizing flow heterogeneities in reservoirs and producing reliable estimations of petrophysical properties, as porosity and permeability. Several methods that correlate pore-throat size with permeability and porosity in the core and well-log domains are available in the literature, being the flow zone indicator (FZI) method the most common used in both clastic and carbonate reservoirs. Extrapolating the flow units rock typing from the core and well-log scales into the whole reservoir is a major challenge due to the lack of correlation with sedimentological facies and available data scale differences. Most 3D generations of flow units and petrophysical properties are merely a geostatistical procedure, without any spatial data constraints (like seismic attribute). We propose a new approach to create flow units occurrence probability volumes as well as seismic derived porosities and permeabilities that are more robust than the usual estimate of petrophysical properties considering sedimentological facies. Considering the seismic scale characteristics and using the concept of decametre flow units and quantitative seismic interpretation in a Brazilian presalt dataset, we indirectly quantified superimposed small-scale effects that obliterate/generate porosity on a larger scale and established a minimum number of correlatable FUs with elastic seismic attributes. We produced 3D volumes of permeability and porosity that are still capable of obtaining complex reservoir flow characteristics and could be directly considered as variables in lateral interpolation of reservoir parameters, seismic 4D interpretations and seismic-assisted history matching.

3.2 Introduction

Generation of adequate static and dynamic models provides better subsidy for the decision-making process, especially in enhanced oil recovery production. For any asset team

working in complex geology settings, as Brazilian presalt carbonates, an assertive description of reservoir heterogeneity and flow behavior in terms of fluid movement is crucial. In that sense, working with flow units in carbonate settings can present an advantage over sedimentary or lithological facies, as it provides better estimation of reservoir petrophysical characteristics. In the presence of complex geological settings with differential diagenesis, the estimation of porosity (ϕ) and permeability (k) performed on a flow unit (FU) basis should be more accurate than lithological or sedimentary facies, as discussed by Aggoun et al. (2006), Daraei et al. (2017), Hatampour et al. (2018), Ghanbarian et al. (2019).

Because flow units do not have any correlation with lithological facies, their incorporation into 3D static models that are essentially built on sedimentological premises can be very disappointing. Depending on the diagenetic history, same lithological facies deposited at a given high-energy setting, for example, can present distinct flow behavior. These rocks would group at the same sedimentological facies, but at different reservoir rock typing (RRT) and flow units because of the distinct porosity generation/obliteration processes. In addition, the difference in scales and the lack of correlation between well logs and seismic data makes the propagation of the petrophysical properties into 3D geological model problematic and purely a geostatistical approach, often resulting in non-realistic flow models. Examples of lateral extrapolations of flow units and petrophysical properties considering only well data are found in Testerman (1962), Svirsky et al. (2004) and Li et al. (2018).

Flow units are rarely a considered technique for geophysicists working with quantitative seismic interpretation (QSI). In literature, the main publications related to QSI (Avseth et al., 2005; Dvorkin et al., 2016; Vernik, 2016) does not mention any definition or workflow to identify and map the FU from elastic seismic attributes. Prasad (2003) is one of the few publications on the usage of flow units constraining seismic velocity-permeability relations. The author showed that grouping and sorting rocks into flow units had strong relationship between P-wave velocity and absolute permeability within each FU in the analyzed dataset.

Recent publications correlate flow units with multiple seismic attributes, producing constrained tridimensional petrophysical properties of porosity and permeability (Rastergania et al., 2016; Iravani et al., 2018; Hatampour et al., 2018). Iravani et al. (2018) considered a single FU regression from the well-log data for the entire reservoir, having the acoustic impedance volume as constraint for the lateral interpolation of petrophysical properties. Rastegania et al. (2016) and Hatampour et al. (2018) used intelligent systems, like probabilistic

neural networks and radial basis function networks, to obtain linear relationships between FU and seismic attributes. The mentioned methods that correlate FU and seismic attributes, are simply an extrapolation of FU classification based on core and well log data into the seismic resolution, regardless of the scale difference between data types. For most cases, the geological setting of the area is a sand-shale intercalation, where a small number of flow units is enough to characterize the reservoir behavior in terms of fluid movement. In more complex geology settings, where numerous FUs are calculated, the lack of seismic vertical resolution must be considered in the process.

We propose a methodology for calculating better seismic derived petrophysical volumes, characterizing large-scale flow characteristics of the reservoir considering flow units as constraints. Using percentiles and a cumulative S-curve in permeability and porosity core measurements from the Mero Field, a Brazilian presalt carbonate reservoir, we calculated a significant number of flow units that correlates with seismic elastic attributes and respond for the large-scale flow characteristics in the reservoir, maintaining part of the local flow complexity (Penna and Lupinacci, 2020). Within each FU, we establish petrophysical relations that calculates more accurate seismic derived 3D volumes of porosity and permeability and compared to volumes calculated using sedimentological k- ϕ relations.

3.3 Study Area and Data Available

The present study is developed using a Mero Field database composed of core, well log and seismic data. This field is a part of the giant Libra discovery, located in the northeastern portion of the Santos Basin, ultra-deep water of the Atlantic Ocean (Fig. 26). Libra Prospect comprises a 2013 consortium of Petrobras (operator), Shell, Total, CNOOC and CNPC, under the new Brazilian production-sharing contract for presalt areas. Libra Prospect initial estimates indicate an oil in place volume of between 8 and 12 billion BOE (Carlotto et al., 2017), with high geological complexity in terms of stratigraphic facies (Penna et al., 2019; Penna and Lupinacci, 2020).

Main reservoir rocks of the Mero Field are bivalve rudstones (coquinas) from the Itapema Formation (Barremian) and shrubs and spherulites from the Barra Velha Formation (Aptian), although high porosity is also found in bioclastic grainstones, packstones, wackestones and others carbonate related facies (Jesus et al., 2019; Gomes et al., 2020). Low porosity fine-grained carbonates, such as mudstone (classified, for simplification, as

microporous sediments) are distinguishable, as well as extrusive and intrusive igneous rocks. Because of the lack of vertical resolution and rock high incompressibility characteristics, Mero seismic data can only distinguish a simplified lithology classification that comprises carbonates, microporous carbonates, and igneous rocks, as discussed by Penna et al., 2019.

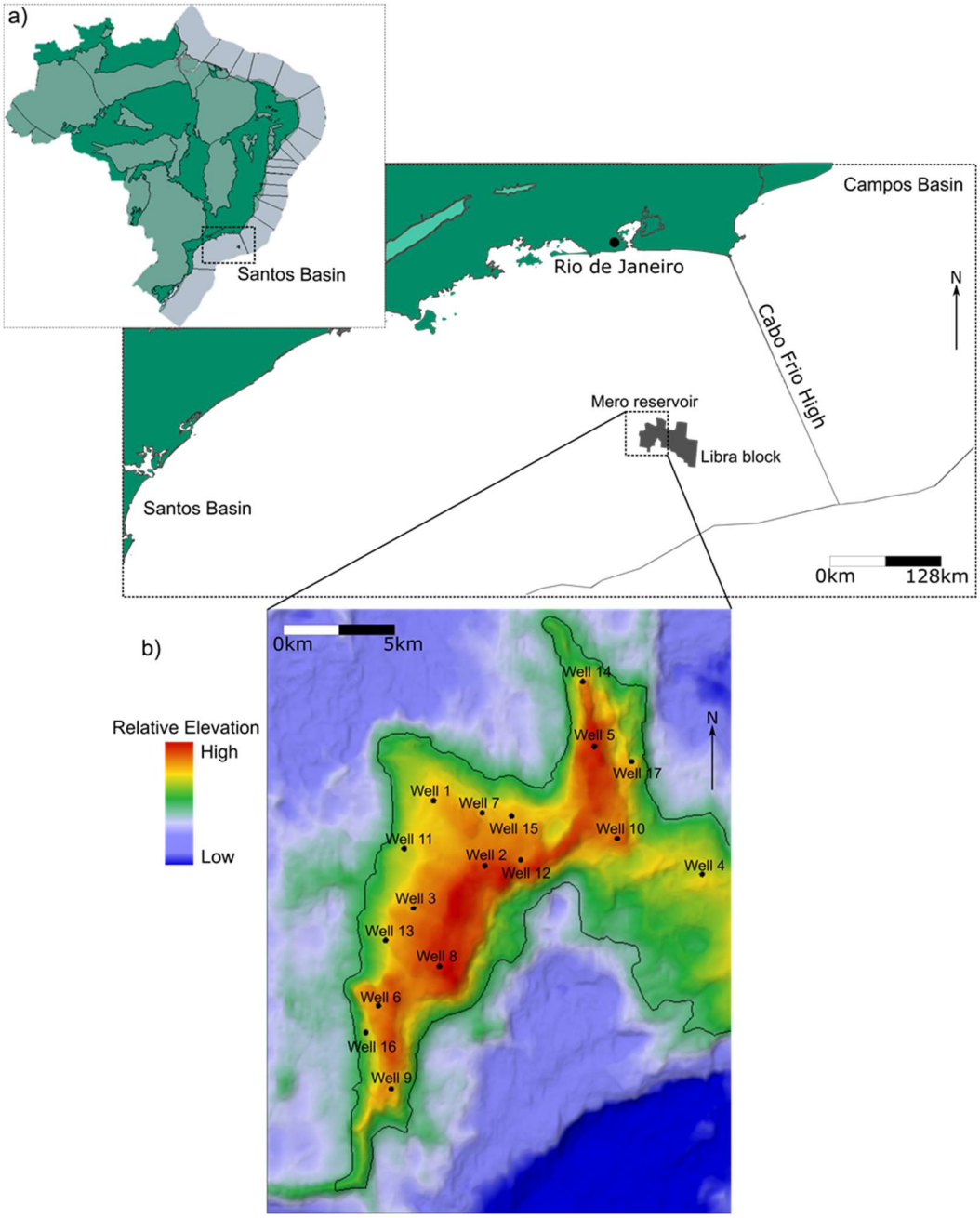

Fig. 26 – (a) Mero Field is located on the northeastern portion of the Santos Basin, southeast Brazil, close to the Cabo Frio high that separates it from Campos Basin. (b) Base of salt horizon (top of the Barra Velha Formation) displays an elongated N-S structure. 17 wells in the study area are represented by circles.

Mero reservoir, like other Brazilian presalt carbonates, shows many static and dynamic indications of fracturing in different stratigraphic levels. However, it is very hard to identify relevant and consistent fractured intervals in well logs and borehole images, especially when the fracture opening is small (this is common due to the high compaction of these reservoirs, and core data tend to highly overestimate fracture opening due to the uncompressing effect at sea level). At decametric scale, however, dissolution and neomorphism, replacement of minerals, silicification and dolomitization are the main effects that controls porosity generation and/or obliteration and fluid movements in the reservoir (Herlinger et al., 2017 and Gomes et al., 2020).

Approximately 500m of cores were taken in different stratigraphic intervals. The dataset comprises about 1700 laboratory core and plug measurements of porosity and permeability from 17 wells, containing both the Barra Velha and Itapema formations. The seismic data is a legacy seismic acquisition that cover an area of 2,484 km², 8 km streamer cable length and 6.25 x 25m grid. This seismic data was reprocessed in 2016 with an initial tilted transversely isotropic (TTI) velocity model over an area of 2,900 km² and a vertical transversely isotropic full waveform inversion (VTI-FWI) from 3 Hz to 45 Hz. Then a multi-layer tomography using both Kirchhoff and Reverse Time Migration (RTM) picks was performed, followed by a TTI-FWI from 7 Hz to 8 Hz applied at the entire geologic sequence (pos-salt, salt and presalt). High and low-salt velocities layers, like anhydrite, taquidrite, carnalite and silvinite, as well as igneous rocks, within the salt stratification, were incorporated for the velocity model. Seifert et al. (2017) provides more details and discussions about this procedure.

We used a model-based constrained sparse-spike prestack seismic inversion (Pendrel, 2001), calculated from six partial angle stacks of the reprocessed RTM data with the well log information of 17 wells drilled in the area. The low-frequency model was built through a lateral interpolation of the acoustic impedance (PI), shear impedance (SI) and density logs. The stratigraphic control is constrained by four interpreted seismic horizons (top of the Barra Velha Fm., top and base of the Itapema Fm. and top of basement. In this inversion method, a minimum number of interfaces continuously simulates the seismic trace in a recursive and iterative scheme. The derived errors from the comparison of the synthetic and the real seismic data should be minimized. Details of the sparse spike inversion method and others available in the industry are found in Veeken and Da Silva (2004).

3.4 Seismic Data Scale Analysis

An important issue to be addressed in the characterization of flow units through elastic volumes is the difference in scales between data and the magnitude of the feasible discretization using available seismic data. In terms of lateral resolution, the seismic scale is relative to the bin size of the seismic acquisition: 6.25 x 25 m. For the seismic vertical resolution, the minimum thickness of a given layer that the seismic data can resolve (separation between top and base of layer interface with the correct thickness) is related to the frequency content, the compressional (P) wave velocity of the medium, and the shape of wavelet (Kallweit and Wood, 1982). Any layer below the minimum vertical thickness will fall into the phenomenon known as tuning, where the amplitudes brighten or diminish due to the constructive and destructive interferences between overlapping seismic reflectors associated with thin layers. Usually, the minimum thickness is considered as one quarter of the signal wavelength (λ) (Kallweit and Wood, 1982).

The seismic data used in this work has frequency content, in the presalt section, between 5 to 35 Hz, with a peak frequency of 15 Hz, and the wavelet phase close to zero degrees for the existing spectra. Based on the frequency content information, an effective way to assess the tuning thickness is through the construction of a wedge model, as shown in Fig. 27. We considered for the central wedge layer an average value of acoustic impedance that represents a flow unit with good permoporous conditions surrounded by layers with low permoporous. Wedge thickness varies from 270 m to zero. Apparent thickness is measured from the bottom of the positive peak to the top of the negative peak (dashed line). In Fig. 27, the tuning thickness is obtained from the lowest value of seismic amplitude, which for this model is approximately 60m. When the wedge is thinner than this, the apparent thickness deviates from the real thickness. This means that the resolution for the flow units is approximately 60m, if we directly use the seismic amplitude as constraint.

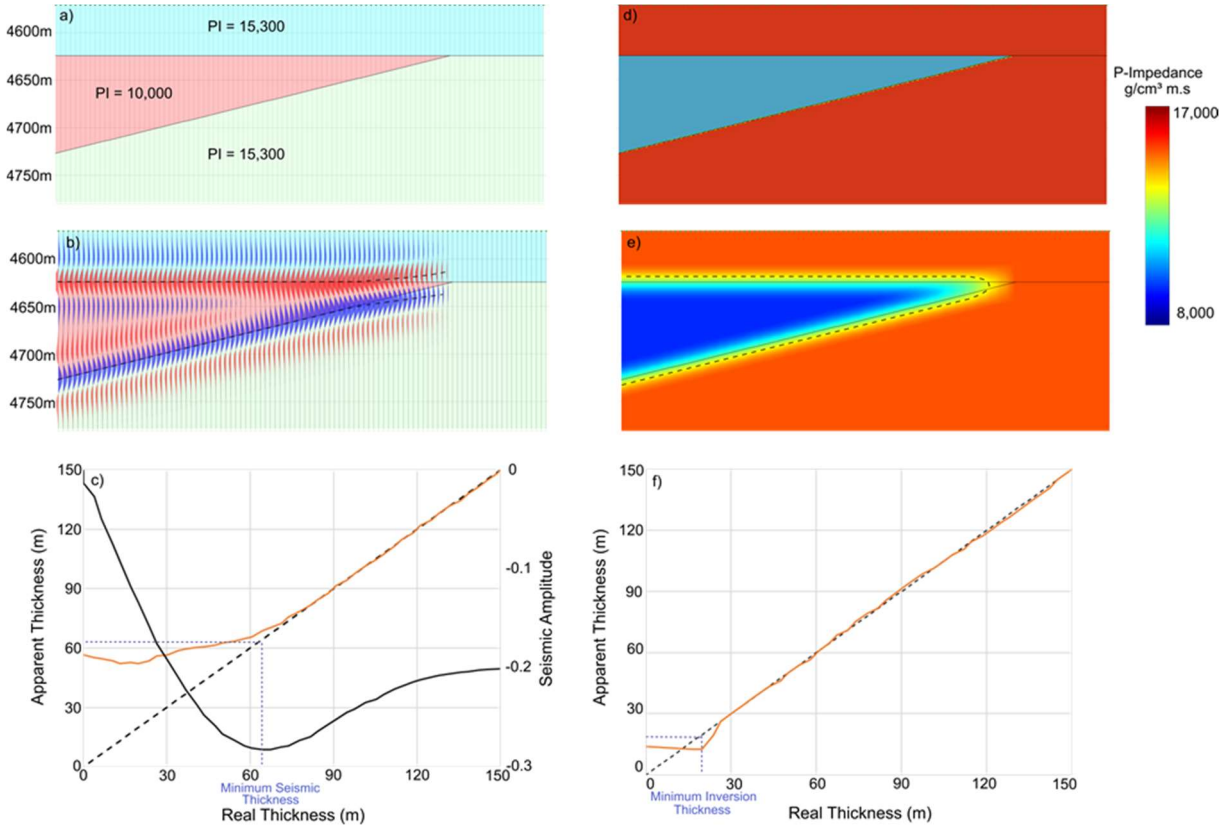

Fig. 27 – (a) A three-layer wedge model. (b) Synthetic seismogram of the wedge model. (c) Apparent (orange line) versus real thickness (black dashed line) graph and the amplitude variation (black line) from the top of the negative peak. (d) Acoustic (P) impedance wedge model. (e) Smoothed P-impedance wedge model for the frequency content obtained from the seismic inversion. (f) Apparent (orange line) versus real thicknesses (black dashed line) from P-impedance wedge model.

An advantage of using elastic volumes over seismic amplitude data is the frequency gain due to the low and high frequency content incorporated during the seismic inversion process. Hill (2005) provides a discussion on this subject, showing that the use of inversion data can provide a reliable thickness estimation of about 1/3 of the tuning thickness. For our seismic inversion method, we considered a sparse-spike algorithm who calculates a blocked impedance volume. The sparse-spike inversion technique is defined through an Lp norm (with $p \leq 1$) applied in the parameter model of the objective function, which favors discontinuous functions in the first derivative of the model (Aster et al., 2004). A blocked impedance solution is only possible through an iterative method that increases the higher frequency content, that is, it increases the resolution. For instance, Aster et al. (2004) states that once you apply the L1 norm in the parameter model, the problem becomes non-linear and for its solution it is necessary to use, for

example, the IRLS (iteratively reweighted least-squares) method. As result in a reflectivity inversion, the reflected pulses become more compressed and well localized and the solution resembles a sparse series of spikes (Oliveira and Lupinacci, 2013). Wang (2014) shows how the amplitude spectra of inverted reflectivity series increases from each iteration using the sparse-spike solution. Gradually, at each iteration, the spectrum is flattened through the increasing high frequency content on the reflectivity series.

We evaluate the vertical resolution gain using the same wedge model described in Fig. 27, but now using the impedance data to estimate the apparent thickness. For this, the wedge model in acoustic impedance was smoothed to the same frequency content of the elastic parameter volumes (0-60Hz) obtained after the prestack inversion. Apparent thickness is measured between the top and bottom transition with constant impedance value (dashed line). We note that now the real and apparent thicknesses are equal after 23 m, a considerable gain compared to the 62 m from the amplitude seismic data. The minimum thickness from inversion is named in this work as the minimum inversion thickness.

The vertical resolution of Mero data indicates that the flow units discretized by the seismic inversion data will have decametre scales. This means that every distinct effect that obliterates or generates porosity identified at centimetric or metric scales will be expressed differently at lower scales. When rock typing for decametre flow units, we are characterizing the combined diagenetic effect from several centimetric higher frequency variations. Rock typing for flow units core or well log data produces different results compared to seismic data, although both represent different stages of the geological building process of a reservoir (Penna and Lupinacci, 2020).

3.5 Flow Units Classification

The most documented method for rock typing into flow units in clastic and carbonate reservoirs is the RQI/FZI (rock quality index/flow zone indicator) method. Since Amaefule and Altunbay (1993) introduced the classification based on the Kozeny equations (Kozeny, 1927; Carman, 1937), the method is widely used due to its simplicity and consistent results. The analysis is based on the permeability (k) in (mD) and effective porosity (ϕ_E) ratio, where the index RQI in μm is:

$$\mathrm{RQI} = 0.0314\,.\,\sqrt{\frac{\mathrm{k}}{\phi_{\mathrm{E}}}}. \tag{19}$$

Then, the FZI is calculated as:

$$\mathrm{RFZI} = \frac{\mathrm{RQI}}{\phi_{\mathrm{Z}}},. \tag{20}$$

where FZI is given in μm and ϕ_{Z} defines as a normalized porosity on the form $\phi_{\mathrm{E}}/1-\phi_{\mathrm{E}}$. Taking log on both sides of Eq. 20 and rearranging, we have:

$$\log \mathrm{RQI} = \log \mathrm{FZI} + \log \phi_{\mathrm{Z}}. \tag{21}$$

Considering Eq. 21, a constant value of FZI produces an inclined straight line in log-log plot of RQI versus ϕ_{Z} (Amaefule and Altunbay, 1993). Samples with similar flow characteristics and, consequently, same FZI values, cluster around a corresponding unit-slope, determining a flow unit. Samples with different FZI values are plotted on different parallel lines and grouped in distinct flow units.

Clustering core data and FZI values into flow units can be performed in different approaches, depending on the complexity of the reservoir and classification objectives. As FZI is strongly dependent on permeability and usually exhibits log-normal distribution, a histogram discretization of log (FZI) values can be enough in relatively simple geology areas. Other clustering methods like iterative multi-linear regressions were detailed by Al-Ajmi and Holditch (2000). Penna and Lupinacci (2020) used percentiles and cumulative S-curves to produce a significant number of flow units aiming decametre flow characterization. In Penna and Lupinacci (2020), different methodologies for creating a minimum amount of flow units in the well domain were performed, along with a seismic feasibility study considering the vertical scale characteristics of the seismic data.

FZI is considered a robust method of permeability estimation and reservoir prediction in terms of flow heterogeneities, due to petrophysical correlations between permeability and flow units (see e.g.: Emami Niri and Lumley 2016 and Iravani et al. 2018). Despite being widely used in the industry to characterize flow behavior in reservoirs, the FZI method is purely petrophysics. Concepts as depositional environments, sedimentological texture and grain type are not considered in the flow unit classification. This is the main problem with the FZI

technique and flow units rock typing, because, due to the lack of correlation with the local geology, is extremely difficult to propagate the flow units in a sedimentary-based geological model. Furthermore, obtaining seismic attributes correlations to use as constraints to geostatistical procedures is often incipient due to the scale difference between the core and seismic data.

We calculated the stratigraphic modified Lorenz plot (SMLP) (Gunter et al., 1997) using the storage capacity and flow capacity of both Barra Velha and Itapema formations from the core laboratory permeability and porosity measurements (Fig. 28). In Gunter et al. (1997) proposed that the interpretation of each FU is performed observing the slope of the curve: flat segments corresponds to seals or baffle zones, as they may present some level of porosity, but have no contribution of permeability. Steep segments correspond to "speed zones" of the reservoir, they can have low or high porosity, but provide major contributions to the reservoir flow performance in terms of fluid movement. In this study, we did not used the SMLP to address any discretization in terms of FU. We did use as a graphic tool to indicate how FUs will present at different scales. This is a concept like sequence stratigraphy studies where higher and lower orders of cyclicity can be individualized using the Wheeler Diagram (Wheeler, 1958) for example, as a graphic tool.

We can measure different scales in the SMLP plot. Higher and lower orders of slope variations are present, expressed by the green (higher order) and black (lower order) lines in Fig. 28. We see clearly that variations of the low and high frequency are correlational since the slope of the low frequency curve depends on the constructive effect of each high frequency curve. Considering the study's objectives of characterize decametre flow units using the seismic data as constraints, as discussed in the Seismic Scale section, we considered, as a starting point for our analysis, the number of four FU, which corresponds to the lower order of slope variation in Fig. 28 (black lines). We found the same high and low frequency variations in the depth versus accumulated normalized FZI plot, as suggested by Da Rocha et al. (2019).

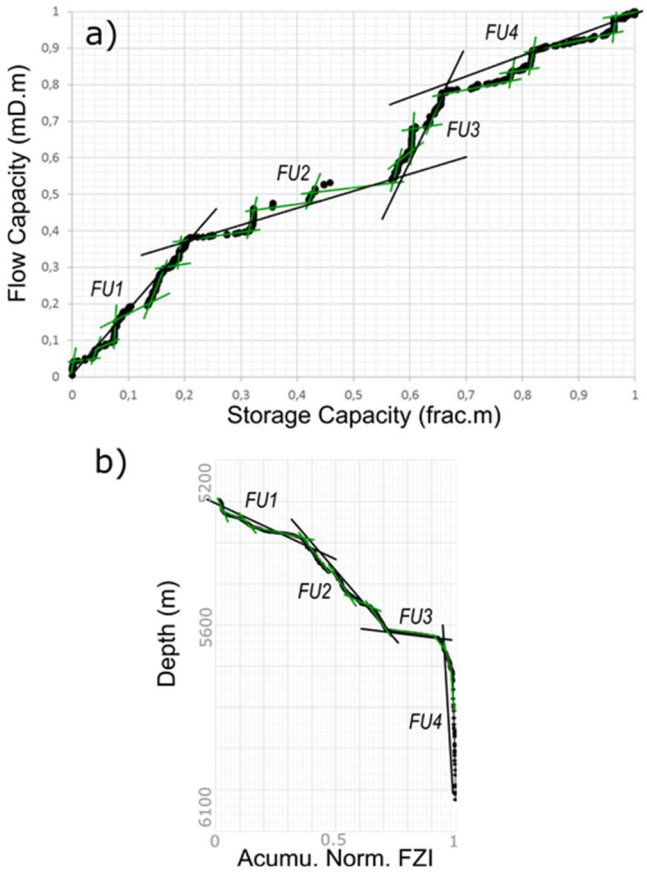

Fig. 28 – (a) SMLP from the core permeability and porosity measurements. (b) Depth versus accumulated normalized FZI values, also evidencing the same FU orders of variation. We can observe higher (green lines) and lower (black lines) orders of flow units.

We choose the RQI/FZI method for rock typing into flow units for the study area because of the large number of core permeability and porosity measurements. Due to the high geological heterogeneity of the Mero reservoir, a conventional analysis of RQI/FZI produces a large number of FUs, as evidenced by the small-scale variation in Fig. 28. Given the scale differences between the core and well log data and the seismic data, we prefer to discretize the RQI/FZI rock typing using percentiles values and a cumulative S-curve of core permeability/porosity data, and then analyze the slope variation of this plot. The steps to construct the RQI/FZI curve are:

1- Calculate porosity and permeability percentiles of the core dataset;
2- Calculate RQI and FZI values using Eq. 19, Eq. 20 and the percentiles values;
3- Order the data with increasing values of log (FZI);
4- Accumulate and normalize the percentiles of permeability values;
5- Calculate the slope of the curve for each sample.

As we observed in the SMLP, two ranges are observable in the derivative data: one on a small scale (higher order), related to metric variations, and other on a large scale (lower order), related to decametre variations (Penna and Lupinacci, 2020). The four decametre FU detected in the SMLP graph are expressed in the RQI/FZI calculation as the major jumps in the derivative data, here named as FU1 to FU4. We can infer that the use of percentiles and cumulative data comprises a powerful tool to visualize higher order variations in the data. This is understandable, given that a running sum in the frequency domain works as a high-cut frequency operator.

FU1 is considered a barrier or baffle zone and corresponds to the initial flat segment of the curve with near zero permeability. FU2 relates to the initial detachment of the curve, with reduced but considerable flow capacity in the decametre scale. FU3 relates to the first ramp up after the FU2 cut-off value and an increasing steep curve. This is a reservoir rock with greater permeability and good flow performance. Finally, FU4 corresponds to the better flow characteristics and relates to the final step of the S-curve. We used the log (FZI) values as cut-offs for the segmentation of each rock typing, shown in Table 5.

Table 5 — FU and log (FZI) cut-offs from the FZI S-curve.

	Log (FZI) values
FU1	below -0.5
FU2	-0.5 to 0.67
FU3	0.67 to 1.49
FU4	above 1.49

We constructed a k versus ϕ semi-log plot and created regressions per flow units from core permeability and porosity (Fig. 29). It is evident that there is a scatter around each FU regression line, suggesting that a higher frequency classification is more adequate to this dataset. However, using the concept of decametre flow units, we expect to gain lateral predictability of the petrophysical properties, even that means losing vertical resolution. This is a constant trade-off that we must manage when integrating data with scale differences. For comparison, Fig. 29 also exemplify porosity versus permeability regressions using the lithology description facies distinguishable at seismic scale. These facies (carbonates, microporous and

igneous rocks) are based on the rock texture and have no correlation to the FU classification by no means, as discussed in Penna and Lupinacci (2020). Note that, for our dataset, reasonable permoporous correlations per lithology are difficult. This relates to the fact that the lithological description neglects diagenetic effects that occur differently in later stages of the geology history of the reservoir. However, those effects are indirectly estimated using flow units.

From the effective porosity and permeability of the nuclear magnetic resonance (NMR) logs, we calculated the RQI/FZI values using Eq. 19 and Eq. 20 for the wells drilled in the area. We consider the Schlumberger-Doll Research permeability estimation (Al-Ajmi and Holditch, 2001), that uses the log mean of relaxation time T2 of NMR logging (small relaxation time corresponds to small pores, while large relaxation time reflects the larger pores). Fig. 30 shows the flow units rock typing applied for the wells 1, 3 and 7. In these wells, it is evidenced that most carbonates with recrystallized silica were classified as FU1, low porosity-permeability values. This is quite notable at the bottom of the Itapema Formation in Well 1, where the silicon content raises to about 25% and the FU1 is predominant. Igneous rocks were also characterized as FU1. Low-energy carbonates with fine sediments, as mudstones, were classified mostly as FU2, as seen in segments where gamma ray values increase. Carbonates with better permoporous conditions were classified as FU3 or FU4, depending on the silicon content and porosity/permeability values.

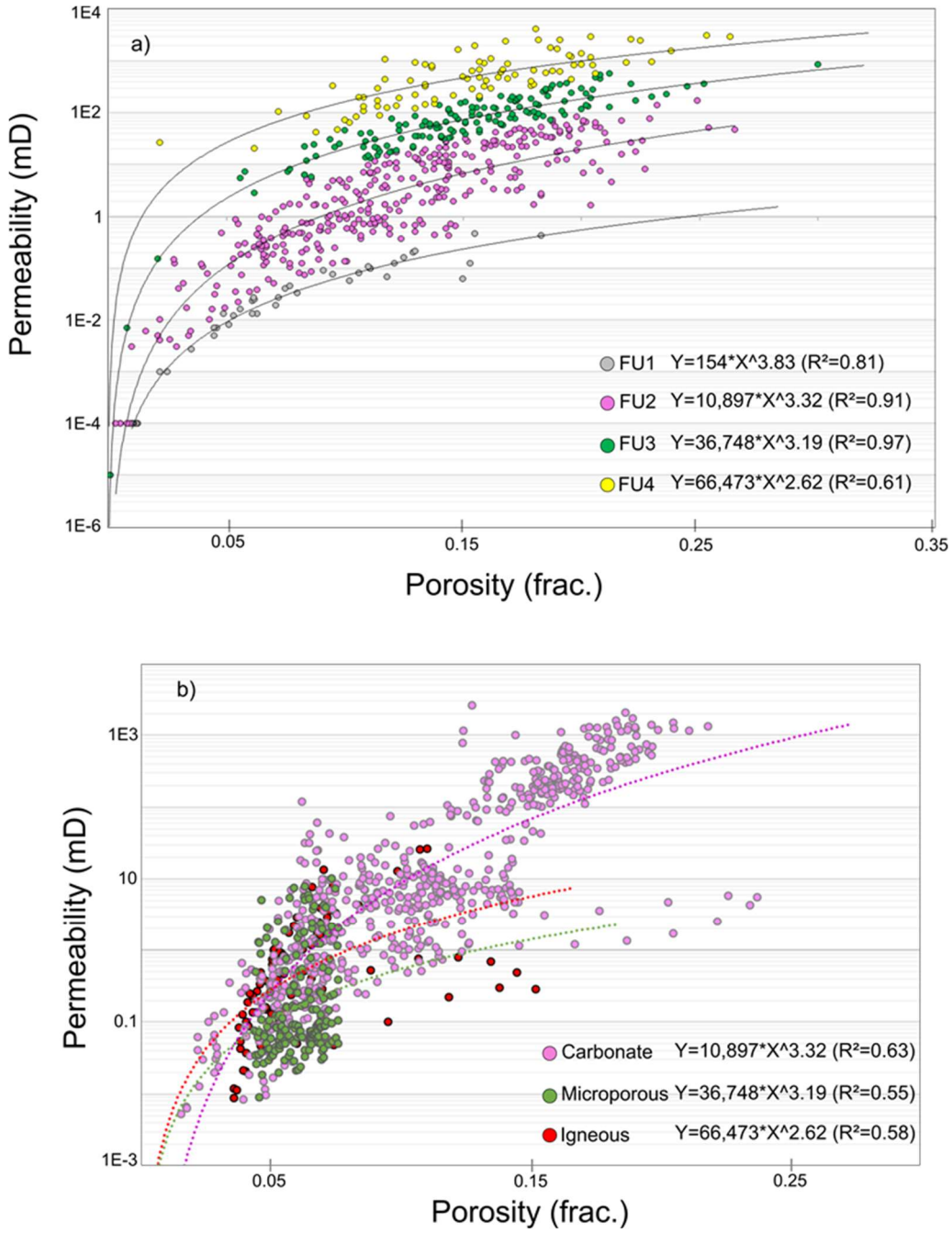

Fig. 29 – (a) Porosity versus permeability regressions per flow units according to the discretization proposed in Table 5. (b) Porosity versus permeability regressions per lithology description.

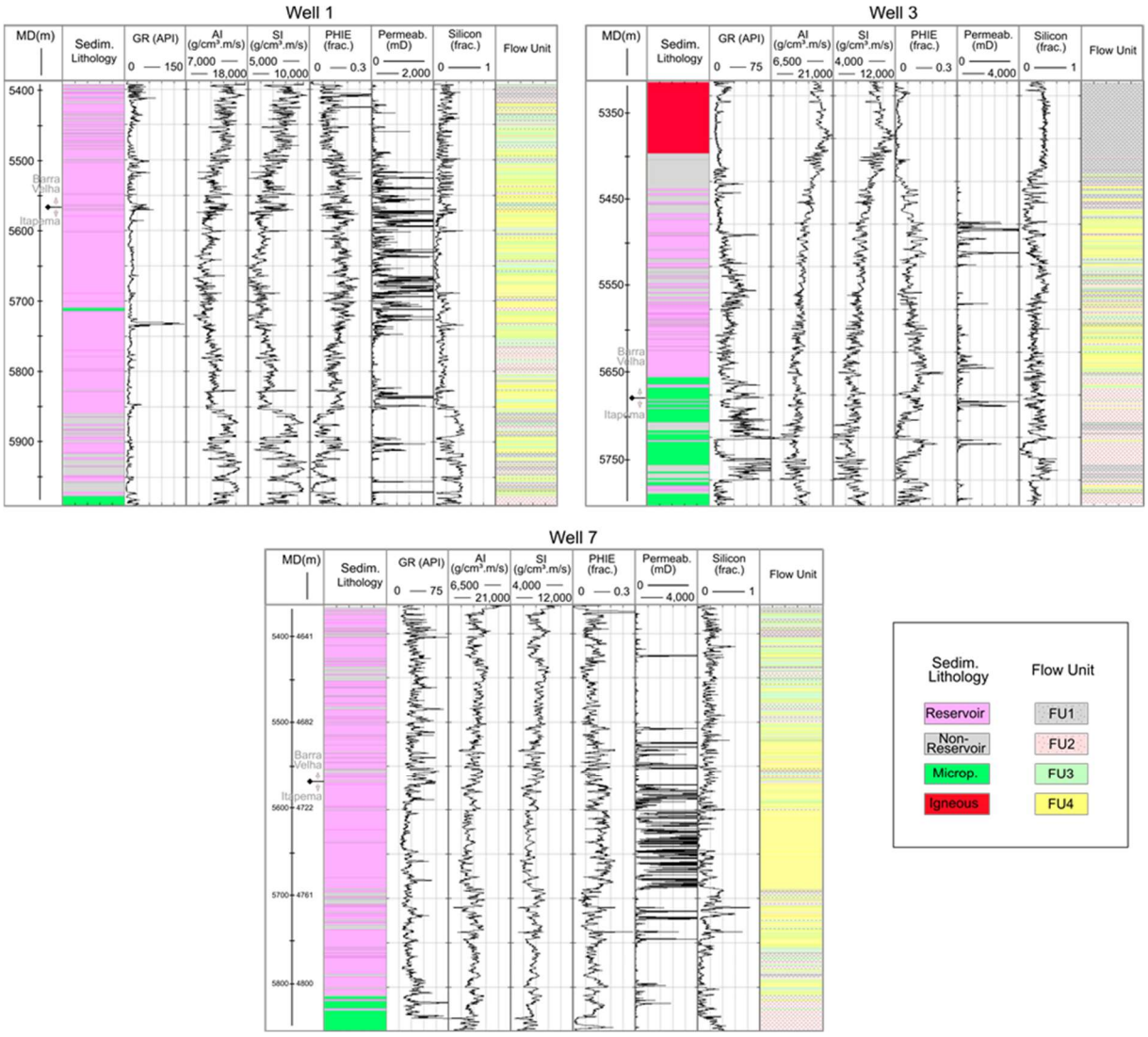

Fig. 30 – FZI rock typing applied to wells 1, 3 and 7 using the cut-offs defined in Table 5. FU1 correspond to the worse decametre flow unit in term of reservoir flow performance, while FU4 denotes high-permeability facies. The first track is the sedimentary classification and the last track is the flow unit classification.

3.5.1 Seismic 1D Feasibility

To verify how the discretization of decametre flow units behaves in the elastic space, considering the vertical resolution of the Mero seismic dataset, we performed a 1D feasibility study using time-filtered versions of well logs for the frequency content of the elastic parameter volumes (0-60Hz), that is, with minimum inversion thickness of 23 m. For discrete well logs, like the flow units, we considered the upscaled facies as the one that occurs with the greatest frequency given a running analysis window.

Fig. 31 shows how each flow unit separates in the filtered elastic domain, considering the P- and S-impedances values within each decametre FZI. As seen also in well logs in Fig. 30, FU1 tends to present higher values of impedances, while FU4 corresponds to lower values. This is expected, considering that FU1 and FU2 are mostly comprised of low porosity and silicon cemented carbonates, while FU3 and FU4 correspond to higher porosity and calcium-pure carbonates. Due to the reduced number of FU used in the study, we can note some superimposed zones between each of the four FUs in the elastic domain. This mean that a single pair of P-impedance and S-impedance values can relate different flow units, resulting in some level of classification errors when predicting petrophysical parameters within FUs. Similar analysis from the elastic characteristics of Mero lithological facies reservoir can be seen in Penna et al. (2019).

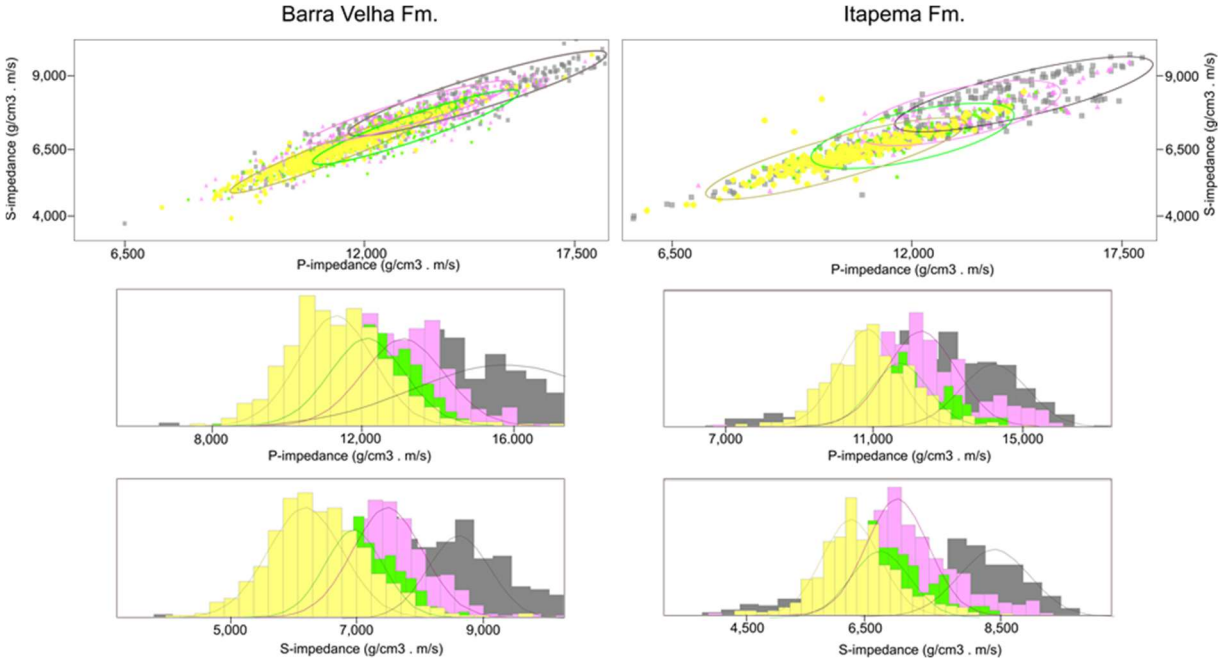

Fig. 31 – P-impedance and S-impedance crossplots (top) and histograms (bottom) of the RQI/FZI flow units distributions in the filtered elastic domain with the probability density functions (pdfs) for each FU. Left plots correspond to the Barra Velha Formation and right plots correspond to the Itapema Formation.

We performed a Bayesian classification to provide a quantitative analysis of the probability occurrence from each flow unit, given the high-cut filtered version of the well logs as inputs. Bayesian's theorem describes the posterior probability $p(m \mid z)$ of the parameters model m given the observed data z:

$$p(m \mid z) = \frac{p(m)\,.\;p(z \mid m)}{p(z)}, \tag{22}$$

where $p(m)$ and $p(z)$ are the probabilities of observing m and z independently, respectively, and $p(z \mid m)$ is the conditional probability the z given m.

Given the 3D discretization of FU using seismic derived elastic property volumes, we can rewrite Eq. 22 as:

$$p(FU \mid PI, SI) = \frac{p(FU)\,.\;p(PI,\ SI \mid FZI)}{p(PI,\ SI)}, \tag{23}$$

where $p(FU)$ is a priori estimation of occurrence probability for each facies. For that, we used a relative FU facies count for each well. The term $p(PI,\ SI \mid FU)$ corresponds to the probability density function adjusted for each FU in the P-impedance (PI) versus S-impedance (SI) crossplot (as seen in the histograms in Fig. 31), and $p(PI,\ SI)$ is a normalization factor (joint probability of PI and SI). Fig. 32 shows the resulting classification, considering all the time-filtered inputs. Note that because of the seismic vertical resolution, several thin layers are not identified in the Bayesian classification. However, the results are consistent and the main units are well ranked on the scale of impedance volumes.

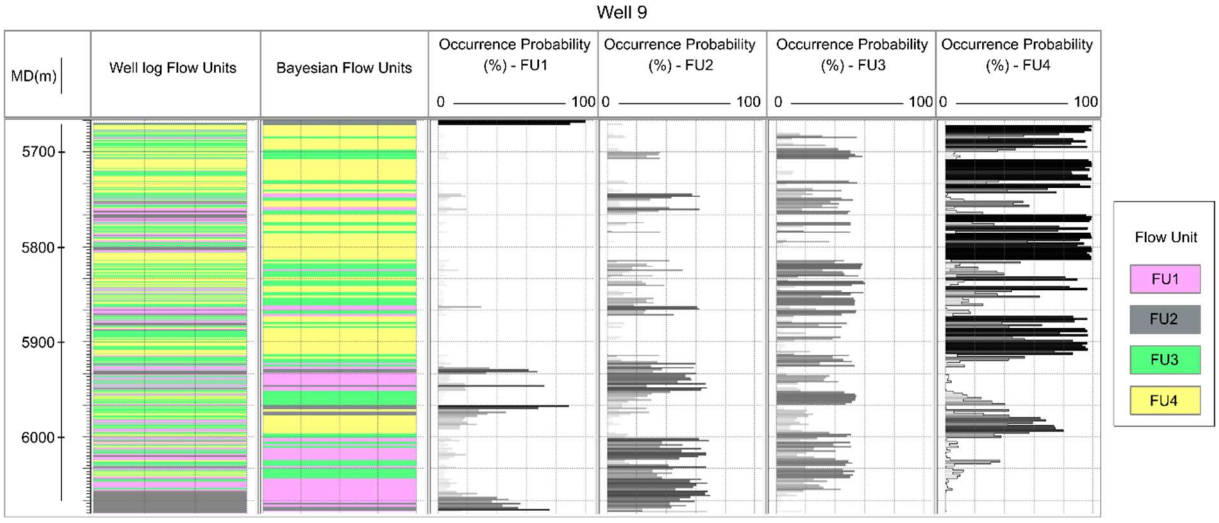

Fig. 32 – Bayesian classification of RQI/FZI flow units in decametric seismic inversion scale in Well 9. Note that the lower vertical resolution intrinsic in inverted data results in some vertical detectability loss of thin layers.

3.5.2 Prestack Seismic Inversion

We performed the calculation of P-impedance (PI) and S-impedance (SI) volumes through a sparse-spike prestack seismic inversion (Pendrel, 2001) using seven partial angle stacks derived from the RTM data (Penna et al., 2019). We analyzed the AVO response of the reservoirs of the Mero Field to generate the angle stacks, considering four degrees of overlap between each stack. The angle ranges are 6-14º, 10-18º, 14-22º, 18-26º, 22-30º and 24-32º. Individuals wavelets were calculated from each angle stack using a combination of zero phase long-window wavelets and well-constrained short-window wavelets.

We constructed a low frequency model up to 4 Hz using four seismic interpreted horizons: base of salt (top of the Barra Velha Formation), top of the Itapema Formation, base of the Itapema Formation (top of the Piçarras Formation), and the Basement top. The PI and SI well logs were interpolated using an ordinary kriging technique (Azevedo and Soares, 2017). We did not consider any uncertainty analysis of the low-frequency influence on the final PI, SI and density volumes, because we assume that the amount of wells drilled in the area is enough to obtain an accurate low-frequency model. We discussed some of the quantitative results obtain with accuracy using the elastic seismic attributes in Penna et al. (2019). As previously discussed, working with elastic inversion volumes provides an advantage over amplitude seismic due to the increase of vertical resolution brought by low and high frequency content. Low frequencies are artificially incorporated using the well logs, while high frequencies result by the seismic amplitude deconvolution process.

Fig. 33 exemplify one NW-SE section resulting from prestack inversion in Mero reservoir. In general, the results show a good correlation between the original (well logs) and inversion impedance values, which confirm the robustness of the seismic inversion results. Most of the P-impedance errors are concentrated in the high values of the intrusive rocks. This is due to these rocks are mostly found near the base of salt, where occurs a lot of tuning effects and high impedance contrasts between the salt and carbonate layers. Even with the vertical resolution increase with the seismic inversion, it is hard to correctly reproduce the real thickness and impedance values in these conditions. The dispersion around the S-impedance estimation is commonly higher than the P-impedance for Brazilian presalt data, explained due to the worse signal/noise ratio in the far angle stacks, compared to the near angle stacks (Penna et al., 2019).

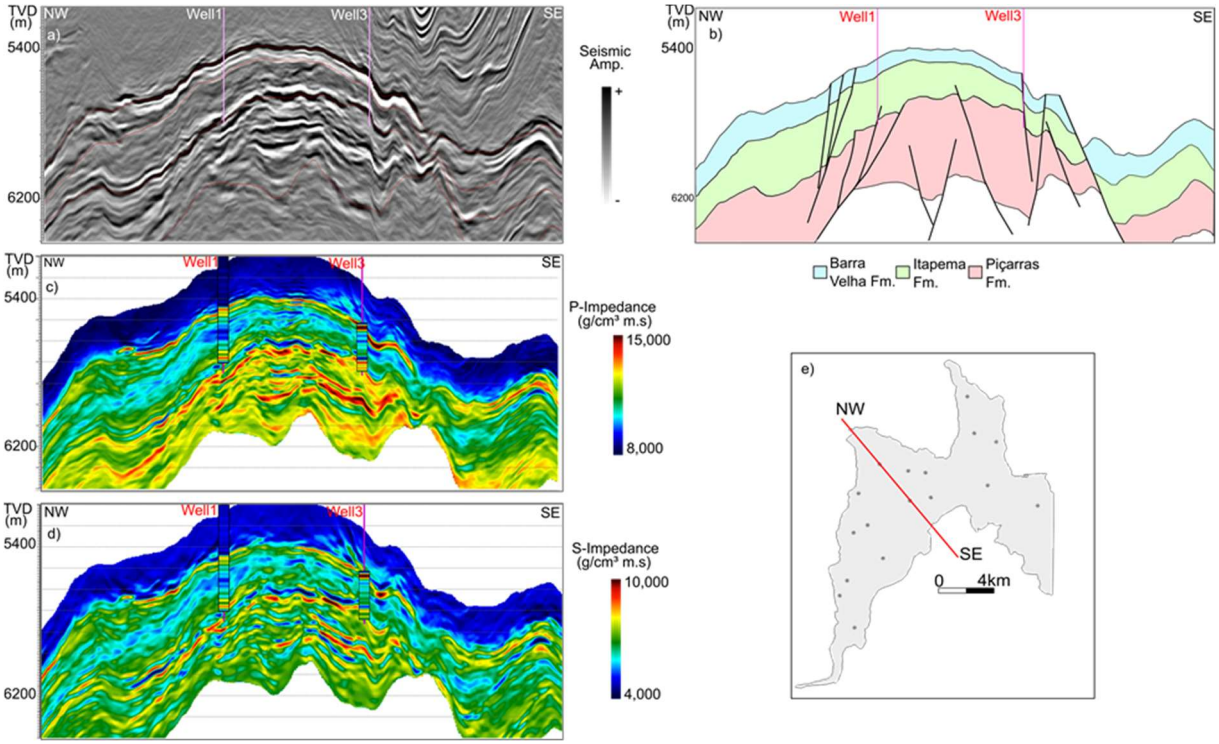

Fig. 33 – NW-SE (a) seismic amplitude, (c) P- and (d) S-impedance sections resulting from the sparse-spike prestack inversion. (b) The interpreted horizons are, from top to bottom, base of salt, top of the Itapema Formation, base of the Itapema Formation and the Basement. (e) Mero Field baseline with the NW-SE section.

3.5.3 Seismic Quantitative Interpretation for Decametre Flow Units

We applied Eq. 23 to obtain occurrence probability of decametre flow units in the 3D grid using the P-impedance and S-impedance volumes. For this, we calculated distinct probability density functions (pdfs) for the Barra Velha and Itapema formations, considering the impedance logs, as shown in Fig. 31. The priori probabilities volumes for each FU were built using a relative proportion of FU per well that were extrapolated to the grid through ordinary kriging, considering the interpreted seismic horizons as stratigraphic control.

The outputs of the Bayesian inference were five volumes: one discrete, called most probable FU and four different occurrence probability volumes for each decametre flow unit. The most probable volume consists of the corresponding discrete data with the higher occurrence probability for a given sample. Each occurrence probability volume varies from zero to one, and the sum of all the probabilities for a given sample is always one.

Fig. 34 exemplifies an E-W section with the five calculated Bayesian probabilities. The thick FU4 response in the upper-middle part of the Itapema Fm. corresponds to a large bivalve

rudstone (coquina) bank, deposited during the late stage of the rift phase. This lithofacies is one of the best reservoirs of the Mero Field in terms of permoporosity, and a detailed study about the textural and taphonomic characteristics of this type of reservoirs is found in Chinelatto et al. (2020). Most of the Barra Velha Fm. presents FU3, which also has good conditions. At the upper part of the Barra Velha Fm. has continuous layers of FU1 and FU2, especially near the western flexural edge. This is related to an increased silica concentration, as seen in the top of well 1 and well 3 in Fig. 30. The predominance of FU1 is notable in the eastern part of the section, but, in this case, it is due to the presence of intrusive igneous rocks, probably related to the fault plane presents in that part. Microporous sediments (mostly clay-enriched carbonate) also appear as a continuous FU1 layer near the base of the Itapema Fm.

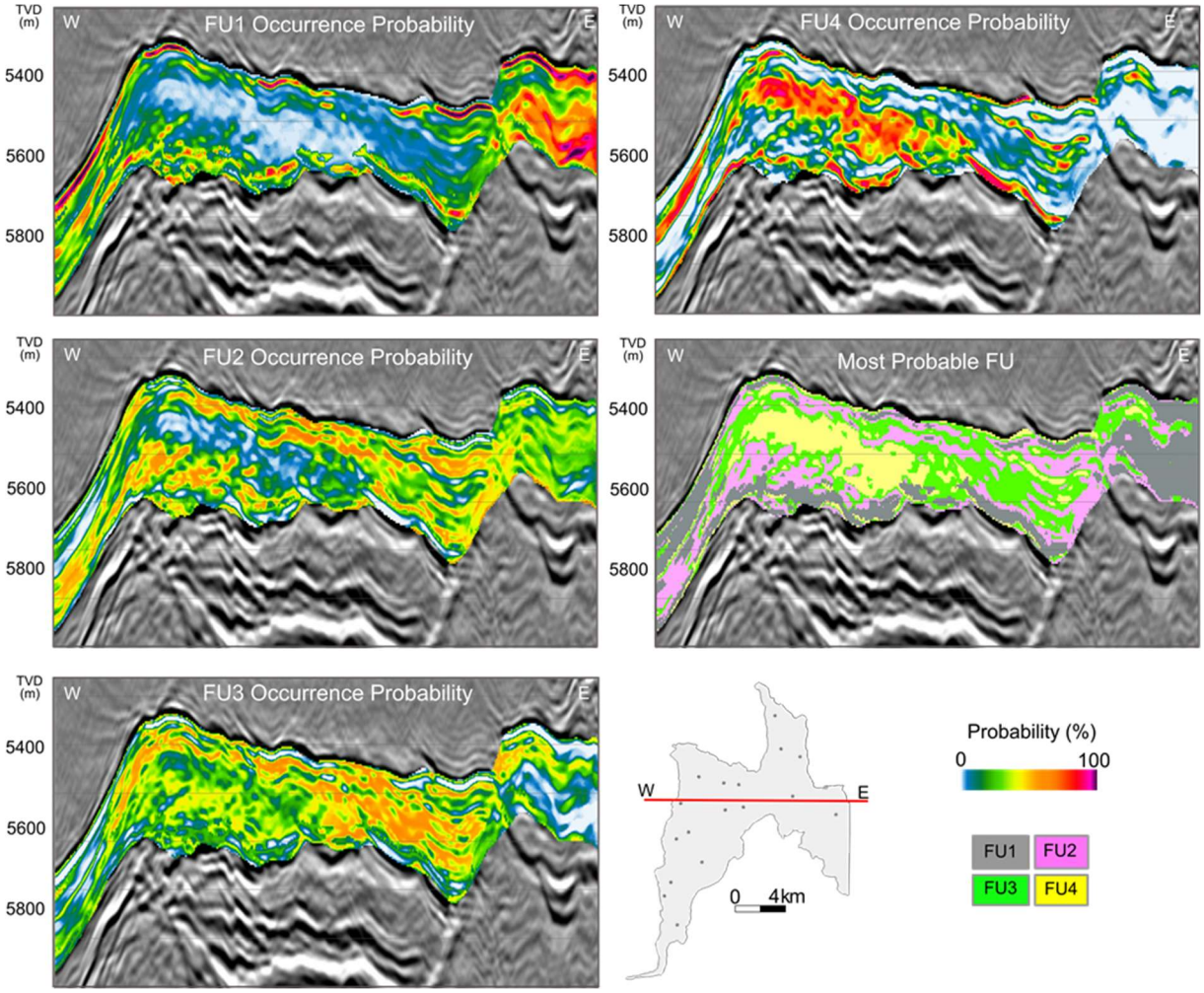

Fig. 34 – Section E-W showing occurrence probability for four decametre flow units and the most probable FU.

Toward the generation of seismic derived petrophysical parameters considering the decametre flow units concept as constraints, we created empirical PI versus ϕ regressions for each FU. The link between porosity and P-impedance is one of the most important rock physics relation for seismic quantitative interpretation. Several rock physics models use this link to characterize and predict the permoporous reservoir behavior (Avseth et al., 2005, Ferreira and Lupinacci, 2018; Peçanha et al. 2019, Lupinacci et al., 2020). Fig. 35 shows the PI versus ϕ relations for each FU stablished using the P-impedance and the NMR effective porosity of well logs. We also presented a comparison of the FU-porosity versus the lithology-porosity (in this case, using regressions for reservoir and non-reservoir carbonates, igneous and microporous sediments). It is important to mention that due to the bulk compressibility characteristics of the reservoir (relatively high values of bulk and shear modulus), the discretization of carbonates using the lithology description is quite incipient. For instance, a separation between rudstones and shrubs or even water-saturated carbonates between oil-saturated carbonate are not possible through elastic attributes.

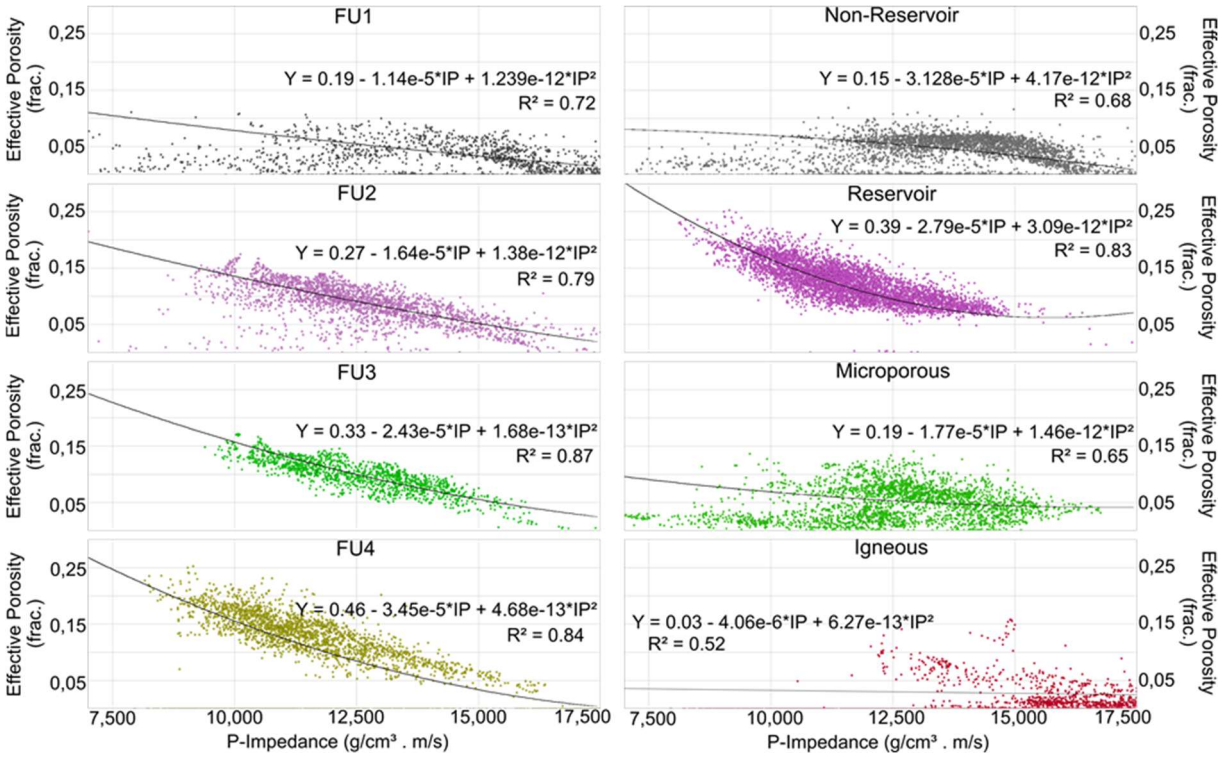

Fig. 35 – PI versus porosity regressions for decametre flow units (left) and lithologies (right).

We can observe that the PI versus ϕ dispersions around each lithological facies are higher than the dispersions around each FU (Fig. 35). In general, constraining the seismic porosity estimation using flow units provides results that are more accurate, as seen in the well

logs, percent errors and crossplots in Fig. 36. The usage of lithological facies to constrain the seismic estimation of porosity overestimate low-porosity values and underestimate high-porosity values.

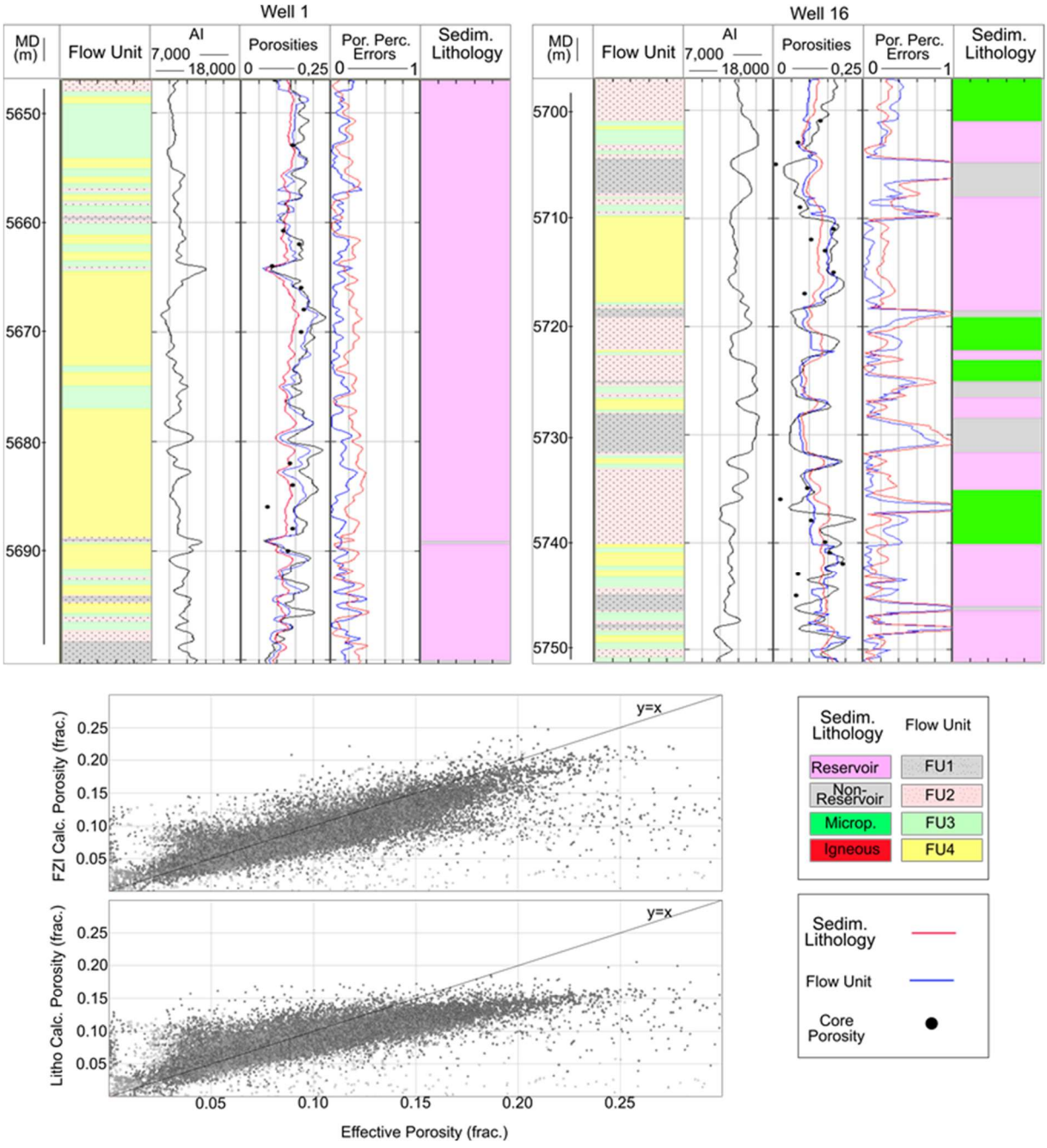

Fig. 36 – (top) Comparison between porosities obtained from regressions by FU (blue curve) and by lithology (red curve) with NMR porosity (black curve) in well 1 and 16. (bottom) NMR porosity (x-axis) and porosities using regressions by FU and by lithology (y-axis) considering all wells.

The relations established in the well logs between FU-porosity and lithology-porosity (Fig. 35) were extrapolated in the 3D grid on the decametric scale using, respectively, the most likely models of FU and lithologies obtained by the Bayesian classification. For more details of 3D modeling for lithologies using the Bayesian classification in the study area see in Penna et al. (2019). Fig. 37 shows a comparison in two sections of the porosities obtained from FU and from lithology. The results using FU were more accurate and with a higher resolution in estimating porosity for thin layers. From our approach, we can identify layers with an intermediate range of porosity that were not previously invisible considering the lithological restriction. As shown in Fig. 36, the porosity from FU shows higher values, above 0.20, mainly at the top of the Itapema Fm., where the bivalve rudstones (coquina) are predominant. The observation is also valid for lower porosity values, below 0.05, more noticeable in the upper part of the Barra Velha Fm., due to the presence of intrusive igneous rocks and the silica recrystallization in carbonates.

Extending the petrophysical properties, we calculated permeabilities based on the decametre flow unit concept (permeability-porosity regressions using equations shown in Fig. 29), and compared them with the permeabilities estimated from the lithologies (permeability-porosity regressions per lithology). For this, we considered the NMR effective porosity as inputs and the Schlumberger-Doll Research permeability as a benchmark (Fig. 38). The usage of decametre flow units as constraints provides a much better permeability estimation in Mero reservoir. The crossplots of the permeability measured and estimated in Fig. 38 demonstrate that percent errors using FU are generally between zero and 3%, while using the lithology the percent error is spread above 10%.

The resulting permeabilities from the FU and lithology constraints are shown in sections and maps in Fig. 39. It is evident that the use of the decametre FU provides a better estimation of the permeability volume, in terms of the layer definition and the permoporous conditions. The same analyzes performed with porosity apply to the results of permeability, although the differences are more evidenced between the permeability volumes per FU and per lithology.

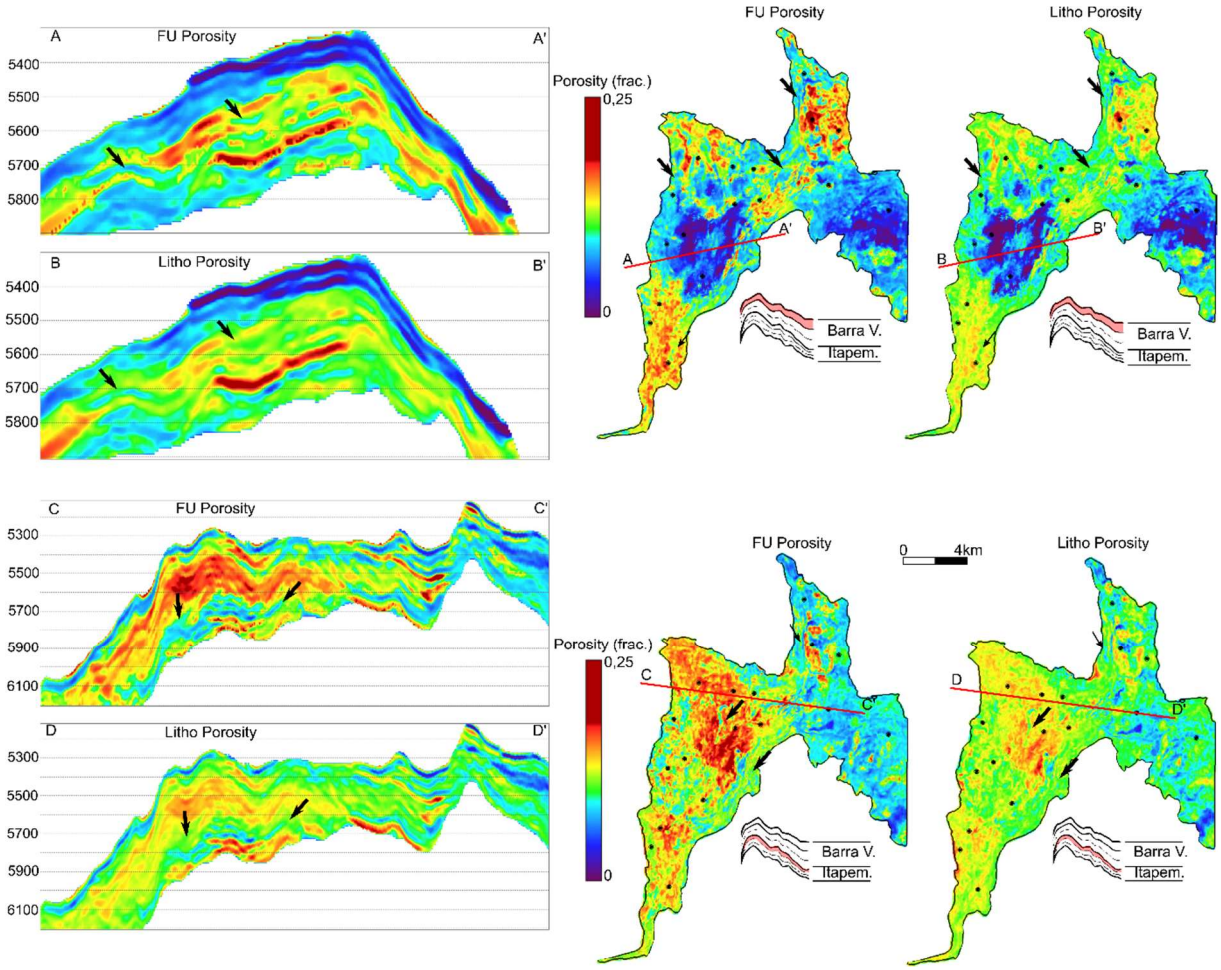

Fig. 37 – Comparison between the porosities from FU and from lithology. Sections of FU-porosity (A and C) and lithology-porosity (B and D). Average porosity maps of the tops of the (top) Barra Velha and (bottom) Itapema Formations.

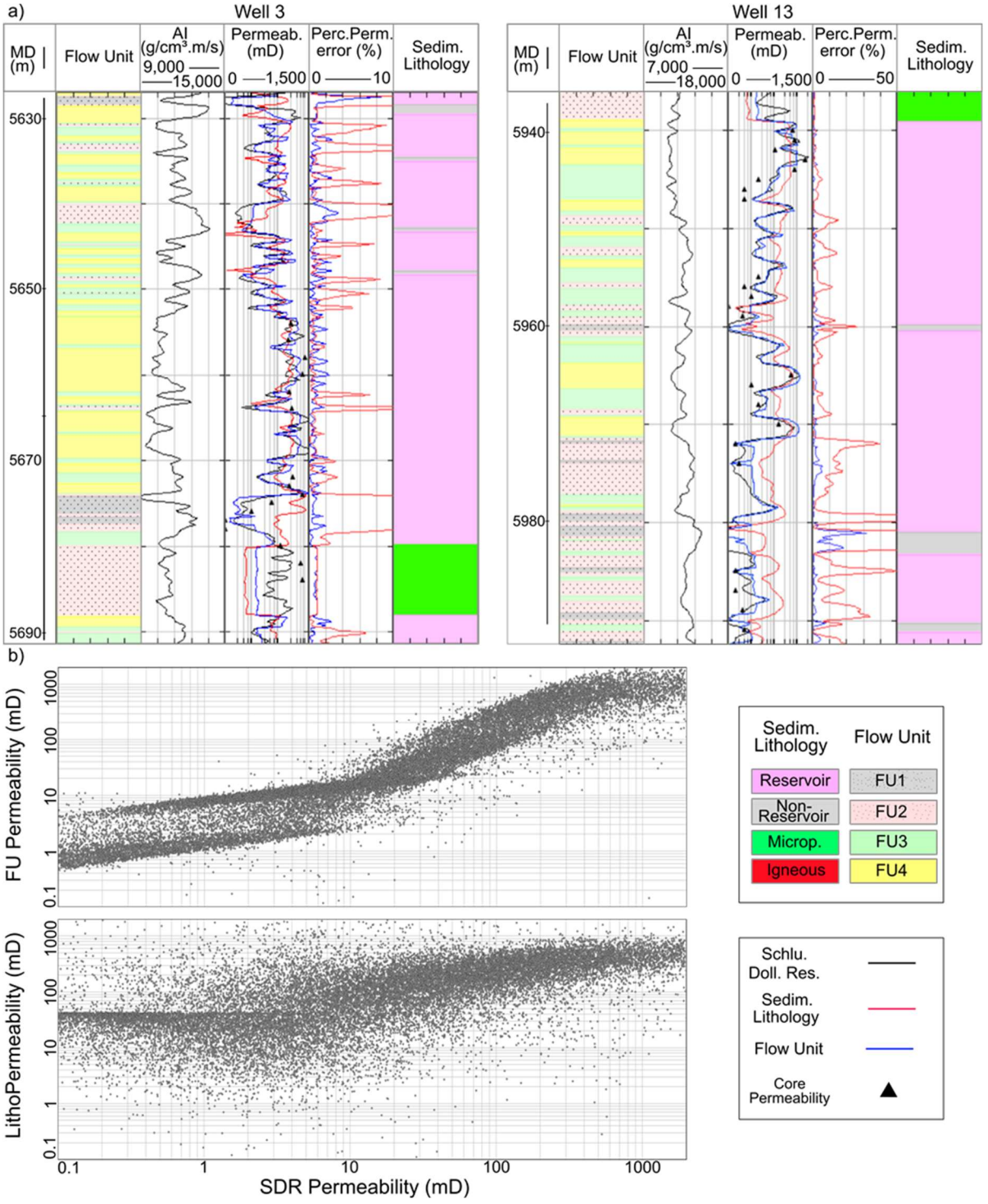

Fig. 38 – (a) Comparison between permeabilities obtained from regressions by FU-porosity (blue curve) and by lithology-porosity (red curve). (b) SDR permeability (x-axis) and permeabilities using regressions by FU-porosity and by lithology-porosity (y-axis).

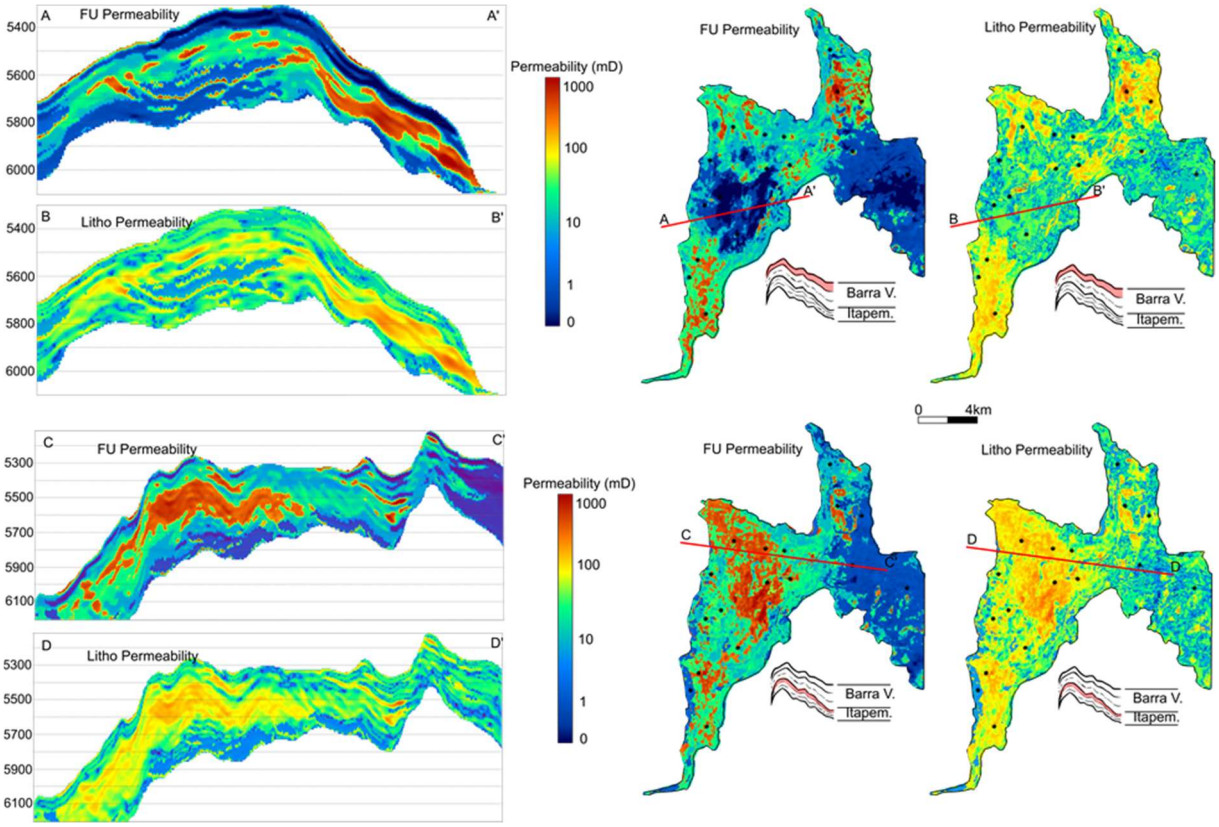

Fig. 39 – Comparison between the permeabilities from FU-permeability and from lithology-permeability. Sections of FU-permeability (A and C) and lithology-permeability. (B and D). Average permeability maps of the tops of the (top) Barra Velha and (bottom) Itapema formations.

To validate our three-dimensional results, we compared the porosity and permeability values extracted in well locations from the sections discussed in Fig. 37 and Fig. 39. We called these extracted values as pseudologs, and the comparison between estimated and profiled ϕ and k are displayed in Fig. 40. We can see, apart from the scale differences (seismic inversion derived results are a smoothed version of the well logs), that the results are quite consistent, capturing the main variations of porosity and permeability. This is what we expect for the decametric characterization of the reservoir: to evidence variations of a lower order in terms of fluid movements. However, some differences between the estimated and profiled values are notable, most of them related to seismic noise or signal degradation in those places. For example, near the depth 5650 m in Well 11 (Fig. 40), it is possible to notice that the porosity and permeability derived from the seismic inversion are overestimated when compared to the well logs. In that location, the seismic signal is degraded in the Barra Velha section due to the presence of a seismic migration artifact, which is repeat near the top of the Itapema Formation,

also generating errors near the depth 5760 m. P- and S-impedance estimates are affected when the seismic signal is compromised, and, consequently, porosity and permeability estimates are also affected. Small errors and miscalculation are also present, and we relate this to the dispersion of the P-impedance versus porosity fit in the decametric FU template, as shown in Fig. 35. In almost the whole section, the FZI calculated permeability and porosity is more accurate than the lithology calculated ones.

Analyzing the porosity and permeability calculated on the decametric scale, we note that the response of the flow units in terms of pore generation/obliteration processes comprises a sum of all factors that occur at smaller metric scale. Although some indication of fracture permeability and transmissibility are seen in EWT and dynamic data, at seismic-decametric scale, we do not believe that high permeability corridors or layers will be detectable or successfully classified using our technique. Fig. 41 shows that the FU1 and FU2, with worse permoporous conditions, are related to intrusive igneous rocks as well as both silicification and dolomitization processes (silica and dolomite replacing calcite), represented as higher concentrations of calcium, magnesium and silicon, while FU3 and FU4 present dominance of clean calcite carbonates, with little diagenetic effects. These results are same as those found by Vasquez et al. (2019) in their petroacoustics studies in Brazilian presalt carbonates. Although the understanding and identification of each individual diagenetic process is important, as it can show different porosity and permeability relations at metric scale (Grude et al. 2015), they will have the same meaning in terms of flow simulation at decametre scale. Depending on how each individual effect overlaps, the results on decametric scale may be a single flow barrier zone in the reservoir, for example, or a high permeability layer. Usually, most flow simulators grids have decametre cells-size, so they fit for this purpose.

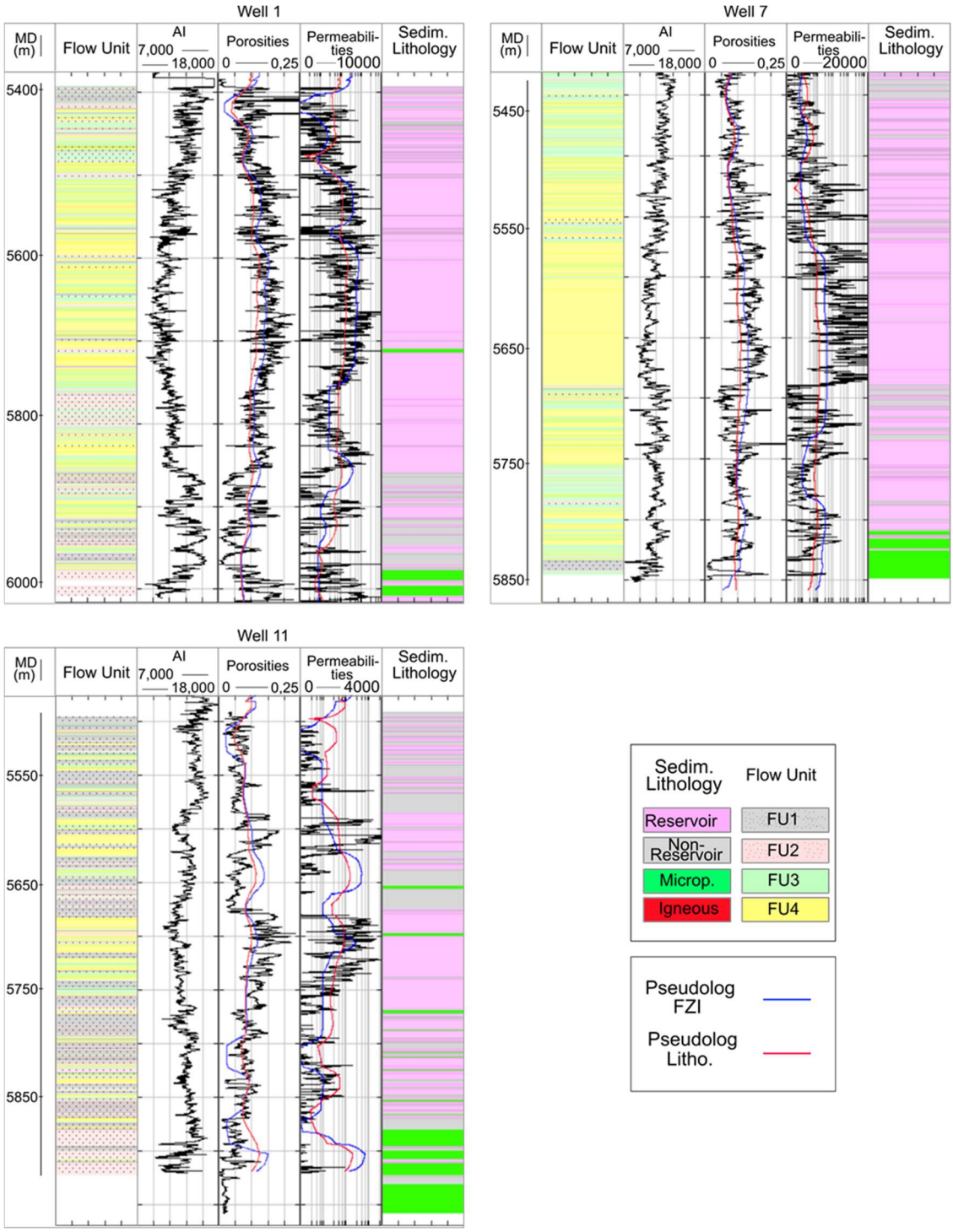

Fig. 40 – Pseudologs extracted at three well locations from the 3D volumes of porosity and permeability compared with the porosity and permeability well logs.

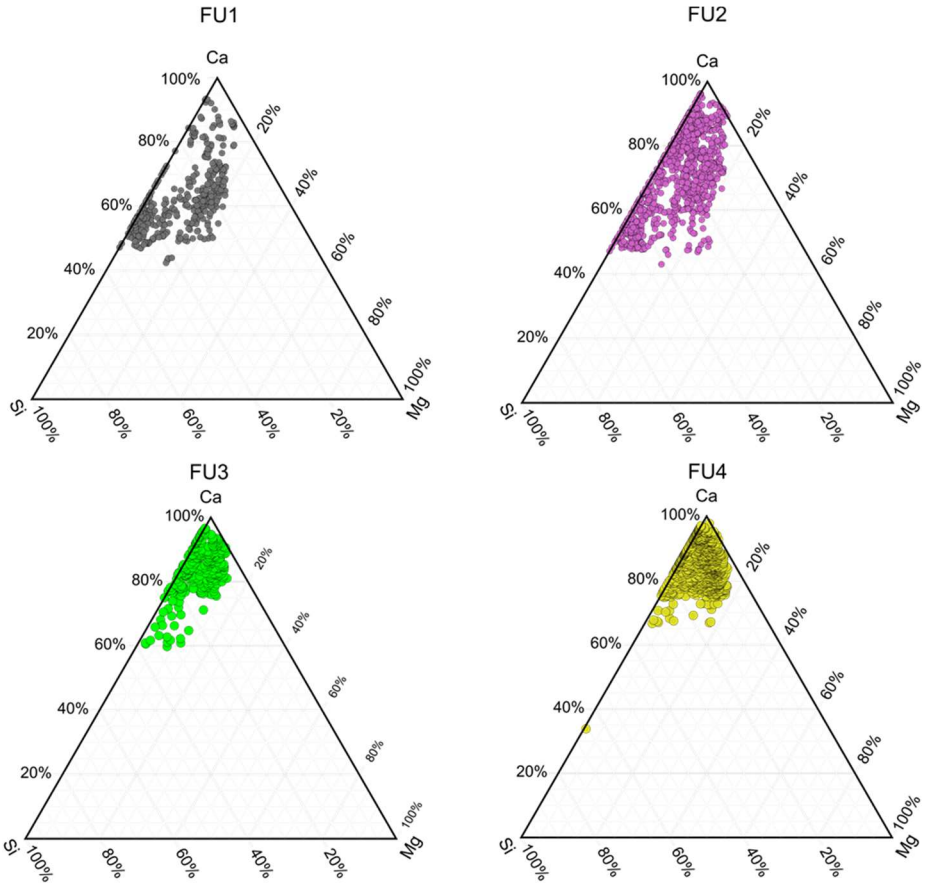

Fig. 41 – Ternary diagram of calcium (Ca), magnesium (Mg) and silicon (Si) by FU in Well 1. In the decametric scale, degrees of pore obliteration due to dolomitization and silicification (Si and Mg substituting Ca) are mixed.

3.6 Conclusions

The use of decametric flow units as a constraint to estimate petrophysical properties at seismic inversion scale produces much better results than using the lithology classification. In our approach, we noticed that the calculated porosity difference is smaller due to the strong impedance-porosity relation independent of the scale. For the permeability estimation, the usage of decametric flow units proved to be crucial to achieve good results due to the indirect consideration of diagenetic effects. We consider that the accurate mapping and comprehension of the flow behavior at decametric scale is the first step to build the dynamic knowledge of the reservoir at smaller scales, especially considering all the concerns and difficulties to incorporate FU into geologic models built essentially on analogs, sedimentary facies and conceptual premises. Our methodology provides ways to generate a minimum amount of FU that calculates porosity and permeability with acceptable accuracy and are correlatable with elastic attributes on seismic inversion scale. We believe that petrophysical estimations derived from decametre

flow units by our approach will have great impact on the static model building, as well as 4D seismic interpretation and seismic assisted history matching. The proposed method shows that the use of seismic elastic inversion laterally predicting decametric flow units and producing reliable petrophysical parameters is possible. However, due to the elastic characteristics of the Mero reservoir, the evident loss of vertical resolution, the need to simplify the analysis reducing the number of FU, and the presence of high superimposed zones of each FU in the elastic domain, we strongly suggest an uncertainty analysis and different decametric flow unit occurrence scenarios using the a posteriori probability volumes later during the static model building stage. We also suggest considering the interpretation of the second most probable FU in the Bayesian calculation as a different occurrence scenario. Areas with similar values of FU occurrence probability should have a closer look.

4. Geostatistical Seismic Inversion and 3D Modelling of Metric Flow Units, Porosity and Permeability in Brazilian Presalt Reservoir

Article submitted to: **Petroleum Science**.

Impact Factor: 4.757

Authors: Rodrigo Penna and Wagner Moreira Lupinacci

4.1 Abstract

Flow units (FU) rock typing is a common technique for characterizing reservoir flow behavior, producing reliable porosity and permeability estimation even in complex geological settings. However, the lateral extrapolation of FU away from the well into the whole reservoir grid is commonly a difficult task and using the seismic data as constraints is rarely a subject of study. This paper proposes a workflow to generate numerous possible 3D volumes of flow units, porosity and permeability below the seismic resolution limit, respecting the available seismic data at larger scales. The methodology is used in Mero, a Brazilian presalt carbonate reservoir located in Santos Basin who presents a complex and heterogenic geological setting with different sedimentological processes and diagenetic history. First, we generated metric flow units using the conventional core analysis and transposed to the well log data. Then, given a Markov chain Monte Carlo algorithm, the seismic data and the well log statistics, we simulated p-impedance, decametric flow units (DFU), metric flow units (MFU), porosity and permeability volumes in the metric scale. The aim is to estimate a minimum amount of MFU able to calculate realistic scenarios porosity and permeability scenarios, without losing the seismic lateral control. In other words, every porosity and permeability volume simulated produces a synthetic seismic that match the real seismic of the area, even in the metric scale. The achieved 3D results represent a high-resolution fluid flow reservoir modelling considering the lateral control of the seismic during the process and can be directly incorporated in the dynamic characterization workflow.

4.2 Introduction

Complex geology reservoir systems present many challenges to generate coherent static and dynamic models for reservoir simulation. The representation of reservoir heterogeneities

and flow patterns comprehend the most important step to predict subsurface fluid movement, production and injection, especially in giant oil fields where forecast errors can result in a great loss of investment.

Flow units (FUs) reservoir rock typing can present an advantage over lithological rock typing in the 3D model building process using seismic data as a constraint, as FU provides better estimations of reservoir petrophysical properties, like porosity (ϕ) and absolute permeability (k), even in complex geological settings (Penna and Lupinacci, 2021). Once FUs may not have any relation with the lithology, incorporating FUs into reservoir models, which are essentially built with geological premises, is quite challenge for any asset team. Lithological facies, for instance, can comprehend two distinct FUs, depending on the diagenetic evolution of both rocks. Due to pore obliteration or generation processes, lithological facies would present different fluid flow and petrophysical patterns, and different consequences when submitted to production or injection (Penna and Lupinacci, 2020).

FU rock typing has been performed from flow zone indicator (FZI) (Nabawy et al., 2018), electrical parameters (Ghanbarian et al., 2017), FZI-star (Mirzaei-Paiaman et al., 2018; Rocha et al., 2019) and mercury injection capillary pressure (Liu et al., 2019), demonstrating how FUs are a powerful tool to predict storage and flow capacity of the reservoir, regardless of the geological complexity. Penna and Lupinacci (2021) show that the 3D porosity and permeability performed based on FU is a valuable and accurate tool to be incorporated into workflows in the construction of reservoir models.

Because of the FU incorporation difficulties and lack of correlation with lithological facies, most 3D static models built from FU are merely a geostatistical procedure away from the well control, without any lateral constraint of the facies interpolation (Li et al., 2018; Zhang et al., 2018). However, recent studies have incorporated seismic data into the FU modelling workflow for the FU interpolation. Iravani et al. (2018) considered the acoustic impedance as constraint for the lateral interpolation of petrophysical properties in a FU template. Yarmohammadi et al. (2014), Rastegania et al. (2016), Hatampour et al. (2018) applied artificial intelligence to obtain linear relationships between FU and seismic attributes, creating their constraints to the 3D FU facies modelling. Penna and Lupinacci (2021) used a cumulative S-curve analysis to create a decametric FU rock typing, and, through a Bayesian probabilistic model, modeled 3D porosity and permeability, adequate to the seismic acoustic impedance resolution. All these seismic-generated FU models can later be successfully incorporated in the

static modelling workflow of the reservoir, as hard constraints or secondary variable in co-kriging techniques.

The usage of seismic attributes provides lateral control for FU interpolation away from the well and is especially relevant in large reservoirs with a reduced number of drilled wells. However, the vertical resolution of deterministic seismic inversion products is limited to the decametric scale, above 20m for Brazilian presalt reservoirs (more details in Penna and Lupinacci, 2021). In seismic-incorporated FUs and fluids movements detection, the scale of observation is crucial as, for instance, porous fractured media will be more or less connected depending on the grid size (Haridy et al., 2020). Conventional methods of seismic facies classification do not extrapolate the vertical resolution further from the input data limit and, considering that most of the FU classifications are made in the core scale (millimetric) and then transposed to well log scale (centimetric), several upscale and downscale assumptions are needed to incorporate the decametric seismic results (Penna and Lupinacci, 2021).

This paper proposes an approach to estimate seismic derived petrophysical property volumes at the metric scale. Using data percentiles and a cumulative S-curve from the core porosity and absolute permeability, we calculated a significant number of decametric and metric flow units that correlates with seismic acoustic impedance and responds for both large and small scales flow characteristics of the reservoir. Within each iteration of decametric and metric flow units from the geostatistical seismic inversion, we co-simulated 3D volumes of petrophysical properties that respect the well information in the metric scale and are laterally consistent with the local geology and the acquired seismic data, regardless of the input resolution limit.

4.3 Study Area and Geological Settings

Mero reservoir, part of the Libra block, locates in the northeast portion of the Santos Basil, Brazil (Fig. 42). The consortium that operates the field consists of Petrobras, Shell, Total, CNOOC and CNPC, under the new Brazilian production-sharing contract ruled by Pré-Sal Petróleo S.A. (PPSA). The initial exploratory phase of the block estimates an oil in place volume between 8 to 12 billion BOE (Carlotto et al., 2017), with high-complexity geology, igneous rocks occurrence (Oliveira et al., 2019; Penna et al., 2019; Penna and Lupinacci, 2020; 2021) and diagenetic effects (Leite et al., 2020; Sartorato et al., 2020).

One of the main hydrocarbon fluid characteristics from Mero Field is the high CO2 content (44% in the gas phase), which imposes several challenges to the reservoir management.

The production design comprises a Floating Production Storage and Offloading (FPSO) designed to reinject all the gas produced (Moczydlower et al., 2019). The drilled wells by the consortium are keepers and will be used as producers or water alternating gas (WAG) injectors.

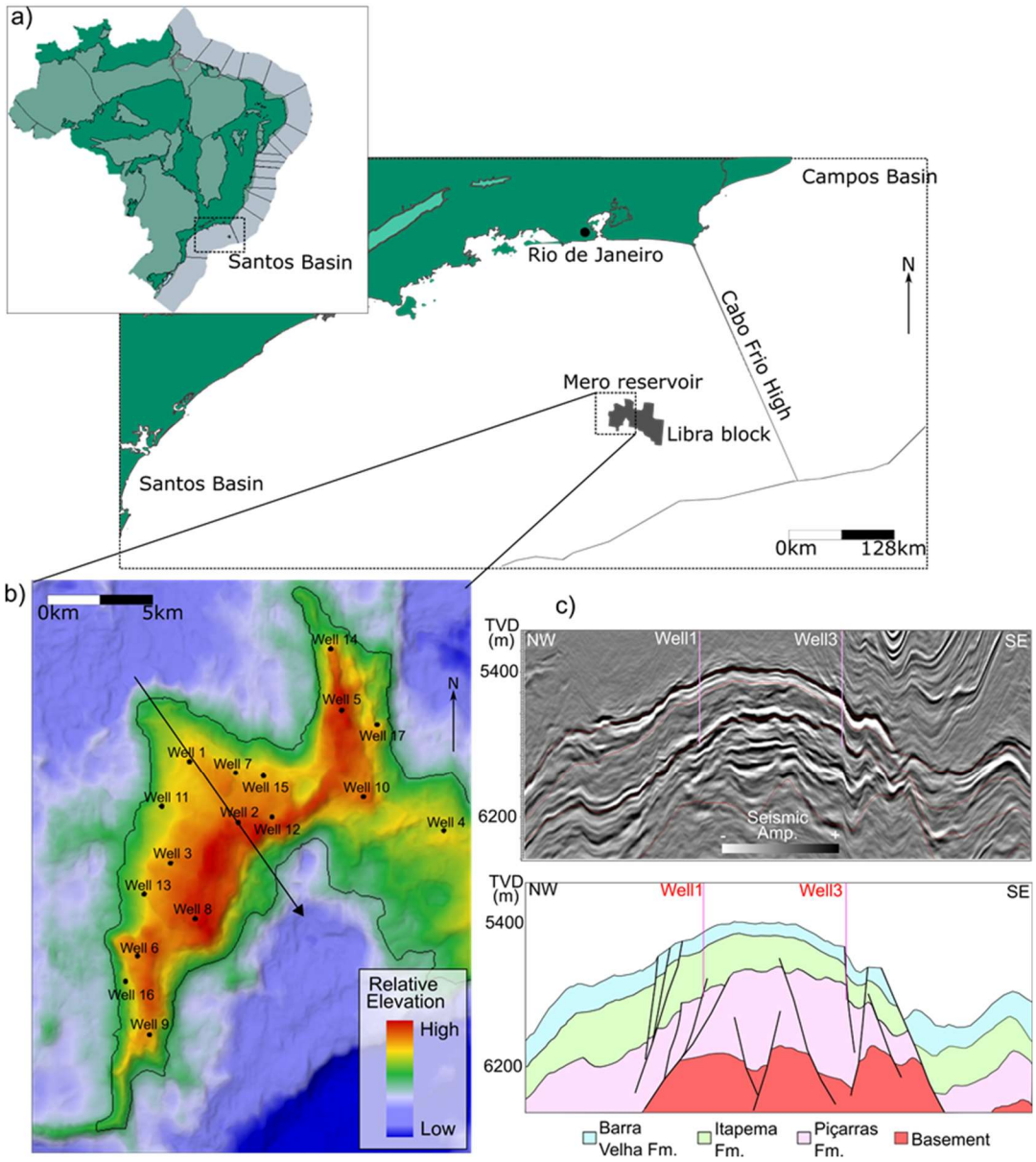

Fig. 42 – (a) Mero reservoir and Libra block location in southeast Brazil. (b) Top of reservoir (Barra Velha Formation) structural map. (c) NW-SE seismic section a stratigraphic interpretation (after Penna and Lupinacci, 2021).

Santos Basin evolution history (also Libra block, consequently) initiates with basalts from Camburiú Formation (138 to 130 million years) as the response for the initial Gondwana breakup. Piçarras Formation (Barremian age) corresponds to the initial rift stage of the continental breakup, with sandstones, mudstones and shales deposited in lacustrine

environments. From the Neobarremian until Eoaptian ages, rudstones from Itapema Formation were deposited in high energy platform settings. In lower energy settings, usually in relative structural low, organic rich shales occur. These rocks are considered the main hydrocarbon source in the Santos Basin. The Barra Velha Formation deposits are from transitional environments between continental to shallow marine settings, the lower part to the intra-Alagoas unconformity still belongs to the rift phase and the upper part belongs to the sag phase. The base of the sequence are predominantly grainstones and packstones (reword facies), while in the top shrubs, spherulites and laminites (in-situ facies) occur more frequently (Gomes et al., 2020). In the late Aptian, already in marine environment, a thick salt sequence from Ariri Formation were deposited. This layer is the main Santos basin hydrocarbon seal and is mainly composed by halite and anhydrite (Moreira et al., 2007). Fig. 43 shows the Santos Basin pre-salt lithostratigraphy, tectonic evolution and unconformities adopted in this work.

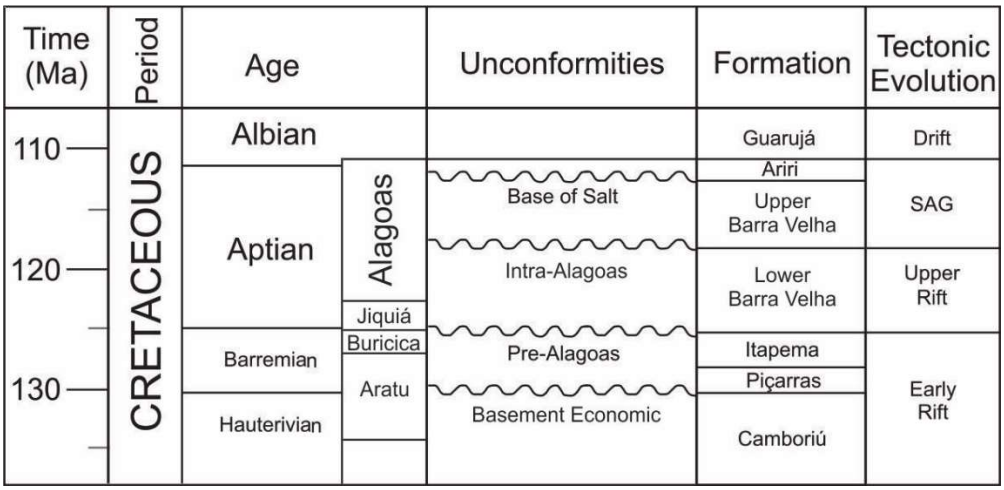

Fig. 43 – Santos Basin pre-salt lithostratigraphy, tectonic evolution and unconformities (After Buckley et al., 2015; Wright and Barnett, 2015; Neves et al., 2019).

Mero Field main reservoir rocks are bivalve rudstones (coquinas) from the Itapema Formation and shrubs and spherulites from the Barra Velha Formation, although high porosity is also found in rework facies as bioclastic floatstone, grainstones and, packstones (Jesus et al., 2019; Penna and Lupinacci, 2020; Penna and Lupinacci, 2021). Several diagenetic effects of dissolution and neomorphism, replacement of minerals, silicification and dolomitization are identified, and corresponds to the main effects that controls porosity generation and/or obliteration and, consequently, fluid movements in the reservoir (Herlinger et al., 2017, Gomes et al., 2020, Leite et al., 2020 and Sartorato et al., 2020).

A unique feature of Libra block and Mero reservoir is the abundant igneous rocks presence (Oliveira et al., 2019; Penna et al., 2019). Extrusive igneous rocks are Barremian/Aptian age and are mainly composed by tholeiitic basalts, more commonly found below Itapema Formation (Penna et al., 2019). Intrusive igneous rocks are from Santonian/Campanian ages, mainly alkaline, and can occur anywhere in the stratigraphy cutting surrounding rocks or concordant to the sedimentary layering (e.g., top of the Barra Velha Formation). The correct mapping and prediction of these rocks are very relevant for the characterization and management of the reservoir, once they penalize the total oil in place volume, can act as flow barriers (or even high permeability layers, if fracturing is high enough) and contributes to the regional aquifer and pressure maintenance.

4.4 Data Available

The consortium that operates the field performed an extensive core program with approximately 500m of linear samples taken in both Barra Velha and Itapema formations. 1700 conventional core and plug analysis measurements of porosity and permeability are available in different stratigraphic levels from seventeen drilled wells. We organized and analyzed this datasheet for the purpose of flow unit classification. Twelve well logs are also available and comprehends sets of both logging while drilling (LWD) and wireline: gamma ray, resistivity, compressional and shear slowness, density, nuclear magnetic resonance porosities (total, effective and free fluid) and permeability and elements (e.g., calcium, potassium and magnesium)

The seismic data is a legacy seismic acquisition that cover the whole Libra block with an 8 km streamer cable length, 6.25 x 25m grid and 5m of vertical sampling. This data was pre-stack reprocessed in 2016 with an initial tilted transversely isotropic (TTI) velocity model and a vertical transversely isotropic full waveform inversion (VTI-FWI) from 3 Hz to 45 Hz. Then, a multi-layer tomography using both Kirchhoff and Reverse Time Migration (RTM) picks was performed, followed by a TTI-FWI from 7 Hz to 8 Hz applied at the entire geologic sequence (pos-salt, salt and presalt) as detailed by Araujo et al. (2015). For the FWI velocity model, high and low-salt velocity layers, like anhydrite, taquidrite, carnallite and sylvinite, as well as igneous rocks, within the salt stratification, were incorporated. This procedure is presented and discussed and by Seifert et al. (2017).

In the presalt interval, the seismic data has approximately 15 Hz of peak frequency, with bandwidth of 5 to 35 Hz. Based on the local geology petrophysical characteristics and the seismic spectral distribution, Penna and Lupinacci (2021) created a wedge model to estimate the vertical resolution of the full-stack seismic considering the true thickness resolving capacity. According to their analyses, the vertical resolution is 62m when considering the seismic amplitude and 23m from inverted acoustic impedance volume, thus any layer below these limits will be falsely estimated in terms of thickness. This means that facies or flow unit mapped from seismic amplitude or inverted acoustic impedance volumes will present decametric proportions.

4.5 Metric Flow Units Facies Discretization and Rock Typing Statistics

Considering the amount of conventional core analysis available in Mero reservoir, we used two methods based on permeability (k) versus porosity (ϕ) for flow unit discretization. First, we considered Gunter et al. (1997) stratigraphic modified Lorenz plot (SMLP) as a visual aid to estimate a minimum number of flow units and identify local reservoir flow trends in both decametric and metric scales. Then, we calculated rock quality index/flow zone indicator (RQI/FZI) for the discretization (Amaefule and Altunbay, 1993). Those are both extensively documented methods successfully applied in both clastic and carbonate geological settings.

The SMLP was first introduced by Gunter et al. (1997) by plotting the percent storage capacity (product of porosity and thickness) versus percent flow capacity (product of permeability and thickness), providing a visual guide to estimate how many flow units (FUs) are necessary to honor the geologic framework in terms of fluid movement in the subsurface. Fig. 44 shows the SMLP plot of both Barra Velha and Itapema formations. The minimum number of FU estimation is performed observing the slope and behavior of the curve: as the mean storage and flow capacity increases, we have better flow units in terms of its permoporous characteristics. In that sense, flat segments can correspond to seals, baffle zones or low-production zones, as they may present some level of porosity, but have limited contribution of permeability. Steep segments correspond to “speed zones” of the reservoir, they can have low or high porosity, but provide major contributions to the reservoir flow performance.

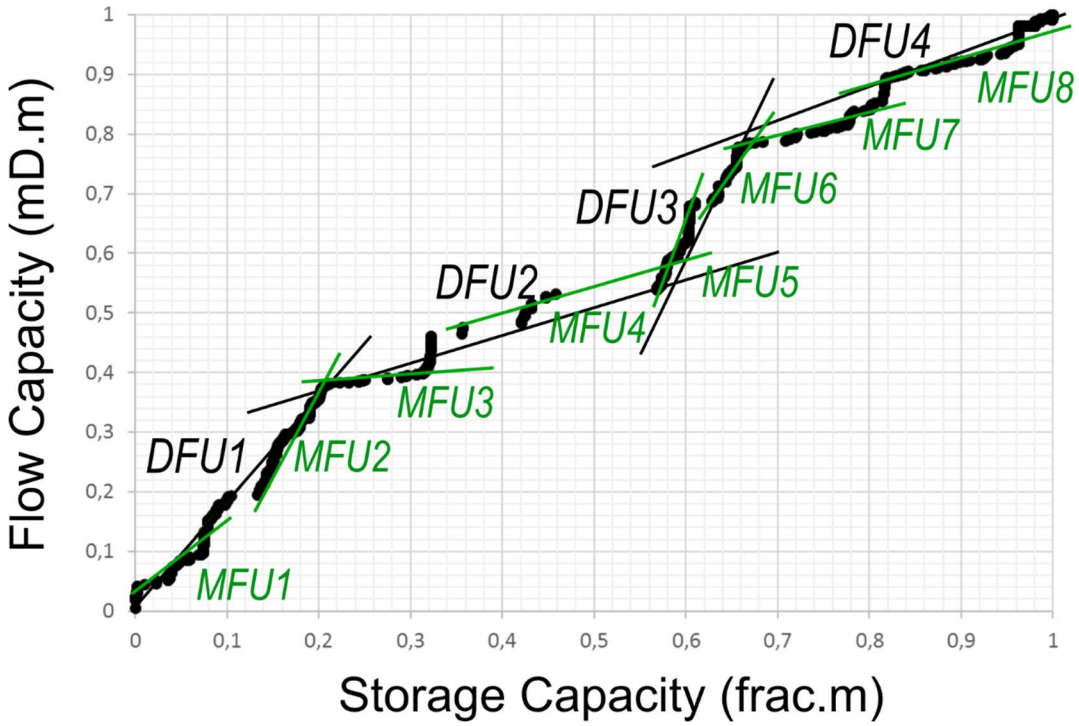

Fig. 44 – Barra Velha and Itapema formations SMLP. Black lines: decametric scale flow units. Green lines: metric scale flow units.

We estimated the minimum number of flow units in the SMLP using a sequence stratigraphy reasoning for high order and low order variations, like a Wheeler Diagram interpretation (Wheeler, 1958). The plot in Fig. 44 clearly demonstrates how the flow unit characterization is scale dependent. Variations of the low- and high- frequency cycles are correlational since the slope of the low frequency curve depends on the constructive effect of each high frequency curve. Penna and Lupinacci (2021) introduced a workflow for the detection of decametric flow units using inverted acoustic and shear impedance volumes, considering the black lines as decametric trend (Fig. 44). However, our purpose here is to characterize higher orders of fluid movements in the reservoir as metric flow units using the acoustic impedance as constraints obtained from a geostatistical inversion. For this, eight FU are considered as metric flow trends (green lines) in Fig. 44.

The flow unit discretization is performed in the core analysis using the rock quality index/flow zone indicator (RQI/FZI), and then transposed to the well log data. This method is based on permeability (k) in (mD) and effective porosity (ϕ_E) ratio and derived from a Kozeny-Carmen equations generalization (Kozeny, 1927). It was introduced by Amaefule et al. (1993)

and is widely used due to its simplicity and assertive results. Let the index RQI (reservoir quality index, in μm) be:

$$\mathrm{RQI} = 0.0314 \,.\, \sqrt{\frac{\mathrm{k}}{\phi_{\mathrm{E}}}}, \tag{24}$$

where k is the absolute permeability (in mD) and ϕ_{E} the effective porosity. Then, the FZI is given by:

$$\mathrm{FZI} \ = \frac{\mathrm{RQI}}{\phi_{\mathrm{Z}}}, \tag{25}$$

where ϕ_{Z} is an effective porosity normalization on the form $\phi_{\mathrm{Z}} = \phi_{\mathrm{E}}/1 - \phi_{\mathrm{E}}$. Since its derivation from Kozeny-Carmen equations, FZI value is approximates an average pore throat radius for a given porous media, relating effective porosity, and permeability. Different sedimentation environments, late diagenetic processes and reservoir geometry are also controlling parameters of FZI (Tiab and Donaldson, 2004).

Taking log on both sides of equation 25 and rearranging it, we verify the linearity between FZI, RQI and ϕ_{Z}:

$$\log \mathrm{RQI} = \log \mathrm{FZI} + \log \phi_{\mathrm{Z}}, \tag{26}$$

In log-log plot of RQI versus ϕ_{Z}, a constant value of FZI produces an inclined straight line. The inference is that samples with similar flow behavior falls around a corresponding slope line, determining a single flow unit (FU). Samples with distinct flow characteristics are plotted in different parallel lines and arrange distinct flow units.

Different methodologies for clustering samples around FZI values and creating FU are available in the literature and applied in different geological scenarios. In some cases, a simple log(FZI) histogram discretization is enough to discretize the flow units (considering that the samples show strong FZI versus permeability correlation and a log-normal FZI distribution). More complex methods, such as iterative multi-linear regressions (Ajmi and Holditch, 2000) and normal probability plots (cumulative distribution function, Mahjour et al., 2016) are also widely used, especially in more complex geological settings. Penna and Lupinacci (2020; 2021) showed that the usage of percentiles and a cumulative S-curve produced a significant minimum

amount of flow units with statistical relevance without compromising the estimation of petrophysical properties. This is particularly relevant to the scope of this study, considering the amount of k and ϕ measurements, the high complexity degree of the Mero reservoir and the aim to correlate the FU to seismic data with respect to its vertical resolution limit.

The steps to construct the RQI/FZI cumulative S-curve, as presented by Penna and Lupinacci (2021), are:

1. Take all the core porosity and permeability measurements and calculate statistical relevant percentiles (the number can vary, depending on the data characteristics. Each percentile is a representative sample from a given interval).
2. Calculate RQI and FZI values using Eq. 24, Eq. 25 and the percentiles values.
3. Order the data with increasing values of log (FZI).
4. Accumulate and normalize the percentiles of permeability values.
5. Calculate the slope of the curve for each sample (Fig. 45).

As described in the SMLP, at least two scales of variations are observable in the derivative data Fig. 44): one on a small scale (higher order), related to metric variations, and other on a large scale (lower order), related to decametre variations. Penna and Lupinacci (2021) choose to interpretate the major jumps in the slope curve as the decametric flow characteristics changes in the reservoir, although this can be extended to many scales. The lower scale of observation responds to low frequency variations in the SMLP and FZI S-curve plots, and higher order of variations responds to high frequency variations. This was fit for purpose, as the scope of their work were to characterize flow units in the decametric scale and then correlate with elastic attributes. Given that the aim of the present study is to get a step further, discretizing metric flow units with the seismic data, we interpret the major jumps in the slope plot, first order variation, that corresponds to the decametric FU, same as Penna and Lupinacci (2021), and the second order variation, as the metric FU.

Using both effective porosity and permeability from the nuclear magnetic resonance (NMR) well logs, the RQI/FZI values are calculated for each well through Eqs. 24 and 25. The discretization of FU in the metric (MFU) and decametric (DFU) scales in the S-curve plot are shown in Fig. 45. Eight metric flow units are interpreted considering the changes in the FZI S-curve slope. Note that the number of metric flow units correlates to the SMLP interpretation as a higher order variation from the decametric scale. The cut-offs in log(FZI) used for discretizing the flow metric units (MFU) are shown in Table 6.

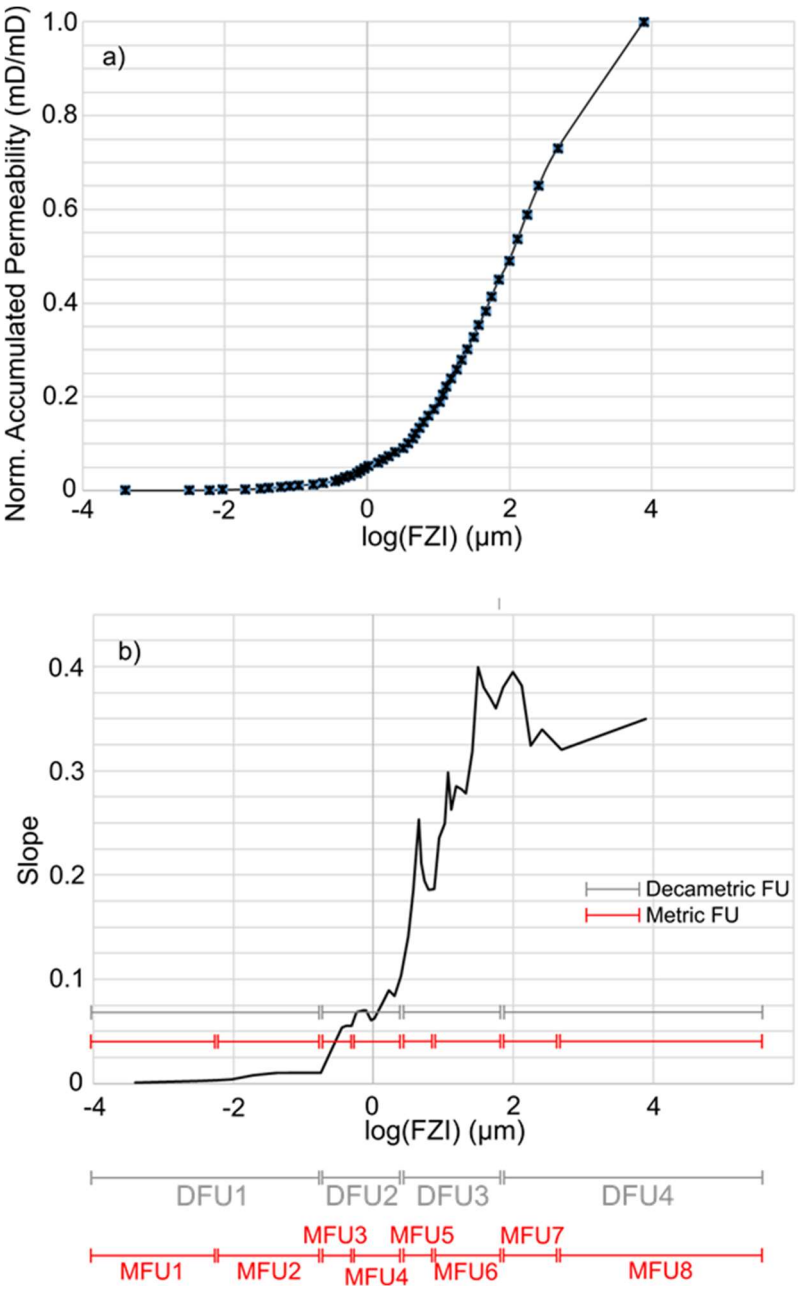

Fig. 45 – log(FZI) S-curve for MFU discretization. Grey line corresponds to decametric FU classification (after Penna and Lupinacci, 2021) and red line corresponds to metric FU classification.

Table 6 – Metric FU (MFU) cut-offs from the FZI S-curve.

	Log (FZI) values
MFU1	below -2.2
MFU2	-2.2 to -0.5
MFU3	-0.5 to -0.2
MFU4	-0.2 to 0.4
MFU5	0.4 to 0.8
MFU6	0.8 to 1.9
MFU7	1.9 to 3.7
MFU8	Above 3.7

The initial flat segment parallel to the X axis of the curve shown in Fig. 45 describes FUs that have no contributions to the flow behavior of the reservoir in the metric scale. Therefore, MFU1 and MFU2 are considered seals or baffle zones that retain fluid flow, acting as vertical and horizontal barriers. In general, rocks with reduced matrix porosity like igneous rocks, cemented and clay-rich carbonates are into these units.

The initial detachment of the curve from the X axis denotes MFU3 and subsequently MFU4 (Fig. 45). These FUs have some flow capacity but are very poor in terms of overall reservoir flow behavior. This is the typical behavior of carbonates with some late diagenetic effects, like quartz and dolomite cementation obliterating the original matrix porosity of the rock. Although not directly considered for production, they are important for maintaining reservoir pressurization over production time.

The first ramp up of the curve characterizes MFU5 and MFU6 (Fig. 45), with better permoporous reservoir characteristics then the previous units. Although some level of diagenetic effect can occur, they will have considerable contributions to reservoir flow during production. Some bioclastic grainstones, packstones and wackestones belongs to MFU5 and MFU6, for example. The end of the curve corresponds to the better FUs in terms of

permoporous characteristics of the reservoir, MFU7 and MFU8. They have considerable porosity and remarkable flow performance during production. In general, MFU7 and MFU8 correspond to clean calcite carbonates like bivalve rudstones (coquinas) from the Itapema Formation and shrubs (stromatolites) from the Barra Velha Formation, with little or none late diagenetic effects (Penna and Lupinacci, 2021).

Fig. 46 demonstrates how the new classification differs from the decametric flow unit (DFU), presented by Penna and Lupinacci (2021), and considering the seismic vertical resolution limitation. The relationship between DFU1 and MFU1 and MFU2, for instance, are quite notable, as the latter are a one-step upscaling of the first one. The mean, median and standard deviation of acoustic impedance (PI), effective porosity (ϕ) and Schlumberger-Doll Research (Al-Ajmi and Holditch, 2000) permeability (k) for each metric flow units are displayed in

Table 7. The calculations were performed using the well logs. Note that the overall values of PI tend to decrease from MFU1 to MFU8, while porosity and permeability increase. This is expected, as MFU1 corresponds to low-FZI values (small pore throat radius) and MFU8 are high-FZI values (large pore throat radius). In general, the distribution of PI, porosity and permeability for MFU are close to symmetric, with little mean versus median differences.

4.6 Geostatistical Seismic Inversion for Metric Flow Units

4.6.1 Stochastic Seismic Inversion Method

Geostatistics is a modelling tool that plays an important role in constructing earth models. In geoscience, initially developed with the constant grow of the mining industry, geostatistical concepts and algorithms have been widely adopted in the oil exploration and production for many purposes (Pereira et al., 2017; Feng et al., 2018; Kneller et al., 2019). These techniques are traditionally used to interpolate the target property, most commonly facies, porosity and permeability, between well data within a stratigraphic framework. The most common method is the Sequential Gaussian Simulation (SGS, Deutsch and Journel, 1992).

Since the introduction by Haas and Dubrule (1994), seismic stochastic inversion is an active topic of interest, as the technique introduces seismic data as a constraint to generate possible earth models (Doyen, 2007). However, the direct use of seismic as secondary data for reservoir modelling is usually frustrating because of vertical scale differences between seismic (usually decametric resolution) and well logs (centimetric). Finding a relationship between, for instance, seismic amplitude and/or impedance volumes and well log porosity is constantly difficult, making the incorporation of seismic data directly into the SGS workflow a challenge for reservoir characterization (Azevedo and Soares, 2018).

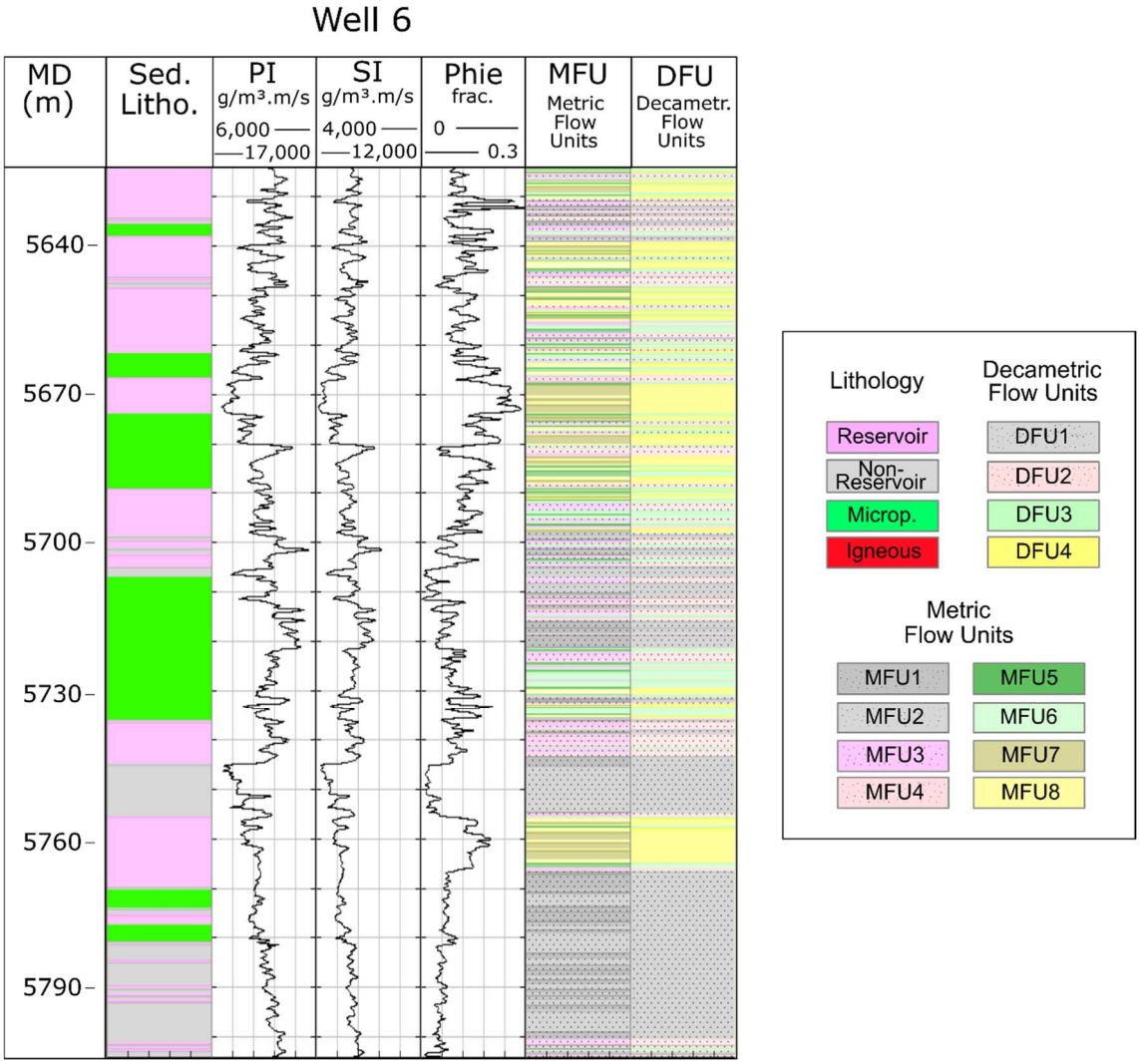

Fig. 46 – Application of log(FZI) cut-off discretization in Well 6 using the effective porosity from the magnetic resonance data. Lithologies on the left correspond to a simplified classification for seismic facies analysis purposes (after Penna et al., 2019).

Table 7 – Mean, median and standard deviation of Acoustic impedance (PI), porosity (ϕ) and permeability (k) from MFU1 to MFU8 considering both Barra Velha and Itapema formations.

		PI (g/cm³.m/s)	ϕ (frac.)	k (mD)
MFU1	mean	16,521	0.042	0.016
	median	17,478	0.044	0.005
	std. dev.	2,785	0.019	0.022
MFU2	mean	14,829	0.087	0.265
	median	15,276	0.082	0.234
	std. dev.	1,880	0.005	0.126
MFU3	mean	14,482	0.102	1.251
	median	14,869	0.102	1.057
	std. dev.	18,645	0.007	0.634
MFU4	mean	13,874	0.119	5.933
	median	14,112	0.118	5.658
	std. dev.	1,850	0.004	2.023
MFU5	mean	13,047	0.144	28.23
	median	13,814	0.144	25.85
	std. dev.	1,646	0.009	12.69
MFU6	mean	11,928	0.167	80.29
	median	11,022	0.168	78.01
	std. dev.	1,599	0.004	16.77
MFU7	mean	11,522	0.188	232,75
	median	10,874	0.188	199,08
	std. dev.	1,454	0.007	103,68
MFU8	mean	10,633	0,236	1760,67
	median	9,830	0,220	1146,7
	std. dev.	1,674	0,038	1425,33

The most documented and used methods for stochastic seismic inversion are SGS (Escobar et al., 2006), Direct Sequential Simulation (DSS, Soares, 2001), Global Stochastic Inversion (GSI, Soares et al., 2007) and Monte Carlo Markov Chain (MCMC Statmod® MCTM, Sams et al., 2011). Although these methods differ in how to sample prior/posterior pdfs, they essentially produce multiple realizations of petrophysical properties, considering the stratigraphic grid and a given vertical sampling (that can be smaller than the available seismic sampling). Every iteration produces a geologic model that fits the seismic and well log data, i. e., each realization is plausible samples of the reservoir's posterior distribution and a variance measure of the input parameters, considering the seismic data as constrains.

In this study, we perform a Metropolis-Hastings (MH) algorithm within the MCMC method (MCMC Statmod® MCTM, Sams et al., 2011) to simulate the acoustic impedance. There are three main steps in the stochastic inversion workflow, which are detailed further: 1) Statistical modelling, where are estimated the probability density functions (pdfs), variograms and trends for each decametric and metric facies; 2) Bayesian inference, combining the prior model, seismic and well data for compute the posterior distribution; and 3) Sampling, where we used the MH-MCMC algorithm for sampling the posterior pdf. Briefly, the algorithm constructs a pdf that represents P (reservoir | geostatistics, seismic) and sample it for the target property volumes using the MCMC method, i. e., the probability of the produced reservoir model given the input geostatistics and seismic data.

The workflow for the stochastic inversion is represented in Fig. 47. The evidence and assumptions are expressed as a series of pdfs defined over the property volumes. We calculated variograms for continuous and discrete properties and property distributions (multivariate joint pdfs). Then the seismic data is modeled for acoustic impedance using the convolutional model and a normal pdf for the seismic noise is calculated to account for uncorrelated differences between real and synthetic seismic (Saussus and Sams, 2012; Kneller et al., 2019). The steps (Fig. 47) are described as:

1. In the stratigraphic grid, created from seismic horizons, start with an arbitrary reservoir model (res0) and select a random location in the volume (the current state of the chain). The lateral sampling is consistent with the seismic data grid and the vertical sampling is 1m.
2. Randomly generate a modified realization (res1). A synthetic seismic (synth1) is calculated through convolution between the estimated wavelet and res1 acoustic

properties. Considering the Bayesian inference scheme, compute the likelihood function of res1 given the real seismic data: P(seis | synth1).

3. Evaluate the prior distribution of the modified realization (P(res1 | geostats), which reflects the lateral and vertical continuity computed from the variograms and the value of the property at neighboring cells.
4. Multiply the prior distribution P(res1 | geostats) with the likelihood function P(seis | synth1) to compute the posterior probability value given the input information (e.g., statistics, well data, seismic horizons and stratigraphy). This is the Bayesian inference part of the algorithm.
5. Compare the posterior probability value with the current reservoir model res0. If the proposal res1 has a higher posterior probability value than res0, there is, P(res1 | geostats, seis) > P(res0 | geostats, seis), then res1 is accepted and the chain moves to a different random location considering res1 as the new current state. Otherwise, if the value is smaller, res1 can be randomically rejected (and res0 is the current stat for the next step) or accepted as a ratio between P(res1 | geostats, seis) and P(res0 | geostats, seis). Note that this is the Metropolis-Hastings part of the algorithm, avoiding the calculation to be stuck in locals maxima/minima as lower probabilities are sometimes accepted.
6. The process continues updating for the entire seismic volume until P(resn | geostats, seis) is no longer changing. Due to the large number of calculations needed to sweep the entire volume, the MCMC algorithm only calculate the conditional posterior pdf on a small portion of the volume at a time. Combination them all gives the global posterior pdf.

Note that the MCMC algorithm does not change the whole Res0 trace considering a single iteration. Instead, a small portion of the grid is modified a step at a time, until the entire grid is swept. All the pdfs are local, so they are re-calculated every time the calculation moves to another part of the volume.

For our purpose, the stochastic seismic inversion fits very well, once we are taking advantage over the seismic constraint in decametric scale but also explicitly simulating flow units in the metric scale, below the seismic data resolution. The objective is to generate many plausible flow units models (and consequently porosity and permeability models) and coherent

with the decametric and metric seismic scales, given the geostatistics associated with every metric flow unit (MFU).

4.6.2 Inputs and Parametrization

We created the grid using three mains seismic horizons: top of the Barra Velha Fm., top of the Itapema Fm. and top of the Piçarras Fm. (base of the reservoir). The lateral spacing is relative to the seismic grid (25m x 25m), and vertical sampling is set to 1m. For the seismic constraint, a full-stack RTM seismic processing from a VTI-FWI migration was used (see Araujo and Gouveia (2015) for more details about Mero seismic data).

The stochastic inversion is set to invert for acoustic impedance, decametric flow units (defined by Penna and Lupinacci (2021)), and metric flow units (defined from the FZI cut-offs described in Table 6). We maintain the FZI S-curve relation between decametric and metric flow units, that is, MFU1 and MFU2 will only occur if DFU1 is present, for instance. This is compatible to the flow multi-scale of observation reasoning used for discretization.

As input, we considered experimental vertical variograms calculated from well logs for acoustic impedance, decametric and metric flow units. Fig. 48 shows an example of the experimental and modelled variograms. They are a mixture of 60% gaussian and 40% exponential with vertical range of 20m for PI, of 5 to 10m for DFU and of 3 to 6m for MFU. No differences were observed between vertical variograms of the Barra Velha and Itapema formations, so we considered the same variogram parametrization for both layers.

We calculated the experimental lateral variograms through different maps. For the acoustic impedance, we extracted mean values for both Barra Velha and Itapema Formations considering the PI volume derived from the elastic inversion (Penna et al., 2019). For the decametric flow units lateral variograms, we used the mode considering each of the most likely facies volumes derived from the Bayesian classification (Penna and Lupinacci, 2021). The same DFU lateral variogram was considered for the MFU. Also, no considerable differences were found between lateral variograms of the Barra Velha and Itapema formations, therefore we used the same variograms for both formations. In general, they are a mixture between 90% Gaussian and 10% exponential curves with a range around 2,500 m for the PI and 1,000 m for DFU and MFU (Fig. 49).

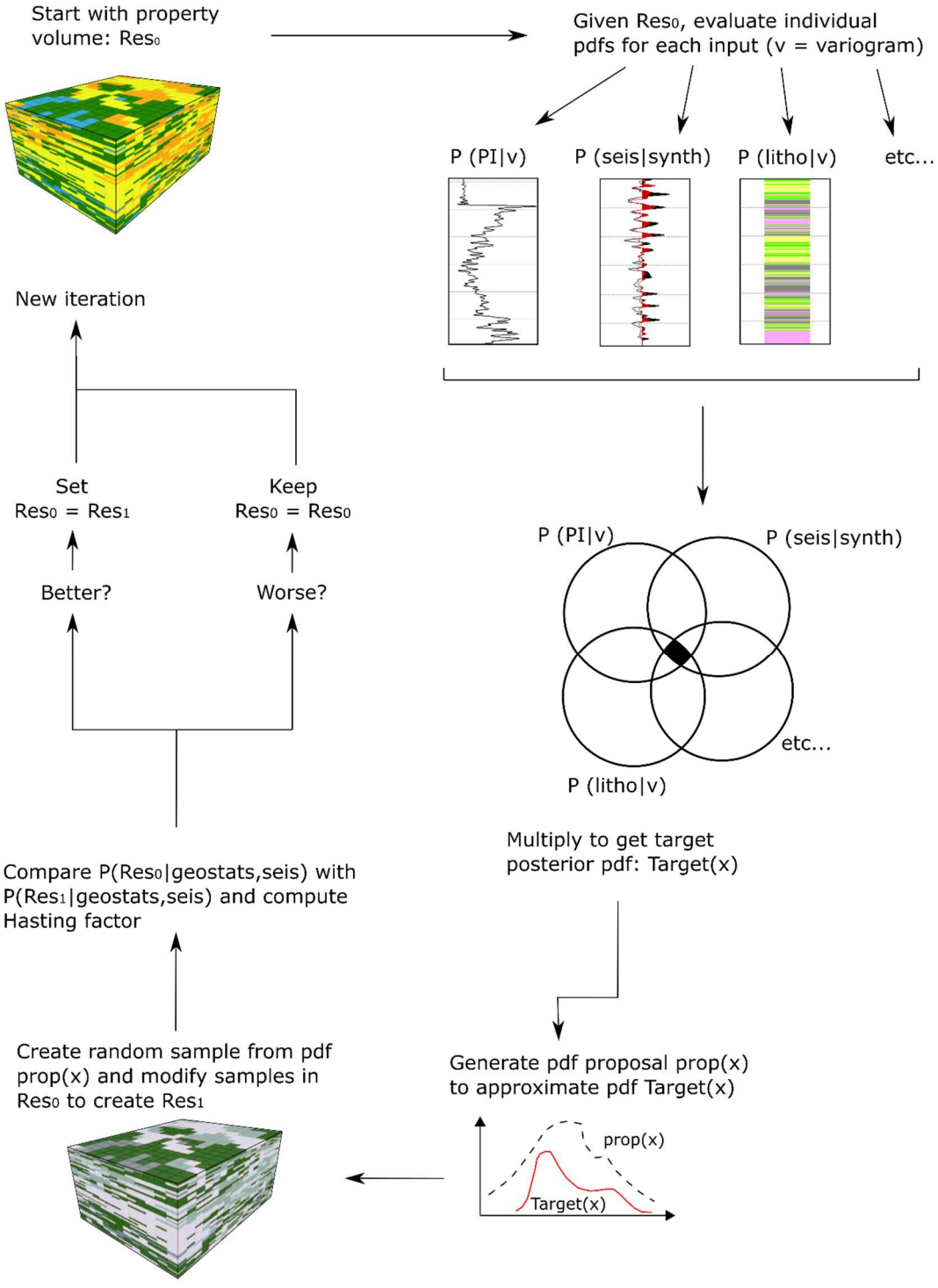

Fig. 47 – MCMC Statmod® MCTM algorithm workflow.

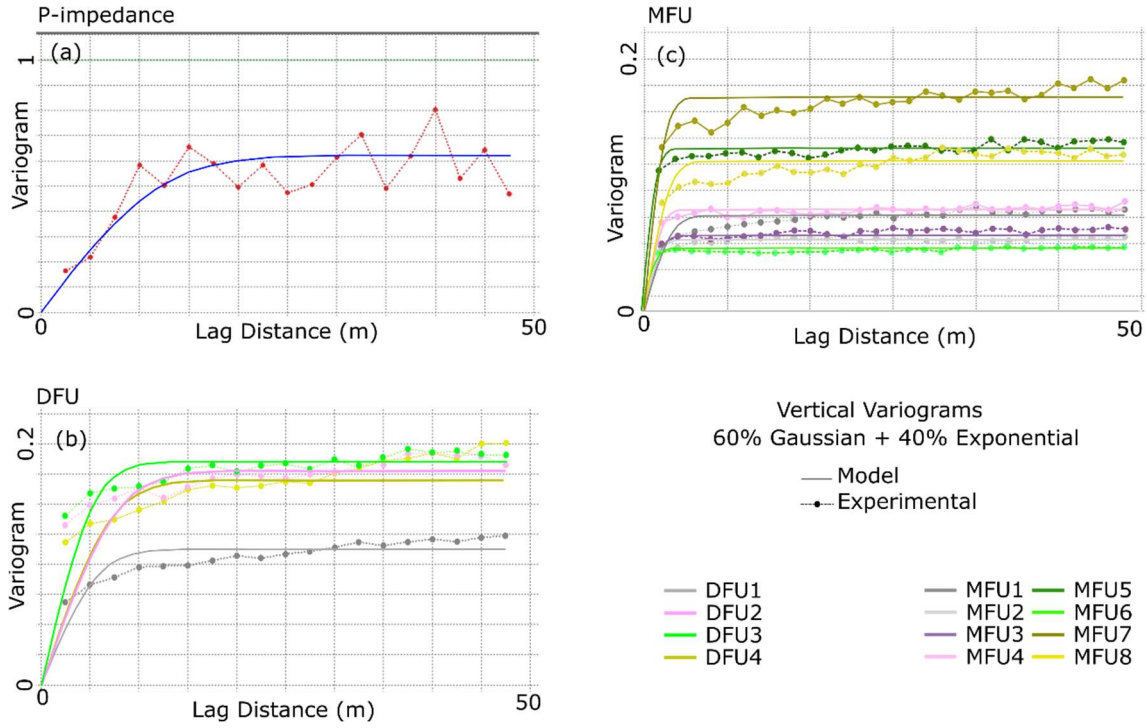

Fig. 48 – Experimental and modelled vertical variograms for (a) Acoustic impedance, (b) decametric flow units and (c) metric flow units. Experimental variograms were calculated from well logs.

Acoustic impedance pdfs for DFU are the same as shown in Penna and Lupinacci (2021). For MFU, we estimated normal PI pdfs separately for the Barra Velha and Itapema formations, as shown in Fig. 50. Due to the high resolution of the discretization, it is expected that the PI superimposition between MFU units would be larger than the DFU pattern. One of the aims is solve this ambiguity through MCMC simulations and several iterations, producing a numerous amount of possible MFU occurrence volumes constrained to the seismic data in decametric scale. The general behavior observed concentrates more MFU1 in higher PI values and MFU8 in lower PI values, like the DFU behavior.

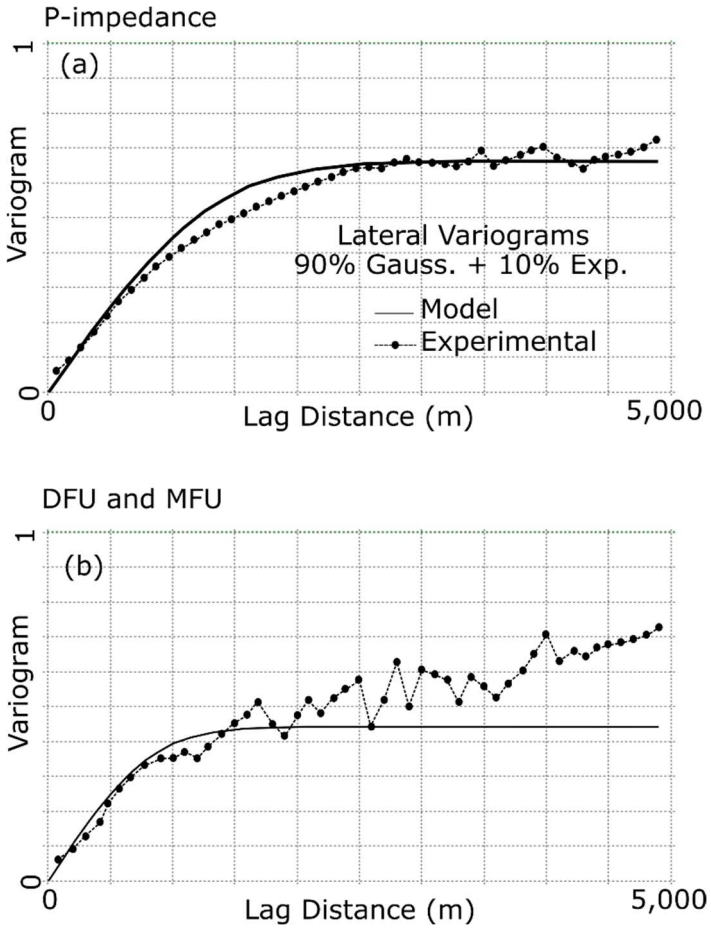

Fig. 49 – Experimental and modelled lateral variograms for (a) acoustic impedance, (b) decametric and metric flow units. We calculated the txperimental variograms considering elastic inversion volumes (PI) and Bayesian facies classification (DFU and MFU).

We chose not to use a constant value for the a priori probability in the Bayesian classification, as the facies are highly heterogenous in carbonate environments. Instead, we constructed a volume regarding the laterally variable a priori probability for each DFU extrapolating, through ordinary kriging, the facies proportion in the wells considering horizons and framework. Since there are no wells drilled in structural lows (therefore sampling low-energy settings) in the study area, we applied a multiplier to raise the prior occurrence probabilities of worse permoporous DFU and MFU away from the Mero main structural high. This behavior is corroborated by numerous presalt analogs that drilled this specific setting (Teixeira et al., 2017; Lima and De Ros, 2018; Neves et al., 2019; Gomes et al., 2020). For each DFU occurrence, there is a prior probability of MFU that corresponds to a mean ratio between its correlated facies obtain from the well data. For example, if DFU1 occur in a given location, a prior probability for MFU1 is 60%, and 40% for MFU2. Fig. 51 exemplifies how a prior

probability varies laterally for DFU4, for exemplification, and a prior probability ratio from MFU1 to MFU8 considering the occurrence of each associated DFU.

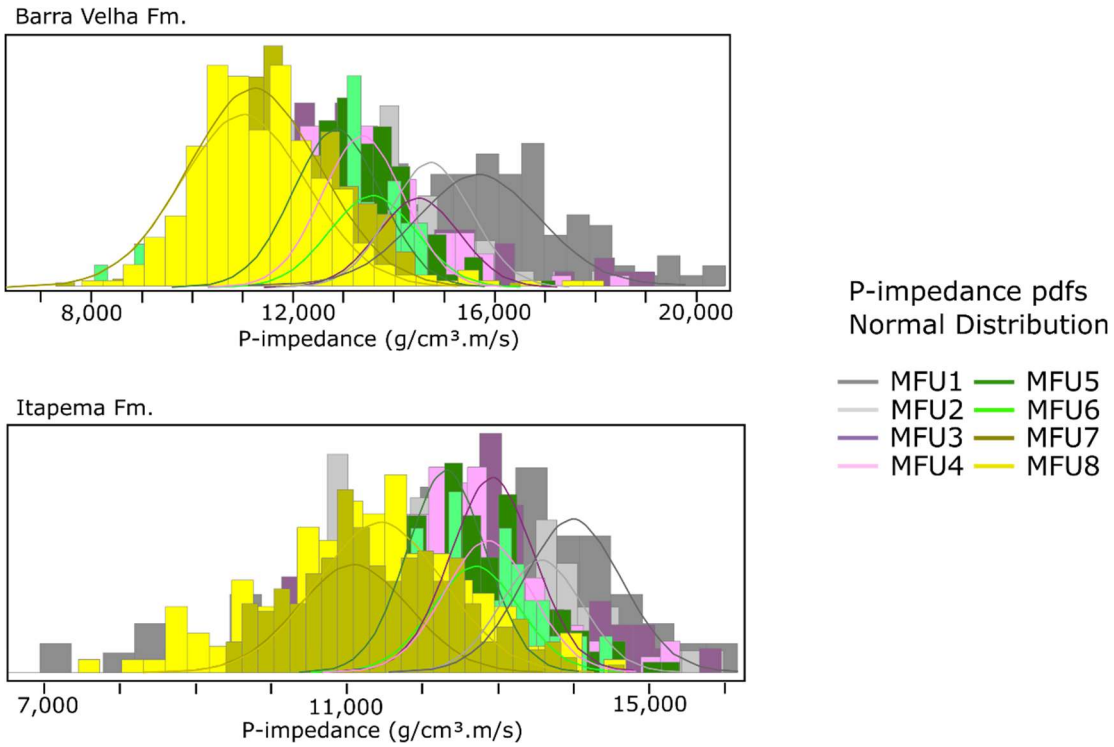

Fig. 50 – P-Impedance pdfs for MFU in both Barra Velha (above) and Itapema (below) formations.

4.6.3 Stochastic Inversion Results and Quality Control (QC)

We performed 100 iterations for the MCMC P-impedance inversion, that is, 100 possible solutions were calculated for the acoustic impedance, DFU and MFU given the seismic data as constraint. The mean wavelet, necessary for the synthetic seismic convolution, is the same used for the seismic inversion by Penna et al. (2019). Initially, we used all the wells with available well-log data as hard constrains for the inversion. Then, we removed three wells to blind-tests and performed the inversion. The presented results below are the blind-test versions of the MCMC inversion.

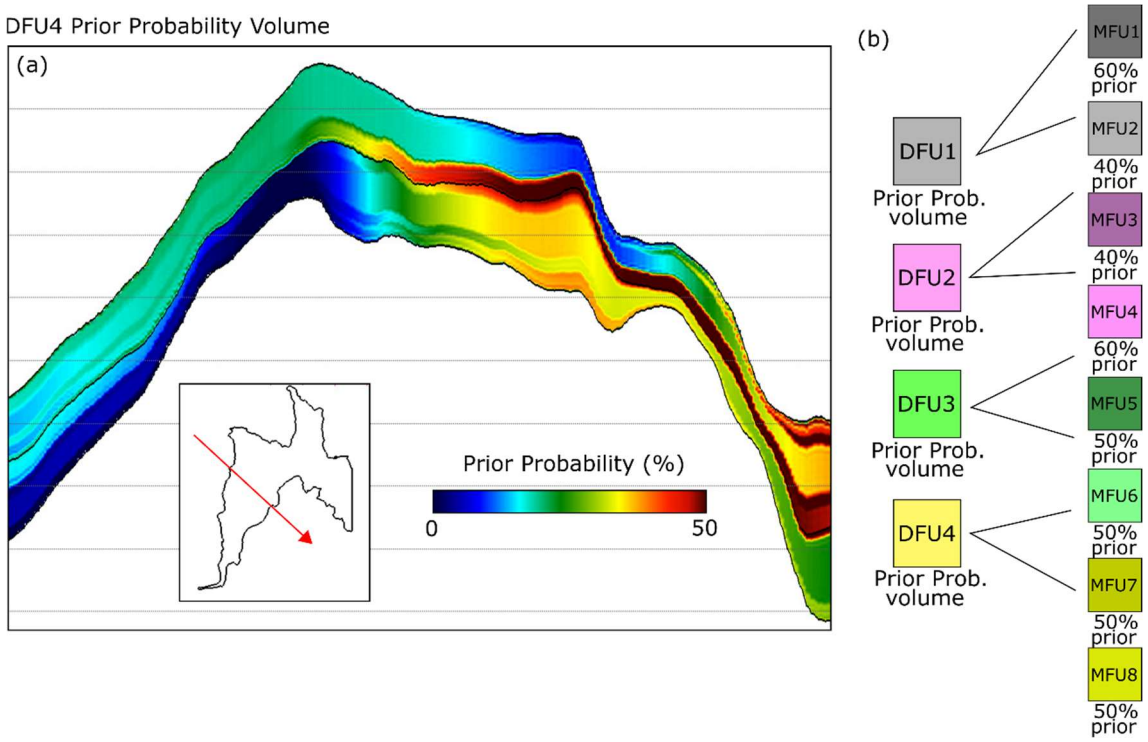

Fig. 51 – (a) A prior probability NW-SE section through DFU4 3D volume and (b) the relation between prior probabilities of DFU and MFU.

The mean PI and DFU and MFU most probable occurrence volumes from the 100 iterations, and the results from two random iterations are presented in Fig. 52. Clearly, one notices the relation and distribution of low-PI values as DFU3 and DFU4 and MFU5 to MFU8, while high-PI values tend to concentrate more DFU1 and DFU2 and, consequently, MFU1 to MFU4. Also, we noted how the occurrence of each MFU is conditioned to the occurrence of its correlated DFU. These sections are a good example of the advantage of using the seismic constraints over decametric scale and stochastic simulation over metric scale, below seismic resolution. To illustrate the special distribution, PI mean and DFU and MFU mode maps from the Itapema Formation are displayed in Fig. 53.

Overall, the prior and posterior pdfs results for PI inversion are consistent, within few errors along Barra Velha and Itapema formations, except for MFU1 and MFU2 (Fig. 54). The reason for the discrepancy for these two flow units is the addition of an increasing a prior probability of DFU1 at lower structural regions (areas without drilled wells), mainly with predominance of mud sediments that corresponds to low PI values. Because of those areas, this pushes the posterior MFU1 and MFU2 PI values to the left of the plot. For the other MFUs,

metrics such as mean, standard deviation, P10 and P90 are in match between prior and posterior pdfs.

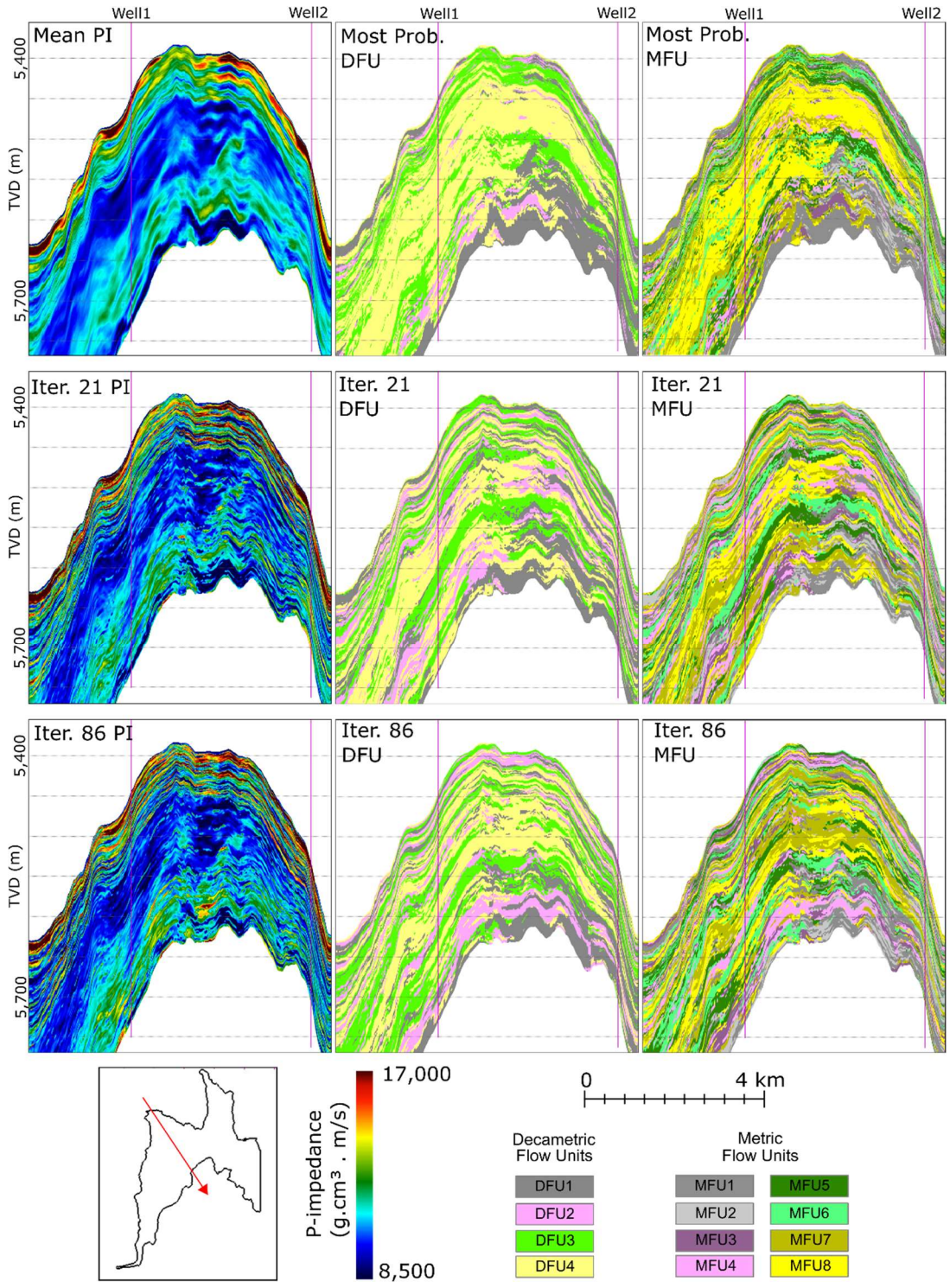

Fig. 52 – (above) Mean PI and most probable DFU and MFU NW-SE section from 100 MCMC iterations. (middle) Iteration 21 PI, DFU and MFU results. (below) Iteration 86 PI, DFU and MFU results.

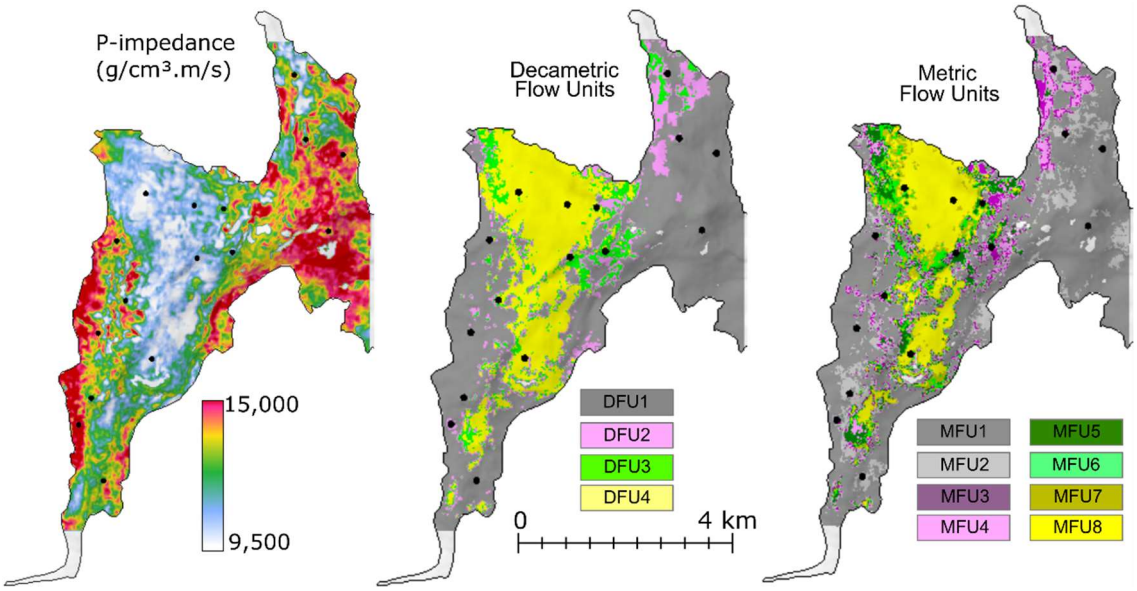

Fig. 53 – (left) Mean PI map from the upper Itapema Formation. (middle) DFU and (right) MFU mode maps from the same stratigraphic layer.

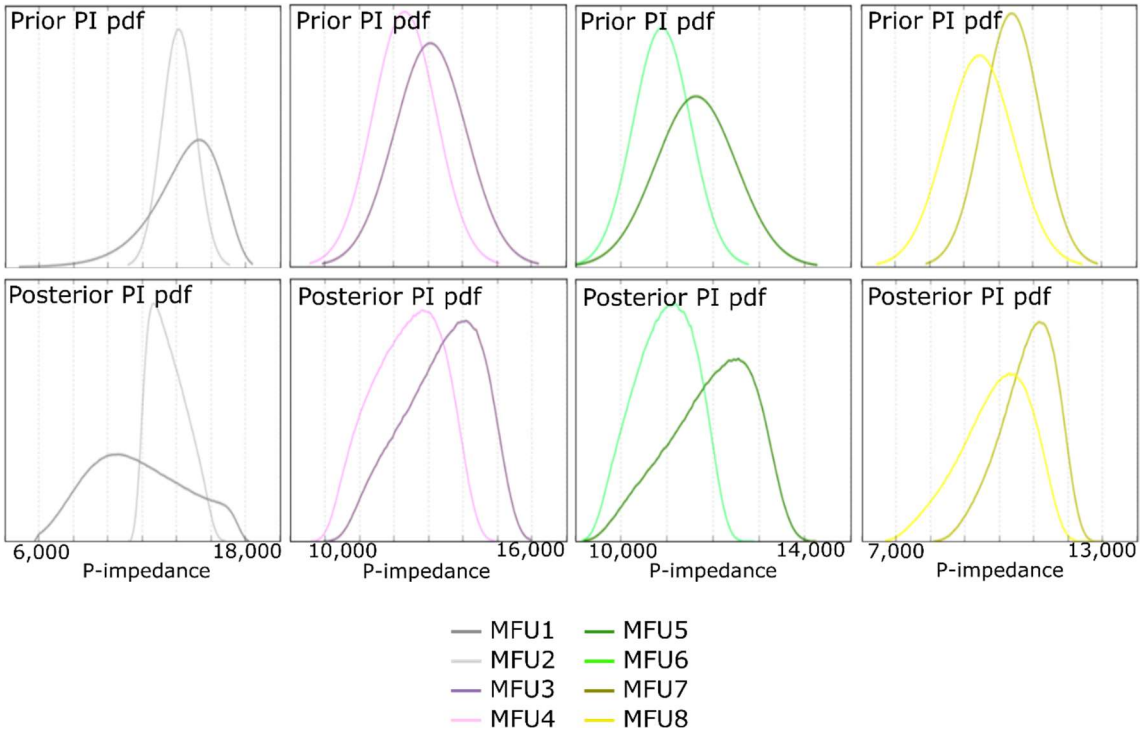

Fig. 54 – A prior and posterior pdfs for the 100 MCMC iterations. MFU1 posterior pdfs deviates from a prior pdfs because of the increasing MFU1 occurrence in structural depressions, areas without any drilled wells sampling mud sediments, usually worse permoporous units with low PI values.

The overall a prior and posterior proportions of DFU and MFU for both Barra Velha and Itapema formations is presented in Fig. 55. MCMC inversion produced occurrence volumes that corroborate the well statistics. DFU, except for the wells used as blind-tests, are a perfect match between a prior and posterior, because they were used as hard constraints at the well location. This is not the case for MFU, whose small deviations are observed between a prior and posterior proportions.

4.6.4 Porosity and Permeability Cosimulation

We cosimulated porosity and permeability for each PI iteration to estimate a numerous quantity of possible ϕ and permeability k volumes, given the MFU distributions calculated by the MCMC inversions. The procedure for the cosimulation is similar to the workflow described in 4.6.2, with the difference that the posterior probability is now coupled with the simulated PI value, there is, we are sampling for P(porosity | geostat, simPI) and P(permeability | geostat, simPI). It is important to emphasize that the porosity and permeability cosimulation is restricted with the MFU, below the seismic resolution. However, MFU is directly related to a specific DFU that is constrained by seismic data. So, at the end, the porosity and permeability are simulated on the metric scale without losing the seismic lateral control.

Through well data analysis and porosity and permeability volumes from the Bayesian classification, the vertical and lateral experimental variograms are like those used to the PI MCMC inversion (Fig. 48 and Fig. 49). The porosity and permeability pdfs used for the cosimulation are showed in Fig. 56. As previously shown in Table 7 basic statistics, MFU1 concentrate worse permoporous samples and MFU8 better. We considered a cosimulation for each MCMC iteration, that is, 100 possible porosity and permeability solutions were calculated given the input variograms, pdfs and PI volumes. Mean and individual results are displayed in Fig. 57, as well as the corresponding MFU from the related MCMC inversion. In practice, given these results, we can stablish pessimistic, optimistic and base scenarios for the Mero reservoir considering parameters such as net to gross, porous volumes, and volume in place.

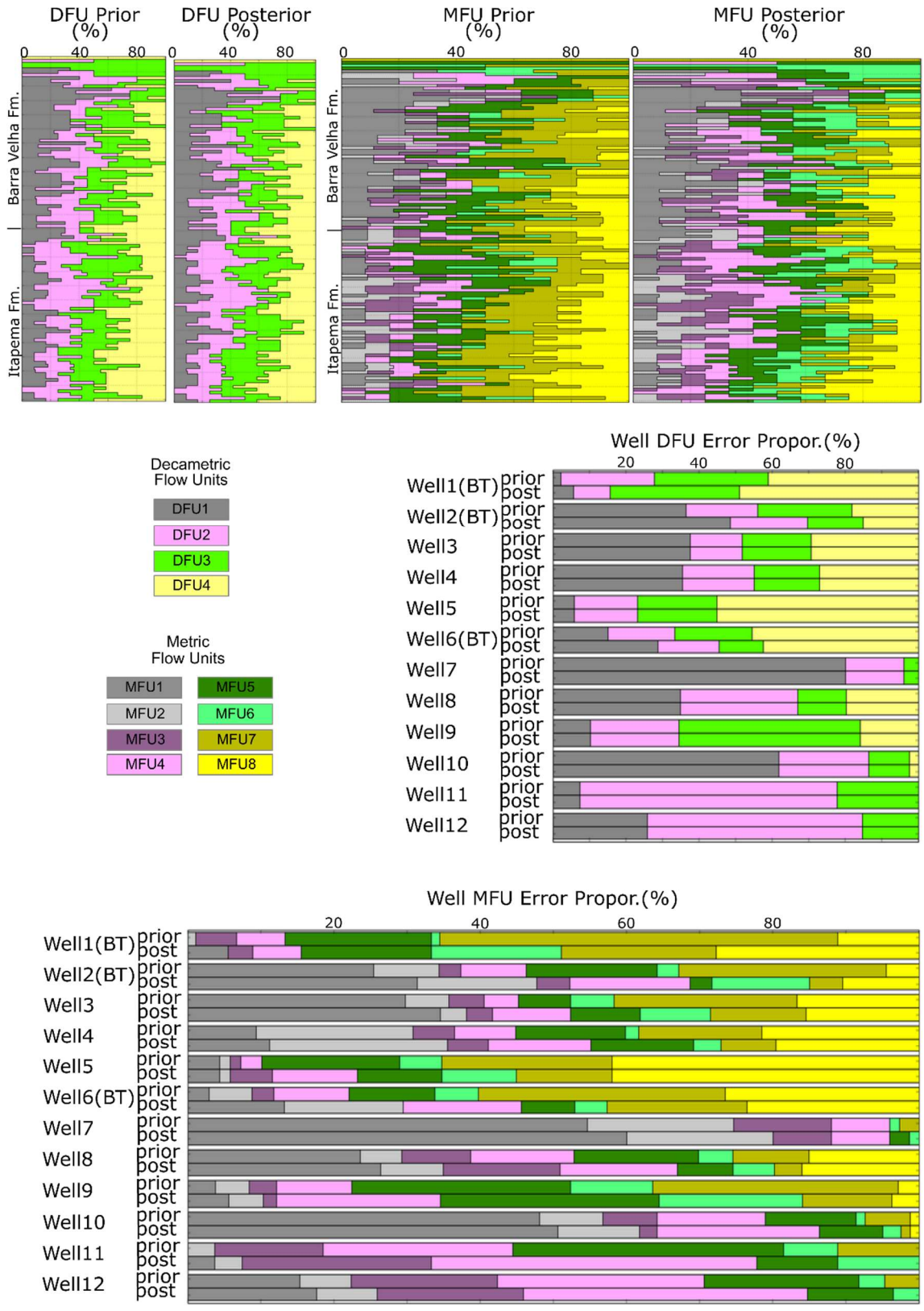

Fig. 55 – Mean prior and posterior proportions for DFU and MFU considering 100 MCMC iterations. Wells marked with BT were considered as blind tests for the inversion.

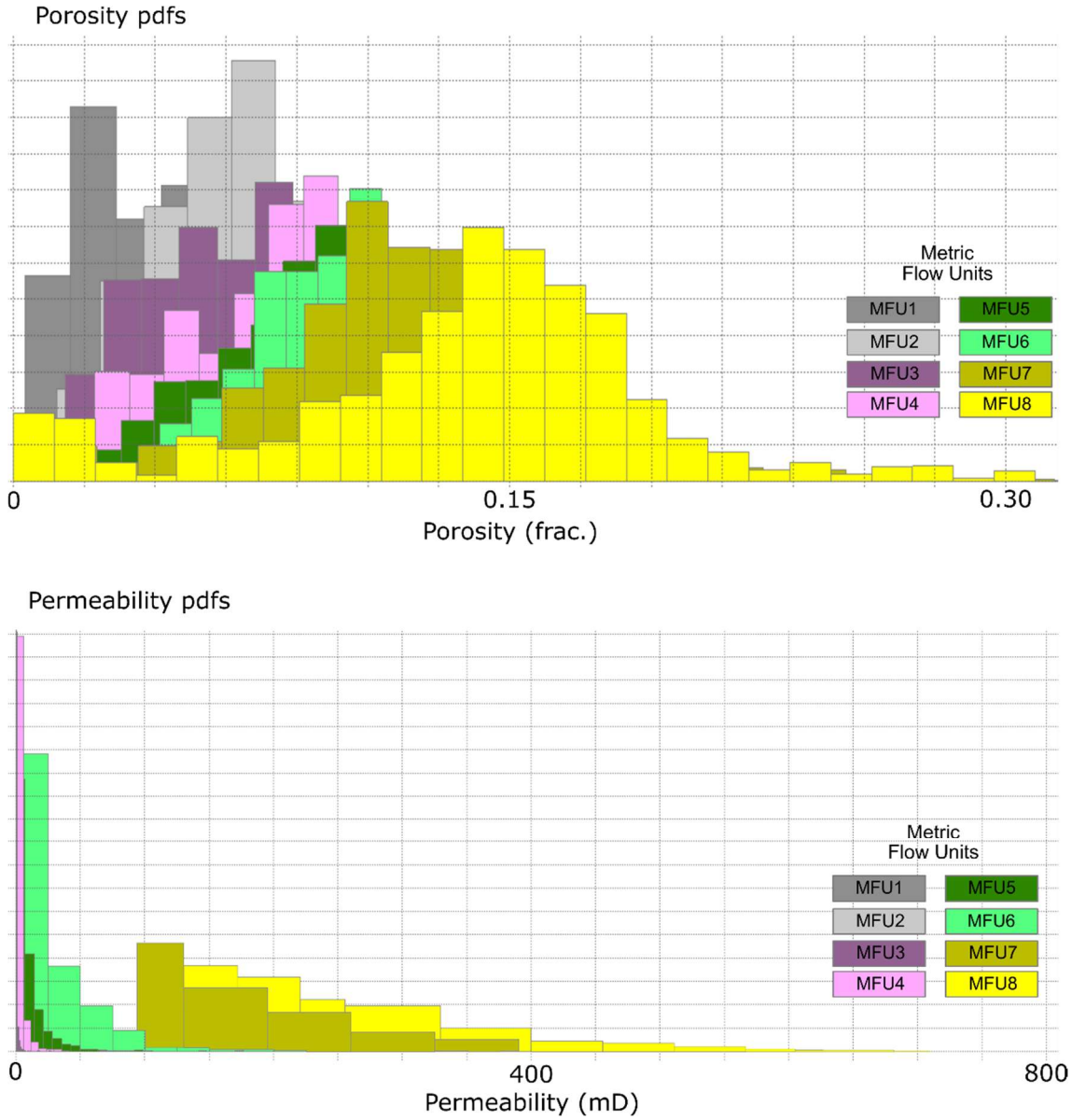

Fig. 56 – Porosity (above) and permeability (below) pdfs for the cosimulation. MFU1 and MFU2 are concentered along the zero-permeability axis. Both Barra Velha and Itapema formations show the same behavior.

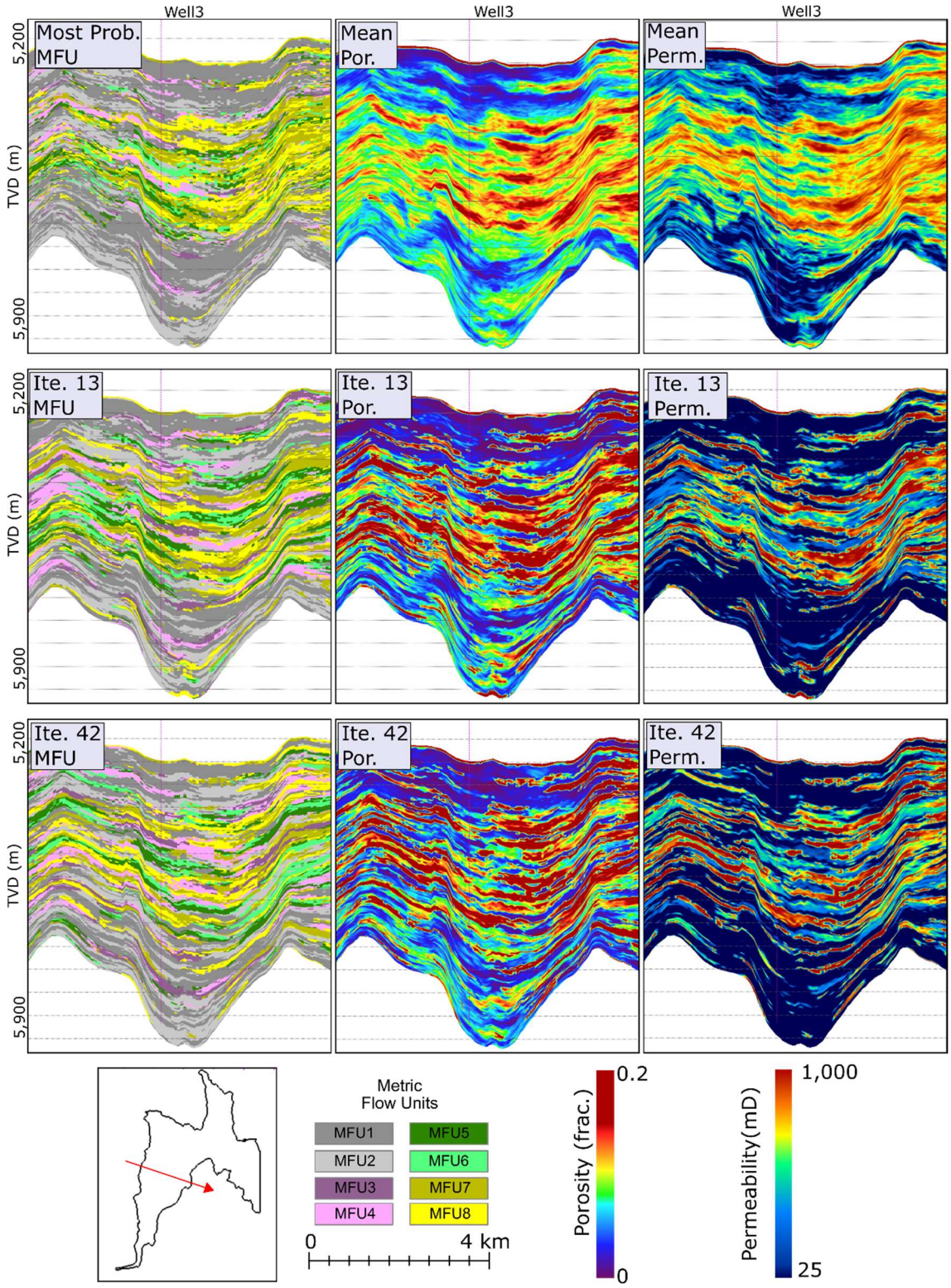

Fig. 57 – (above) Most probable MFU and mean porosity and permeability NW-SE section from 100 cosimulation iterations. (middle) Iteration 13 MFU, porosity and permeability results. (below) Iteration 42 MFU, porosity and permeability results.

We also performed prior and posterior pdfs analysis for the permeability and porosity. As previously shown in the PI QC (Fig. 54), the cosimulation produces results below the seismic resolution that are compatible with the well data statistics, without relevant discrepancies and without losing the seismic constrain in the decametric scale. The comparison is presented in Fig. 58, and the QC results corroborates the robustness of the method. Summarizing, we produced a series of possible PI, DFU, MFU, porosity and permeability volumes through an MCMC inversion and cosimulation, which are laterally compatible with the seismic data and vertically with the well data statistics (Fig. 59).

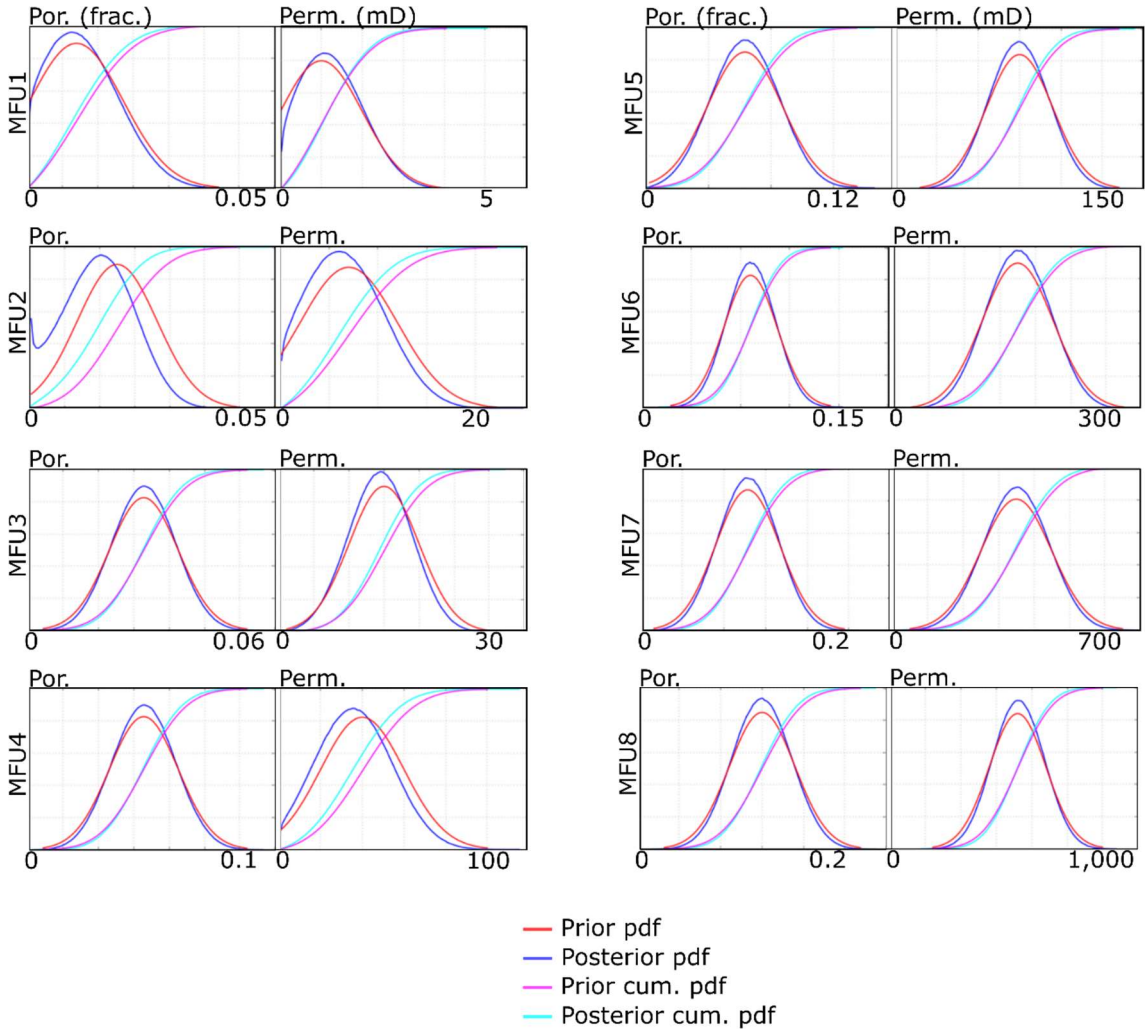

Fig. 58 – Prior and posterior pdfs and cumulative pdfs for the 100 cosimulations for porosity and permeability.

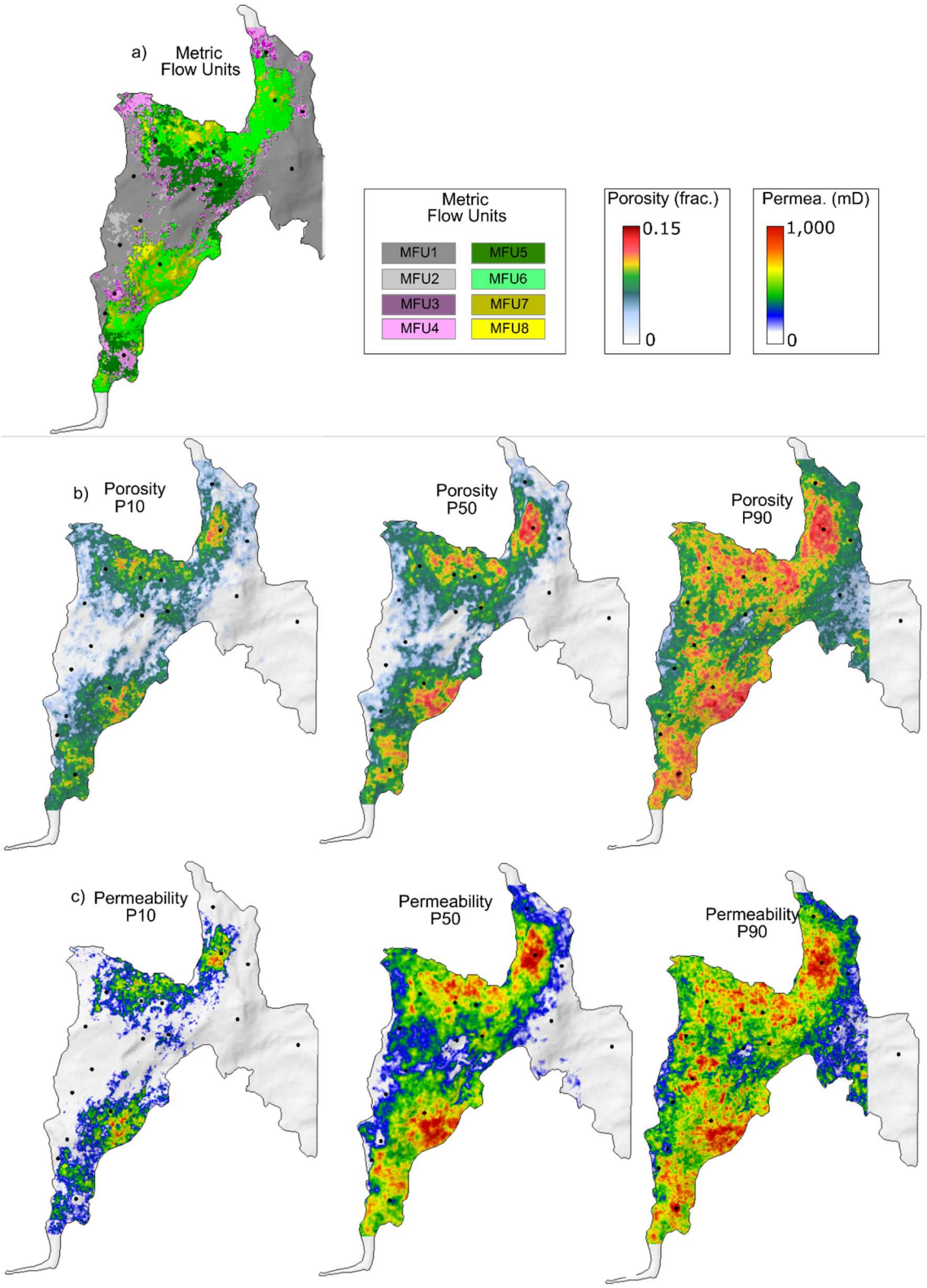

Fig. 59 – (a) MFU mode map from the upper Barra Velha Formation. (b) Porosity and (c) permeability minimum, maximum and mean maps from the same stratigraphic layer.

4.7 Conclusions

The proposed workflow provided means to generate numerous possible porosity and permeability 3D volumes below the seismic resolution limit, respecting the seismic data in decametric scale. Like many seismic Bayesian inference algorithms, the prior information plays an important role in the posterior distribution of PI and, consequently, porosity and permeability. We highly recommended that prior models are built representing local geology aspects or its analogs, constraining some characteristics that sometimes are not sampled even in the presence of numerous wells. That is the case of prior and posterior pdfs for MFU1 and MFU2, which the prior information volume forces the occurrence of worse permoporous facies (clay-rich carbonates) in structural lows, causing a deviation of posterior pdf towards low-PI values. These carbonates were not drilled by wells, once they are below the O/W contact. However, several analog data from other pre-salt reservoirs indicate the presence of such facies.

Even in the presence of high MFU superimposed zones in the acoustic domain, our workflow achieved a satisfactory posterior blind-well proportion. This issue can be addressed by generating a sufficient number of iterations and constraining MFU with its corresponding DFU, guaranteeing the seismic correlation at larger scales. As shown in previous studies, DFU presents a reduced amount of elastic and acoustic superimposition and can be quantified in terms of deterministic inversion and Bayesian probabilistic classification. However, the presence of noise and imaging problems in the seismic can propagate errors in the decametric scale to metric scale, causing porosity and permeability deviations.

Understanding flow behavior at decametric scale is the first step to build the dynamic reservoir knowledge at smaller scales, but detailed analysis can be performed with much more accuracy in the metric scale. In complex reservoir settings, where the fluid flow is inflected by numerous processes, it is important to have more flow units to correctly characterize the flow behavior, producing more accurate porosity and permeability relations and, consequently, a better volumetric distribution of these properties. Uncertainty analysis can be performed through the probabilistic outputs of the workflow. We believe that interpretation of scenarios based on the volumes generated by our methodology (e.g. P10, P50 and P90) will positively impact the static and dynamic model building process, as well as 4D seismic interpretation and seismic assisted history matching.

5. Final Considerations

The proposed methods for incorporating flow units into the seismic quantitative interpretation workflow were able to present important considerations and solutions about the intrinsic problem of constraining porosity and permeability estimations with FU facies. I demonstrated that, with the correct upscaling usage and through probabilistic facies calculation methods, it is possible to obtain better seismic estimations of porosity and permeability, not only in limit by the seismic scale, but also below the seismic resolution limitation.

My results showed that petrophysical parameters calculated through flow units facies were substantially more accurate than when calculated through conventional lithologic facies. This was frequently observed in core and well log studies, with less estimated porosity and permeability errors compared to the measured data. The volumes produced over the proposed workflow will have direct impact on the static and dynamic reservoir 3D modelling, as well as seismic assisted history matching, 4D seismic interpretation and general reservoir planning and management.

In the first core data feasibility study, I showed that cumulative porosity and permeability S-curves are a powerful tool to visualize different scales of observations in the flow units estimation. Through different methods of discretization, I demonstrated that is possible to individualize flow units facies using seismic elastic attributes, as p- and s-impedances. In both core and well log data, the study was able to demonstrate the separation of A utilFU facies in the elastic domain and its usability in a 3D study. Although I opted to use FZI flow units method of facies estimation due to the large porosity and permeability core data availability, I observed some potential in electric methods of discretization. Some karstification intervals with limited pore connectivity are presented as best reservoir facies in the FZI method, but not in the formation factor method. In the presence of more laboratory electrical measurements, it is possible that porosity and especially permeability estimations would be even more accurate than using FZI. This could be an interesting field of study for the upcoming research.

Even with the known FZI method limitations and p- and s-impedances values superimposition in each of the FU facies, the well log results showed that it is possible to separate between upscaled flow units facies in the elastic domain. In contrast to the seismic vertical resolution limits, we can deal with the large units of FU associated with a complex

geological setting using the cumulative S-curve as a method of upscaling, similar to sequence stratigraphy studies of low and high order cycles of sedimentation. This is more accurate than simply combine two or more flow units arbitrarily. I also recommend probabilistic methods of flow units facies classification associated with scenario analysis prior to interpretation, in order to minimize uncertainties associated with the discretization.

The second study transposed core and well logo data FU classification into the 3D domain, using volumetric p- and s-impedance volumes derived from elastic inversion. I considered a Bayesian approach for the facies classification, dealing with the superimposition of facies in the elastic domain on a probabilistic basis. One of the greatest advantages of using this kind of approach is creating occurrence scenarios for each facies, which can be incorporated into uncertainties analysis for reservoir management. Also, using flow units as templates, I calculated permeability and porosity volumes, which we previously showed in the well domain that is more accurate than estimations based on lithologic facies, the standard for reservoir geophysics. However, due to the necessity to limit the number of flow units to match the seismic vertical resolution, and considering that Mero is a complex geological reservoir, errors and miscalculations are still present. Also, FU facies errors due to the acoustic and elastic values superimposition, will also impact the final porosity and permeability results.

The cut-offs values used in the FU discretization, in both metric and decametric scales are vital to porosity and, mainly, for permeability estimation. Once the p-impedance versus porosity relationship varies a lot from facies to facies, and, consequently, the porosity versus permeability relationship, a thorough analysis of the cumulative S-curve determining the cut-offs values are mandatory. Further studies about this discretization are needed, especially in the interpretation of the S-curve as a statistical data. Several areas of science, like biology (i.e., bacteria grown), project management, economics (i.e., market evaluation), geography (i.e., population studies) considers percentiles, most common values and other mathematical techniques to interpret the function.

The third study is an attempt to push the flow unit classification below the seismic resolution limit but maintaining the seismic constraint in the decametric scale. That correspond to say that the inversion and facies calculation were made in the decametric scale considering the seismic as a constraint for the results and the metric flow units and porosity and permeability estimation were made simulating metric flow units facies within each of the decametric facies using a Monte-Carlo stochastic approach. In that case, vertical and horizontal variograms, as

well as the p-impedance and s-impedance pdfs (probability density function) parametrization will represent most part of the uncertainty in the process. Also, the prior probability volumes created considering each of the facies proportions from well logs are a point of attention, as this act as a qualitative interpretation of the posterior probability. In that type of workflow, having many well data is crucial, otherwise calculation errors would be too large to account for.

I believe that there is a lot of studies that can optimize and improve the workflow presented in this thesis. Flow units calculated through electrical methods (both electrical quality index and cementation factor based) showed some good signs of improvement related to non-connected pores, minimizing permeability estimations especially in dissolved carbonates settings. Indeed, other recent flow units methods (e.g. FZI-star) can also be stressed, as they can present better alternatives apart from the classical FZI method. In my research I followed a S-curve visual and qualitative analysis, but it is clear that facies discretization play an important role in the final result for porosity and permeability. More research regarding the S-curve cut-offs criteria in a more quantitative sense is needed, especially in complex settings where uniformizing the study in several reservoir is desired. At last, probabilistic results from both Bayesian classification and geostatistical inversion can input several studies regarding the seismic estimated porosity and permeability uncertainties. This, in turn, is expected to increase acuity for static and dynamic reservoir modelling and, finally, 4D seismic interpretation, seismic assisted history-matching, fluid-flow modelling or any other research where volumetric porosity and permeability is needed.

6. References

Abbaszadeh, M., Fujii, H., Fujimoto, F. 1996. Permeability prediction by hydraulic flow units -theory and applications. SPE Form. Eval. 11, 263–271.

Aggoun, R. C., Tiab, D., and Owayed, J. F. 2006. Characterization of flow units in shaly sand reservoirs—Hassi R'mel Oil Rim, Algeria. Journal of Petroleum Science and Engineering. Vol. 50, Issues 3–4, pp. 211–226. https://doi.org/10.1016/j.petrol.2005.10.006

Alhashmi, N. F., Torres, K., Faisal, M., Segura Cornejo, V., Bethapudi, B. P., Mansur, S. and Al-Rawahi, A. S. 2016. Rock Typing Classification and Hydraulical Flow Units Definition of one of the Most Prolific Carbonate Reservoir in the Onshore Abu Dhabi. Presented at the SPE Annual Technical Conference and Exhibition, Dubai, UAE, 26-28 September, 2016.

Al-Ajmi, F. and Holditch, S. 2000. Permeability Estimation Using Hydraulic Flow Units in a Central Arabia Reservoir. SPE Annual Technical Conference and Exhibition, Expanded Abstracts. SPE-63254-MS. http://dx.doi.org/10.2118/63254-MS.

Altunbay, M., Barr, D., Kennaird, A., and Manning, D. 1994. Numerical Geology: Predicting Depositional and Diagentic Facies Form Wireline Logs Using Core Data. Presented at the SPE Asia Pacific Oil & Gas Conference, Melbourne, Australia, 7-10 November. SPE-28794-MS. https://doi.org/10.2118/28794-MS.

Amaefule, J. O. and Altunbay, M. 1993. Enhanced Reservoir Description: Using Core and Log Data to Identify Hydraulic (Flow) Units and Predict Permeability in Uncored Intervals/Wells. Presented at the SPE Annual Technical Conference and Exhibition, 3-6 October, Houston, Texas. SPE-26436-MS. https://doi.org/10.2118/26436-MS.

ANP, 2021, Boletim da Produção de Petróleo e Gás Natural: Rio de Janeiro, 40 p.

Araujo, S., & Gouveia, W. P. (2015). Improved Presalt Imaging from Post-Salt High-Resolution Velocity Updates. 14th International Congress of the Brazilian Geophysical Society & EXPOGEF, Rio de Janeiro, Brazil, 3-6 August 2015. https://doi.org/10.1190/sbgf2015-215

Archie, G. E. 1942. The Electrical Resistivity Log as an Aid in Determining Some Reservoir Characteristics. Transactions of the AIME. 146(1). 54-62. 1942. SPE-942054-G. Doi:

https://doi.org/10.2118/942054-G

Aster, R. C, Borchers, B. and Thurber, C. 2004. Parameter Estimation and Inverse Problems. First Ed., Elsevier Academic Press.

Azevedo, L. and Soares, A. 2017. Geostatistical Methods for Reservoir Geophysics. First Ed., Springer, New York.

Azevedo, L., and Soares, A. (2018). Geostatistical Methods for Reservoir Geophysics by Azevedo, L. and Soares, A. Mathematical Geosciences, 50(7), 861–863. https://doi.org/10.1007/s11004-018-9748-8

Avseth, P., Mukerji, T. and Mavko, G. 2005. Quantitative Seismic Interpretation: Applying Rock Physics Tools to Reduce Interpretation Risk. First Ed., Cambridge Press, Cambridge

Basbug, Z., and Karpyn, Z. 2007. Estimation of Permeability from Porosity, Specific Surface Area, and Irreducible Water Saturation using an Artificial Neural Network. 2007. Presented in the Latin American & Caribbean Petroleum Engineering Conference, 15-18 April, Buenos Aires, Argentina. SPE-107909-MS. https://doi.org/10.2118/107909-MS.

Box, G. 1976. Science and Statistics. Journal of the American Statistical Association. Vol. 71, Issue 356, pp. 791–799. https://doi.org/10.1080/01621459.1976.10480949

Buckley, J. P., Bosence, D., and Elders, C. (2015), Tectonic setting and stratigraphic architecture of an Early Cretaceous lacustrine carbonate platform, Sugar Loaf High, Santos Basin, Brazil: Geological Society, London, Special Publications, v. 418, no. 1, p. 175–191, doi:10.1144/SP418.13.

Carlotto, M. A., Silva, R. C. B, Yamato, A., Trindade, W., Moreira, J., Fernandes. R., Ribeiro, O. 2017. Libra: A Newborn Giant in the Brazilian Pre-salt Province, in Merrill, R. K., and Sternbach, eds., Giant fields of the decade 2000–2010: AAPG Memoir 113: 165–176. https://org/10.1306/13572006M1133685.

Catuneanu, O. 2019. Scale in Sequence Stratigraphy. Marine and Petroleum Geology, 106, 128-159. Doi: https://doi.org/10.1016/j.marpetgeo.2019.04.026.

Chen, X., Zhou, Y. 2017. Applications of digital core analysis and hydraulic flow units in petrophysical characterization. Adv. Geo-energy Res. 1 (1), 18–30. https://doi.org/ 10.26804/ager.2017.01.02.

Chinelatto, G., Belila, A., Basso, M., Souza, J. P., Vidal, A. A Taphofacies Interpretation of Shell Concentrations and Their Relationship with Petrophysics: A Case Study of Barremian-Aptian Coquinas in the Itapema Formation, Santos Basin-Brazil. Marine and Petroleum Geology. 116, 104317. https://doi.org/10.1016/j.marpetgeo.2020.104317

Cominsky, J. T., Newsham, K. E., Rushing, J. A. and Blasingame, T. A. 2007. A Comparative Study of Capillary-Pressure-Based Empirical Models for Estimating Absolute Permeability in Tight Gas Sands. Presented at the SPE Annual Technical Conference and Exhibition, Anaheim, USA, 11-14 November. 2007.

Da Rocha, H., Costa, J., Carrasquilla, A. and Carrasco, A. 2019. Petrophysical Characterization Using Well Log Resistivity and Rock Grain Specific Surface Area in a Fractured Carbonate Pre-Salt Reservoir in the Santos Basin, Brazil. Journal of Petroleum Science and Engineering. 183(2019), 106372. https://doi.org/10.1016/j.petrol.2019.106372

Daraei, M., Bayet-Goll, A. and Ansari, M. 2017. An Integrated Reservoir Zonation in Sequence Stratigraphic Framework: A Case from the Dezful Embayment, Zagros, Iran. Journal of Petroleum Science and Engineering, 154: 389-404. http://dx.doi.org/10.1016/j.petrol.2017.04.038.

Deutsch, C.V. and Journel, A.G., (1997). GSLIB Geostatistical Software Library andUser's Guide, Oxford University Press, New York, second edition.

Dezfoolian, M. A., Riahi, M. A. and Ilkhchi, A. K. 2013. Conversion of 3D Seismic Attributes to Reservoir Hydraulic Flow Units Using a Neural Network Approach: An Example from the Kangan and Dalan Carbonate Reservoirs, the World's Largest non-Associated Gas Reservoirs, Near the Persian Gulf. Earth Sciences Research Journal, 17 (2): 75-85.

Doyen, P. 2007. Seismic Reservoir Characterization: An Earth Modelling Perspective (EET 2). EAGE Publications bv. https://doi.org/10.3997/9789073781771.

Dvorkin, J., Gutierrez, M. and Grana, D. 2016. Seismic Reflections of Rock Properties, First Ed., Cambridge Press, Cambridge.

D'Windt, A., Quint, E., Al-Saleh, A. and Dashti, Q. 2018. Bayesian Based Approach for Hydraulic Flow Unit Identification and Permeability Prediction: A Field Case Application in a Tight Carbonate Reservoir. Presented in the SPE International Heavy Oil Conference and Exhibition, 10-12 December, Kuwait City, Kuwait. SPE-193752-MS.

https://doi.org/10.2118/193752-MS.

Ebanks, W. J. 1987. Geology in enhanced oil recovery: Reservoir Sedimentology. SEPM Special Publication: 40, 1-14.

El Sharawy, M. and Nabawy, B. S. 2018. Determining the porosity exponent m and lithology factor a for sandstones and their control by overburden pressure: A case study from the Gulf of Suez, Egypt. AAPG Bulleting, Vol.102(9), 1893-1910. https://doi.org/10.1306/03141817262

Emami Niri, M. and Lumley, D. E. 2016. Probabilistic Reservoir Property Modelling Jointly Constrained by 3D Seismic Data and Hydraulic Unit Analysis. SPE Reservoir Evaluation & Engineering. 19(2), 253 - 264. https://doi.org/10.2118/171444-PA.

Escobar, I., Williamson, P., Cherrett, A., Doyen, P. M., Bornard, R., Moyen, R., & Crozat, T. (2006). Fast geostatistical stochastic inversion in a stratigraphic grid. SEG Technical Program Expanded Abstracts 2006. SEG Technical Program Expanded Abstracts 2006. https://doi.org/10.1190/1.2369943

Faria, D., Reis, A. T., and Souza, O. 2017. Three-Dimensional Stratigraphic-Sedimentological Forward Modeling of an Aptian Carbonate Reservoir Deposited during the Sag Stage in the Santos Basin, Brazil. Marine and Petroleum Geology, 88(2017), 676-695.

Feng, R., Luthi, S. M., & Gisolf, D. (2018). Simulating reservoir lithologies by an actively conditioned Markov chain model. Journal of Geophysics and Engineering, 15(3), 800–815. https://doi.org/10.1088/1742-2140/aaa0ff

Ferreira, D. and Lupinacci, W. 2018. An Approach for Three-Dimensional Quantitative Carbonate Reservoir Characterization in the Pampo field, Campos Basin, Offshore Brazil. AAPG Bulletin. 102(11), 2267-2282. https://doi.org/10.1306/04121817352

Ghanbarian, B., Lake, L and Sahimi, M. 2019. Insights Into Rock Typing: A Critical Study. SPE Journal, 24(1), 230-242. SPE-191366-PA. Doi: https://doi.org/10.2118/191366-PA

Grude, S., Landro, M. and Dvorkin, M. 2015. Permeability Variation with Porosity, Pore Space Geometry and Cement Type: A Case History from the Snohvit Field, the Barents Sea. Geophysics. 80(1), D43-D49. https://doi.org/10.1190/geo2014-0064.1

Gomes, J. P., Bunevich, R., Tedeschi, L., Tucker, M. and Whitaker, F. 2020. Facies

Classification and Patterns of Lacustrine Carbonate Deposition of the Barra Velha Formation, Santos Basin, Brazilian Pre-Salt. Marine and Petroleum Geology, 113, 1-21. https://doi.org/10.1016/j.marpetgeo.2019.104176

Gunter, G., Finneran, J. and Miller, J. 1997. Early Determination of Reservoir Flow Units Using an Integrated Petrophysical Method. Presented in the SPE Annual Technical Conference and Exhibition, 5-8 October, San Antonio, Texas. SPE-38679-MS. https://doi.org/10.2118/38679-MS.

Haas, A., & Dubrule, O. (1994). Geostatistical inversion - a sequential method of stochastic reservoir modelling constrained by seismic data. First Break, 12(11). https://doi.org/10.3997/1365-2397.1994034

Haridy, M. G., Sedighi, F., Ghahri, P., Ussenova, K., & Zhiyenkulov, M. (2020, October 25). Comprehensive Study of the Oda Corrected Permeability Upscaling Method. Day 2 Wed, October 30, 2019. SPE/IATMI Asia Pacific Oil & Gas Conference and Exhibition. https://doi.org/10.2118/196399-MS

Hasan, A., and Hossain, M. 2011. Modified Kozeny-Carmen correlation for enhanced hydraulic flow unit characterization. Journal of Petroleum Science and Engineering. Vol. 80, pp. 107-115. https://doi.org/10.1016/j.petrol.2011.11.003

Hassani-Giv, M. and Rahimi, M. 2008. New Correlations for Porosity Exponent in Carbonate Reservoirs of Iranian Oil Fields in Zagros Basin. Journal of Sciences. 34(2). 1-7. 2008.

Hatampour, A., Freez, J. G. and Solelmanpour, I. 2014. Prediction of Flow Units in Heterogeneous Carbonate Reservoirs Using Intelligently Derived Formula: Case Study in an Iranian Reservoir. Arabian Journal for Science and Engineering 39 (7): 5459-5473. https://doi.org/10.1007/s13369-013-0825-5.

Hatampour, A., Schaffie, M. and Jafari, S. 2018. Hydraulic Flow Units' Estimation from Seismic Data Using Artificial Intelligence Systems, an Example from a Gas Reservoir in the Persian Gulf. Journal of Petroleum Science and Engineering 170(2018): 400-408. https://doi.org/10.1016/j.petrol.2018.06.086

Herlinger, R., Zambonato, E.E. and Ros, L. F. 2017. Influence of Diagenesis on the Quality of Lower Cretaceous Pre-Salt Lacustrine Carbonate Reservoirs from Northern Campos Basin, Offshore Brazil. Journal of Sedimentary Research, 87, 1285-1313. 2017. Doi:

http://dx.doi.org/10.2110/jsr.2017.70

Hill, S. 2005. Inversion-Based Thickness Determination. The Leading Edge. 24(5), 449-560. https://doi.org/10.1190/1.1926799

Iravani, M., Rastegarnia, M., Javani, D., Sanati, A. and Hajiabadi, S. H. 2018. Application of Seismic Attribute Technique to Estimate the 3D Model of Hydraulic Flow Units: A Case Study of a Gas Field in Iran. Egyptian Journal of Petroleum. 27(2), 145-157. https://doi.org/10.1016/j.ejpe.2017.02.003

Jesus, I. L., Lupinacci, W. M., Gamboa, L. A. P., Freire, A. F. M. 2019. Electrofacies identification and evaluation in a well of the pre-salt of the Mero Field, Santos Basin. Presented in the 16th International Congress of the Brazilian Geophysical Society.

Kallweit, R. and Wood, L. 1982. The Limits of Resolution of Zero-Phase Wavelets. Geophysics. 47(7), 1035-1046.

Kneller, E., Teixeira, L., Hak, B., Cruz, N. M., Oliveira, T., Cruz, J. M., & Cunha, R. S. (2019). Challenges and Solutions of Geostatistical Inversion for Reservoir Characterization of the Supergiant Lula Field. Petroleum Geostatistics 2019. Petroleum Geostatistics 2019. https://doi.org/10.3997/2214-4609.201902176

Kolodzie, S., Jr. 1980. Analysis of Pore Throat Size and Use of the Waxman-Smits Equation to Determine OOIP in Spindle Field, Colorado. Presented at the 1980 Annual Fall Technical Conference of Society of Petroleum Engineers. 21-24 September. 1980. SPE 9382.

Kozeny, J., 1927. Ueber kapillare Leitung des Wassers im Boden. Sitzungsber Akad 136 (2a), 271–306.

Lalanne, B. and Massonnat, G. 2004. . Presented in the SPE Annual Technical Conference and Exhibition, 26-29 September, Houston, Texas. SPE-91040-MS. https://doi.org/10.2118/91040-MS.

Leite, C., de Assis Silva, C. M., & de Ros, L. F. (2020). Depositional and diagenetic processes in the presalt rift section of a Santos Basin area, SE Brazil. Journal of Sedimentary Research, 90(6), 584–608. https://doi.org/10.2110/jsr.2020.27

Li, P., Zheng, M., Bi, H., Wu, S., and Wang, X. 2017. Pore throat structure and fractal

characteristics of tight oil sandstone: A case study in the Ordos Basin, China. Journal of Petroleum Science and Engineering. Vol. 149, pp. 665–674. https://doi.org/10.1016/j.petrol.2016.11.015

Lima, B. E. M., & De Ros, L. F. (2019). Deposition, diagenetic and hydrothermal processes in the Aptian Presalt lacustrine carbonate reservoirs of the northern Campos Basin, offshore Brazil. Sedimentary Geology, 383, 55–81. https://doi.org/10.1016/j.sedgeo.2019.01.006

Liu, Y., Liu, Y., Zhang, Q., Li, C., Feng, Y., Wang, Y., Xue, Y., & Ma, H. (2019). Petrophysical static rock typing for carbonate reservoirs based on mercury injection capillary pressure curves using principal component analysis. Journal of Petroleum Science and Engineering, 181, 106175. https://doi.org/10.1016/j.petrol.2019.06.039

Lorenz, M. O. 1905. Methods of Measuring the Concentration of Wealth. Publications of the American Statistical Association 9 (70): 209-219.

Mahjour, S. K., Al-Askari, M. K. G., & Masihi, M. (2016). Identification of flow units using methods of Testerman statistical zonation, flow zone index, and cluster analysis in Tabnaak gas field. Journal of Petroleum Exploration and Production Technology, 6(4), 577–592. https://doi.org/10.1007/s13202-015-0224-4

Martin, A., Solomon, S. and Hartmann, D. 1997. Characterizatio n of Petrophysical Flow Units in Carbonate Reservoirs. AAPG Bulletin, V. 81, No. 5, pp. 734-759. https://doi.org/10.1306/522B482F-1727-11D7-8645000102C1865D

Mirzaei-Paiaman, A., Ostadhassan, M., Rezaee, R., Saboorian-Jooybari, H., & Chen, Z. 2018. A new approach in petrophysical rock typing. Journal of Petroleum Science and Engineering. Vol. 166, pp. 445–464. https://doi.org/10.1016/j.petrol.2018.03.075

Moczydlower, B., Pacifico, F. and Pizarro, J. 2019. Libra Extended Well Test – An Innovative Approach to De-Risk a Complex Field Development. Presented at the Offshore Technology Conference. Houston, Texas, USA. 6-9 May 2019.

Nabawy, B. S. and Al-Azazi, N.A.S. 2015. Reservoir Zonation and Discrimination Using the Routine Core Analysis Data: The Upper Jurassic Sab'atayn Sandstones as a Case Study, Sab'atayn Basin, Yemen. Arabian Journal of Geoscience, 8(8), 5511-5530. 2015.

Neves, I. A., Lupinacci, W. M., Ferreira, D. J. A., Zambrini, J. P. R., Oliveira, L. O. A., Olho

Azul, M., Ferrari, A. L., Gamboa, L. A. P. (2019). Presalt reservoirs of the Santos Basin: cyclicity, electrofacies, and tectonic-sedimentary evolution. Interpretation 7, SH33–SH43. https://doi.org/10.1190/INT-2018-0237.1.

Nooruddin, H. A., Hossain, M. E., Al-Yousef, H. and Okasha, T. 2014. Comparison of Permeability Models Using Mercury Injection Capillary Pressure Data on Carbonate Rocks Samples. Journal of Petroleum Science and Engineering, 121, 9-22. Doi: https://doi.org/10.1016/j.petrol.2014.06.032

Ohen, H. and Ajufo, A. 1995. A Hydraulic (Flow) Unit Based Model for the Determination of Petrophysical Properties from NMR Relaxation Measurements. Presented in the SPE Annual Technical Conference and Exhibition, 22-25 October, Dallas, Texas. SPE-30626-MS. https://doi.org/10.2118/30626-MS.

Oliveira, L., Rancan, C. e Oliveira, M. J. (2019). Sill emplacement mechanisms and their relationship with the Presalt stratigraphic framework of the Libra Area (Santos Basin, Brazil). Presented at the LASI 6 Conference, Malargue, Argentina, 25-29 November 2019.

Oliveira, G.P., Roque, W.L., Araújo, E.A., Diniz, A.A.R., Simoes, T.A., Santos, M.D., 2016. Competitive placement of oil perforation zones in hydraulic flow units from centrality measures. J. Petroleum Sci. Eng. 147, 282–291. https://doi.org/10.1016/j.petrol.2016.06.008

Oliveira, S. and Lupinacci, W. 2013. L1 Norm Inversion Method for Deconvolution in Attenuating Media. Geophysical Prospecting. 61, 771-777. https://doi.org/10.1111/1365-2478.12002

Penna, R., Araujo, S., Geisslinger, A., Sansonowski, R., Oliveira, L., Rosseto, J. and Matos, M. 2019. Carbonate and Igneous Rock Characterization Through Reprocessing, FWI Imaging and Elastic Inversion of a Legacy Seismic Data Set in Brazilian Pre-salt Province. The Leading Edge 38 (1) 11-19. https://doi.org/10.1190/tle38010011.1.

Penna, R., & Lupinacci, W. M. 2020. Decameter-Scale Flow-Unit Classification in Brazilian Presalt Carbonates. In SPE Reservoir Evaluation & Engineering (Vol. 23, Issue 04, pp. 1420–1439). Society of Petroleum Engineers (SPE). https://doi.org/10.2118/201235-pa

Penna, R., & Moreira Lupinacci, W. 2021. 3D modelling of flow units and petrophysical

properties in brazilian presalt carbonate. In Marine and Petroleum Geology (Vol. 124, p. 104829). Elsevier BV. https://doi.org/10.1016/j.marpetgeo.2020.104829

Peçanha, A., Lupinacci, W., Ferreira, D. and Freire, A. 2019. A Workflow for Reservoir Characterization Applied to Presalt Coquinas from the Linguado Field, Campos Basin, Brazil. Journal of Petroleum Science and Engineering. 183, 106451. https://doi.org/10.1016/j.petrol.2019.106451

Pendrel, J. 2001. Seismic Inversion – The Best Tool for Reservoir Characterization. CSEG Recorder. 26(1), 1-20.

Prasad, M. 2003. Velocity-Permeability Relations within Hydraulic Units. Geophysics. 68(1), 108-117. https://doi.org/10.1190/1.1543198

Pritchard, T., Scotellaro, C. and Webber, R. 2010. Carbonate Facies and Permeability Estimation using Rock Physics and Flow-Zone Facies. Presented at the SEG 2010 Annual Meeting, Denver. USA. Technical Program Expanded Abstracts: 2654-2658. https://doi.org/10.1190/1.3513392

Porras, J. C., and Campos, O. 2001. Rock Typing: A Key Approach for Petrophysical Characterization and Definition of Flow Units, Santa Barbara Field, Eastern Venezuela Basin. SPE Latin American and Caribbean Petroleum Engineering Conference. SPE. https://doi.org/10.2118/69458-ms

Rahimpour-Bonab, H. and Aliakbardoust, E. 2014. Pore Facies Analysis: Incorporation of Rock Properties Into Pore Geometry Based Classes in a Permo-Triassic Carbonate Reservoir in the Persian Gulf. Journal of Geophysics and Engineering. 11, 1-20. https://doi.org/10.1088/1742-2132/11/3/035008

Rastegarnia, M., and Kadkhodaie, A. 2013. Estimation of Flow Zone Indicator Distribution by Using Seismic Data: A Case Study from a Central Iranian Oilfield. Iranian Journal of Oil & Gas Science and Technology, 2(4). https://doi.org/10.22050/ijogst.2013.4793

Rastegarnia, M., Sanati, A. and Javani, D. 2016. A Comparative Study of 3D FZI and Electrofacies Modeling Using Seismic Attribute Analysis and Neural Network Technique: A Case Study of Cheshmeh-Khosh Oil Field in Iran. Petroleum, 2, 225-235. https://doi.org/10.1016/j.petlm.2016.06.005

Rebelle, M. and Lalanne, B. 2014. Rock-Typing in Carbonates: A Critical Review of Clustering Methods. Presented at the Abu Dhabi International Petroleum Exhibition and Conference, Abu Dhabi, UAE. 10-13 November, 2014.

Rebelo, T. B., Batezelli, A., Mattos, N. H. S., & Leite, E. P. 2022. Flow units in complex carbonate reservoirs: A study case of the Brazilian pre-salt. In Marine and Petroleum Geology (Vol. 140, p. 105639). Elsevier BV. https://doi.org/10.1016/j.marpetgeo.2022.105639

Rezaee, M. R., Motiei, H. and Kazemzadeh, E. 2007. A New Method to Acquire m Exponent and Tortuosity Factor for Microscopically Heterogeneous Carbonates. Journal of Petroleum Science and Engineering. 56(4). 241-251. 2007. Doi: https://doi.org/10.1016/j.petrol.2006.09.004

Riazi, Z. 2018. Application of Integrated Rock Typing and Flow Units Identification Methods for an Iranian Carbonate Reservoir. Journal of Petroleum Science and Engineering 160, 483-497. https://doi.org/10.1016/j.petrol.2017.10.025.

Rocha, H. O., da Costa, J. L. S., Carrasquilla, A. A. G., & Carrasco, A. M. V. (2019). Petrophysical characterization using well log resistivity and rock grain specific surface area in a fractured carbonate presalt reservoir in the Santos Basin, Brazil. Journal of Petroleum Science and Engineering, 183, 106372. https://doi.org/10.1016/j.petrol.2019.106372

Sams, M., Millar, I., Satriawan, W., Saussus, D., & Bhattacharyya, S. (2011). Integration of geology and geophysics through geostatistical inversion: a case study. First Break, 29(8). https://doi.org/10.3997/1365-2397.2011023

Sartorato, A. C. L., Tonietto, S. N., & Pereira, E. (2020). Silicification and dissolution features in the brazilian Presalt Barra Velha formation: impacts in the reservoir quality and insights for 3D geological modeling. Rio Oil and Gas Expo and Conference, 20(2020), 68–69. https://doi.org/10.48072/2525-7579.rog.2020.068

Saussus, D., & Sams, M. (2012). Facies as the key to using seismic inversion for modelling reservoir properties. First Break, 30(7). https://doi.org/10.3997/1365-2397.2012009

Seifert, I., Penna, R., Maul, A., & González, M. (2017). Accurate Velocity Model Refinement through the use of Acoustic Impedance for Evaporite Seismic Facies differentiation of

Presalt Reservoir Prospects in Santos Basin. 15th International Congress of the Brazilian Geophysical Society & EXPOGEF, Rio de Janeiro, Brazil, 31 July-3 August 2017. https://doi.org/10.1190/sbgf2017-351

Shenawi, S., Al-Mohammadi, H. and Faqehy, M. 1999. Development of Generalized Porosity-Permeability Transforms by Hydraulic Units for Carbonate Oil Reservoirs in Saudi Arabia. Presented at the 2009 SPE/EAGE Reservoir Characterization and Simulation Conference. Abu Dhabi, UAE. 19-21 October 2009.

Simm, R., & Bacon, M. 2014. Seismic Amplitude. Cambridge University Press. https://doi.org/10.1017/cbo9780511984501

Soares, A. (2001). Mathematical Geology, 33(8), 911–926. https://doi.org/10.1023/a:1012246006212

Soares, A., D. Diet, J., & Guerreiro, L. (2007). Stochastic Inversion with a Global Perturbation Method. EAGE Conference on Petroleum Geostatistics. EAGE Conference on Petroleum Geostatistics. https://doi.org/10.3997/2214-4609.201403048

Soleymanzadeh, A., Jamialahmadi, M., Helalizadeh, A. and Soulgani, B. S. 2018. A New Technique for Electrical Rock Typing and Estimation of Cementation Factor in Carbonate Rocks. Journal of Petroleum Science and Engineering. 166. 381-388. 2018. Doi: https://doi.org/10.1016/j.petrol.2018.03.045

Strasser, A., Hilgen, A. and Heckel, P. 2007. Cyclostratigraphy - Concepts, Definitions and Applications. Newsletters on Stratigraphy. Vol. 42 (2007). 75-114. 2007.

Svirsky, D., Ryazanov, A., Pankov, M., Corbett, P. W., and Posysoev, A. 2004. Hydraulic Flow Units Resolve Reservoir Description Challenges in a Siberian Oil Field. SPE Asia Pacific Conference on Integrated Modelling for Asset Management. SPE. https://doi.org/10.2118/87056-ms

Testerman, J. D. 1962. A Statistical Reservoir-Zonation Technique. Journal of Petroleum Technology. 14(8), 889-893. https://doi.org/10.2118/286-PA

Tiab, D., Donaldson, E.C. (2004). Petrophysics: Theory and Practice of Measuring reservoir Rock and Fluid Transport Properties. s.l.: Gulf Professional Publishing.

Udegbunam, E. and Amaefule, J. 1998. An Improved Technique for Modeling initial Reservoir

Hydrocarbon saturation Distributions: applications in Illinois (USA) Aux Vases oil Reservoirs. Journal of Petroleum Science and Engineering. Vol. 21, pp.143-152. https://doi.org/10.1016/S0920-4105(98)00075-8

Vasquez, G., Morschbacher, M., Wense, C., Parisek, Y., Madrucci, V., Justen, J. 2019. Petroacoustics and Composition of Presalt Rocks from Santos Basin. The Leading Edge. 38(5), 322-416. https://doi.org/10.1190/tle38050342.1

Veeken, P. and Da Silva, M. 2004. Seismic Inversion Methods and Some of their Constraints. First Break. 22, 15-38. https://doi.org/10.3997/1365-2397.2004011.

Vernik, L. 2016. Seismic Petrophysics in Quantitative Interpretation: Society of Exploration Geophysics, Houston

Xin, C., Jianlin, L., Yong, L., Qihai, N., Xiaohuan, Y., Wenwen, Y., Lu, L., Dengyi, X., Bo, P., Qiang, L., Fuli, A., Caiqin, L., Wang, B., Xiaoli, G., Yamiao, L., & Chen, Y. 2022. Permeability Estimates of Carbonate Reservoir by Using Flow Unit Theory and Bayes Discriminant Seismic Inversion Method. In 83rd EAGE Annual Conference & Exhibition. 83rd EAGE Annual Conference & Exhibition. European Association of Geoscientists & Engineers. https://doi.org/10.3997/2214-4609.202210119

Xu, C. and Torres-Verdín, C. 2012. Saturation-Height and Invasion Consistent Hydraulic Rock Typing Using Multi-Well Conventional Logs. Presented at the 53rd SPWLA Annual Logging Symposium, Cartagena, Colombia. 16-20 June. 2012. SPWLA-2012-071.

Yarmohammadi, S., Kadkhodaie-Ilkhchi, A., Rahimpour-Bonab, H., & Shirzadi, A. (2014). Seismic reservoir characterization of a deep water sandstone reservoir using hydraulic and electrical flow units: A case study from the Shah Deniz gas field, the South Caspian Sea. Journal of Petroleum Science and Engineering, 118, 52–60. https://doi.org/10.1016/j.petrol.2014.04.002

Wang, Y. 2014. Seismic Inversion: Theory and Applications. First Ed. Wiley-Blackwell.

Wheeler, H. 1958. Time-Stratigraphy. AAPG Bulletin. 42(5), 1047-1063. https://doi.org/10.1306/0bda5af2-16bd-11d7-8645000102c1865d

Wright V. P., and Barnett, A. J. (2015). An abiotic model for the development of textures in some South Atlantic early Cretaceous lacustrine carbonates. Geological Society, London,

Special Publications 418(1): 209–219.

Zhang, P., Zhang, J., Wang, J., Li, M., Liang, J., and Wu, Y. 2018. Flow units classification for geostatisitical three-dimensional modeling of a non-marine sandstone reservoir: A case study from the Paleocene Funing Formation of the Gaoji Oilfield, east China. Open Geosciences. Vol. 10, Issue 1, pp. 113–120. https://doi.org/10.1515/geo-2018-0009